THE MECHANISM OF ALLOSTERIC REGULATION IN SOLUBLE GUANYLATE CYCLASE

by

Rahul Purohit

A Dissertation Submitted to the Faculty of the

DEPARTMENT OF CHEMISTRY AND BIOCHEMISTRY

In Partial Fulfillment of the Requirements
For the Degree of

DOCTOR OF PHILOSOPHY

WITH A MAJOR IN CHEMISTRY

In the Graduate College

THE UNIVERSITY OF ARIZONA

2014

THE UNIVERSITY OF ARIZONA
GRADUATE COLLEGE

As members of the Dissertation Committee, we certify that we have read the dissertation prepared by RAHUL PUROHIT,

entitled THE MECHANISM OF ALLOSTERIC REGULATION IN SOLUBLE GUANYLATE CYCLASE

and recommend that it be accepted as fulfilling the dissertation requirement for the

Degree of Doctor of Philosophy.

_____ Date: August 19, 2014
Dr. William R. Montfort

_____ Date: August 19, 2014
Dr. Vahe Bandarian

_____ Date: August 19, 2014
Dr. Matthew H. Cordes

_____ Date: August 19, 2014
Dr. Andrew C. Hausrath

Final approval and acceptance of this dissertation is contingent upon the candidate's submission of the final copies of the dissertation to the Graduate College.

I hereby certify that I have read this dissertation prepared under my direction and recommend that it be accepted as fulfilling the dissertation requirement.

_____ Date:
Dissertation Director: Dr. William R. Montfort

STATEMENT BY AUTHOR

This dissertation has been submitted in partial fulfillment of the requirements for an advanced degree at the University of Arizona and is deposited in the University Library to be made available to borrowers under rules of the Library.

Brief quotations from this dissertation are allowable without special permission, provided that an accurate acknowledgement of the source is made. Requests for permission for extended quotation from or reproduction of this manuscript in whole or in part may be granted by the head of the major department or the Dean of the Graduate College when in his or her judgment the proposed use of the material is in the interests of scholarship. In all other instances, however, permission must be obtained from the author.

SIGNED: RAHUL PUROHIT

ACKNOWLEDGEMENTS

First and foremost, I would like to thank my advisor *Dr. Bill Montfort.* When I joined the lab I did not had the expertise, but he showed faith in me and provided me this great opportunity to work in his lab. He has been a source of continuous encouragement throughout my graduate career. He is always excited about the data and always motivated me to try new things. Looking at him in the hallway with a big smile on his face and his patented hand gesture (when he says "Yes" or "Excellent") makes me feel like working even harder. He has been a great mentor and guided me at every step towards my scientific development. Thanks *Bill* for being highly supportive and patient. I am really grateful to you for that.

I am thankful to my committee members *Dr. Bandarian, Dr. Cordes and Dr. Hausrath* for providing me guidance time to time. Some of the work would not have been possible without your help.

I would like to thank *Dr. Andrzej Weichsel* for all his help and suggestions. I could ask him for any help at any time without any hesitation. His training in the crystallization techniques and X-Ray data collection has especially been helpful in my studies. His subtle humor and witty nature creates a happy environment in the lab. I will miss our coffee breaks and talking over world history. I thank *Jacquie Brailey* for training me with all the basic techniques during my initial years. Her care never made me feel away from home. I really miss you *Jacquie* and deeply appreciate your help. Sometimes I feel that I could not have survived in the lab without your support. I would like to thank *Dr. Sue Roberts* for her help in SSRL facility data collection and computer help. I thank *Dr. Cynthia David* for all her help in SPR studies.

I would like to thank all the past and present lab members, who have been wonderful colleagues and friends. All of them have helped me in one or the other aspect of my research. I thank my friend *Satish,* who has been very helpful during my initial years. I miss all our night outs in the lab. *Saumya* and *Hemant* has been very supportive and helpful and kept my spirits high. I thank *Juliana, John* and *Brad* for being good friends and lab mates. I thank *Aaron* for his help in some of the projects. I also thank my current lab members *Sarah* and *Jessica* for their support in the lab. I am thankful to *McEvoy* lab members *Alayna, Kayla* and *Trisiani* for being very cooperative during my long use of the spectrophotometer. I thank my batch mate *Santosh* for being a good friend. I am thankful to *Lori Boyd* and *Mary Griffin* for their wonderful administrative support. I thank my Master's advisor *Dr. Paloth Venugopalan* and *Dr. Tejvir Singh* for their encouragement and support to pursue higher education.

I would like to thank my longtime friends *Dhillon*, *Bhola* and *Gandhi* for being always there whenever I needed and being my continuous support. I thank all my Tucson friends especially *Venoo*, *Swati*, *Anubhab*, *Gaurav*, *Ramaprasad* and *Vishwas* for making my stay here a great experience.

I am extremely thankful to my parents who endured several hardships in their lives to provide me all the support so that I could fulfill my dreams. I could not have been what I am today without your tireless support and unconditional love. I thank my brothers *Raj*, *Maan Singh*, *Deepak*, and my *Bhabhi's*, who are more like friends to me. Thanks for supporting me through all my decisions and for your love and affection. I thank my sweet nephews *Shubham*, *Yuvraj*, and *Gautam*, and my niece *Priya* for keeping alive a child inside me. I love you all. I am thankful to my parent in laws, *Pushpika* and *Hitesh* for their understanding and support. I thank my loving wife *Bhavna* without whom I cannot imagine my life. She became part of my life while I was a graduate student and fully supported me to perform high. Thanks for your understanding and support.

DEDICATION

I dedicate this work to my parents. My mother herself could never attend a school in her life but she strongly believed in the power of education. She sacrificed at every step of her life to make sure that I get the best education possible. My father worked hard all his life and taught me the righteous way of living. Both of you are an inspiration to me.

TABLE OF CONTENTS

TABLE OF CONTENTS - *Continued*

LIST OF TABLES

LIST OF FIGURES

LIST OF ABBREVIATIONS

AC	adenylate cyclase
ALA	5-aminolevulinic acid
ATP	adenosine-5'-triphosphate
BH_4	tetrahydrobiopterin
cAMP	adenosine 3',5'-cyclic monophosphate
CC	coiled-coil region
cGMP	guanosine 3',5'-cyclic monophosphate
CNGC	cyclic nucleotide-gated ion channel
CO	carbon monoxide
DEA/NO	2-(N,N-Diethylamino)-diazenodiolate-2-oxide
DLS	dynamic light scattering
DMSO	dimethyl sulfoxide
DTT	dithiothreitol
E. coli	Escherichia coli
EDTA	ethylenediamine-N,N,N´,N´-tetraacetic acid
eNOS	endothelial nitric oxide synthase
EPR	electron paramagnetic resonance spectroscopy
FAD	flavin adenine dinucleotide
FMN	flavin mononucleotide
FPLC	fast protein liquid chromatography
GC	guanylate cyclase
GTP	guanosine-5'-triphosphate
H-NOX	heme-nitric oxide and/or oxygen binding domain
H-NOXA	heme-nitric oxide and/or oxygen binding associated domain
iNOS	Inducible nitric oxide synthase
IPTG	isopropyl-β-d-thiogalactopyranoside
ITC	Isothermal Titration Calorimetry
LB	Lysogeny broth
β-ME	beta-mercaptoethanol
Ms	*Manduca sexta* (Tobacco Hornworm)
Ms sGC	Manduca sexta soluble guanylate/guanylyl cycles
Ms sGC-NT	truncated Ms sGC with N-terminus retention
MW	molecular weight
Ni-NTA	nickel-nitrilotriacetic acid

nNOS	neuronal nitric oxide synthase
NO	nitric oxide
NOS	nitric oxide synthase
ODQ	1H-[1,2,4]Oxadiazolo[4,3-a]quinoxalin-1-one, an sGC inhibitor
PAS	Per-ARNT-Sim domain
PCR	polymerase chain reaction
PDB	Protein Database Bank
PDE	phosphodiesterase
PKG	cGMP-dependent protein kinase
PPi	pyrophosphate
SDS-PAGE	sodium dodecyl sulfate polyacrylamide gel electrophoresis
sGC	soluble guanylate/guanylyl cycles
SUMO	small ubiquitin-related modifier protein
TB	terrific broth
TCEP	tris(2-carboxyethyl)phosphine
UV	ultraviolet
YC-1	3-(5′-hydroxymethyl-2′-furyl)-1-benzylindazole, an sGC activator

ABSTRACT

Nitric oxide (NO), a reactive diatomic gas and a potent signaling molecule, is required for proper cardiovascular functioning. Soluble guanylate cyclase (sGC), a heterodimeric heme protein, is the key intracellular NO receptor protein which, upon NO binding, undergoes conformational changes leading to catalysis and the cGMP signaling cascade. Several small molecules that allosterically stimulate sGC have been developed for treatment of pulmonary hypertension, but little is known about their binding site or how they stimulate activity. This dissertation describes experiments designed to uncover the molecular basis for signal transduction in sGC by NO and small molecule stimulators. The crystal structure of the α-subunit PAS domain from *Manduca sexta* (*Ms*) sGC was solved at 1.8 Å resolution revealing the expected PAS fold but with an additional β strand and a shorter Fα helix. CO binding measurements on different *Ms* sGC N-terminal constructs and the β_1 (1-380) construct revealed that the α-subunit keeps the β_1 H-NOX domain in an inhibited conformation and this inhibition is relieved by removal of the α-subunit or by addition of stimulatory compounds such as compound YC-1. Linked-equilibria measurements on the N-terminal constructs show that YC-1 binding affinity is increased in the presence of CO. Surface plasmon resonance (SPR) studies on the *in-vitro* biotinylated constructs showed that YC-1 binds near or directly to the β_1 H-NOX domain. Computational and mutational analysis of the β_1 H-NOX domain revealed a pocket important in allostery and drug action. Finally, we show that the coiled coil domain plays

an important role in allosteric regulation of the β_1 H-NOX domain and possibly in signal transduction. Our data are consistent with a model of allosteric activation in which the α-subunit and the coiled coil domains function to keep heme in a low affinity conformation while YC-1 binding to the β_1 H-NOX domain switches heme to a high affinity conformation, and sGC to its high activity form.

CHAPTER I

INTRODUCTION

1.1 *Nitric oxide: A biological messenger*

Nitric oxide (NO) is a reactive, diatomic free radical gas produced in air by atmospheric lightning and the internal combustion engine. NO has long been considered as an air pollutant causing ozone layer depletion and acid rain. During the late 1970's, while the focus was to design catalytic converters to curb the exhaust of nitrogen oxides, scientists discovered that NO is produced in living organisms and is responsible for smooth muscle relaxation and vasodilation (*1*). The earliest reported vasodilatory effect of NO dates back to the 1860's when workers felt relief from their angina symptoms while working with nitroglycerin in Alfred Nobel's dynamite factory, but symptoms would return during weekends. It was a London physician, William Murrell, who successfully employed nitroglycerin for the treatment of patients suffering from angina pectoris (*2*). In fact, almost two months before Nobel's death he was prescribed nitroglycerine for his heart disease, which he refused to take (*3*). It took almost one century to determine the mechanism of action of these vasodilatory compounds.

During the late 1970's, while studying the effect of vasodilatory compounds on smooth muscle cells, Ferid Murad discovered that nitroglycerin caused smooth muscle relaxation through release of nitric oxide. He was able to show that nitric oxide increased cyclic GMP levels through activation of an enzyme called soluble guanylate cyclase

(sGC) (*4-6*). Robert Furchgott found that smooth muscle relaxation depended upon a factor released from the endothelium cells, which he named endothelium derived relaxation factor (EDRF) (*7, 8*). In 1979, Louis Ignarro observed relaxation of preconstricted arteries when he exposed them to NO and showed this relaxation occurs through sGC (*9*, *10*).

Today, the list of biological processes regulated by NO keeps growing. Vasodilation through smooth muscle cell relaxation is the best characterized physiological effect, where NO production in the endothelial cells causes smooth muscle cell relaxation, thereby lowering blood pressure. NO also acts as a neurotransmitter and has been implicated in long-term potentiation and memory formation (*11, 12*). NO production in macrophages is an important component of immune response against viruses, bacteria and even tumor cells (*13*). Recently, NO has been implicated in protein function regulation through *S*-nitrosation (also called *S*-nitrosylation) of cysteine residues as a post-translational modification of proteins (*14-16*). Apart from mammals, NO is important in olfactory sensation in the hawk moth *Manduca sexta* (*17*) and controls flashing in fireflies (*18*). NO production in bacterial cells can impart resistance against antibiotics through chemical modifications (*19*). NO production by commensal bacteria in *C. elegans* enhances longevity (*20*). Now, it is clear that NO is a signaling molecule influencing broad and diverse biology, including tissue development, immune response, blood pressure, neural function, cell growth and cell death. Cells from all kingdoms of life respond to NO but the roles for NO are particularly diverse and pervasive in higher

eukaryotes. In particular, NO is increasingly implicated in tumor growth, cardiovascular disease and asthma (*21*).

1.2 *Biological production of NO and the cGMP signaling pathway*

Nitric oxide is produced in cells by a class of enzymes called nitric oxide synthases (NOS), which oxidize L-arginine to L-citrulline (*22-26*). To date, three isoforms of NOS have been reported and well characterized in animals, namely: endothelial NOS (eNOS, also called NOS3) (*27*), neuronal NOS (nNOS, NOS1) (*28, 29*), and inducible NOS (iNOS, NOS2) (*30*). A fourth NOS protein may occur in mitochondria (mtNOS) (*31-33*). nNOS and eNOS are constitutively produced while iNOS is induced under specific conditions such as inflammation. NOSs function as homodimers and are activated in a Ca^{2+} dependent manner upon calmodulin (CaM) binding whereas iNOS, which binds CaM tightly, is always active. NOSs are remarkable in that they bind five cofactors, namely: NADPH, FAD and FMN to the C-terminal reductase domain, and tetrahydrobiopterin (H_4B) and heme to the N-terminal oxygenase domain. Electrons transfer from NADPH to the flavins and finally to heme upon CaM binding, ultimately oxidizing L-arginine with oxygen to produce NO.

Since NO is uncharged and lipophilic, it readily crosses the membrane without requiring a specific transport mechanism and can diffuse up to a distance of 100 microns. NO, a free radical in nature, is reactive and has a half-life of only 5-15 seconds in biological solutions (*34-36*). NO reacts readily with metal centers in proteins, modifies

thiols to *S*-nitrosothiols and reacts with oxygen species to form nitrite, nitrate and peroxynitrite anions (*37*).

Though NO can undergo a variety of reactions, thereby regulating a plethora of biological processes, the best characterized signaling pathway is through binding to heme in soluble guanylate cyclase (sGC), which stimulates cyclic guanosine 3',5'-monophosphate (cGMP) production and downstream signaling pathways. NO binding to the sGC ferrous heme leads to several hundred fold stimulation of cyclase activity. cGMP acts as a secondary messenger in target cells, which in turn regulates numerous physiological processes including vasodilation, platelet aggregation and neurotransmission (*21*) (outlined in Figure 1.1).

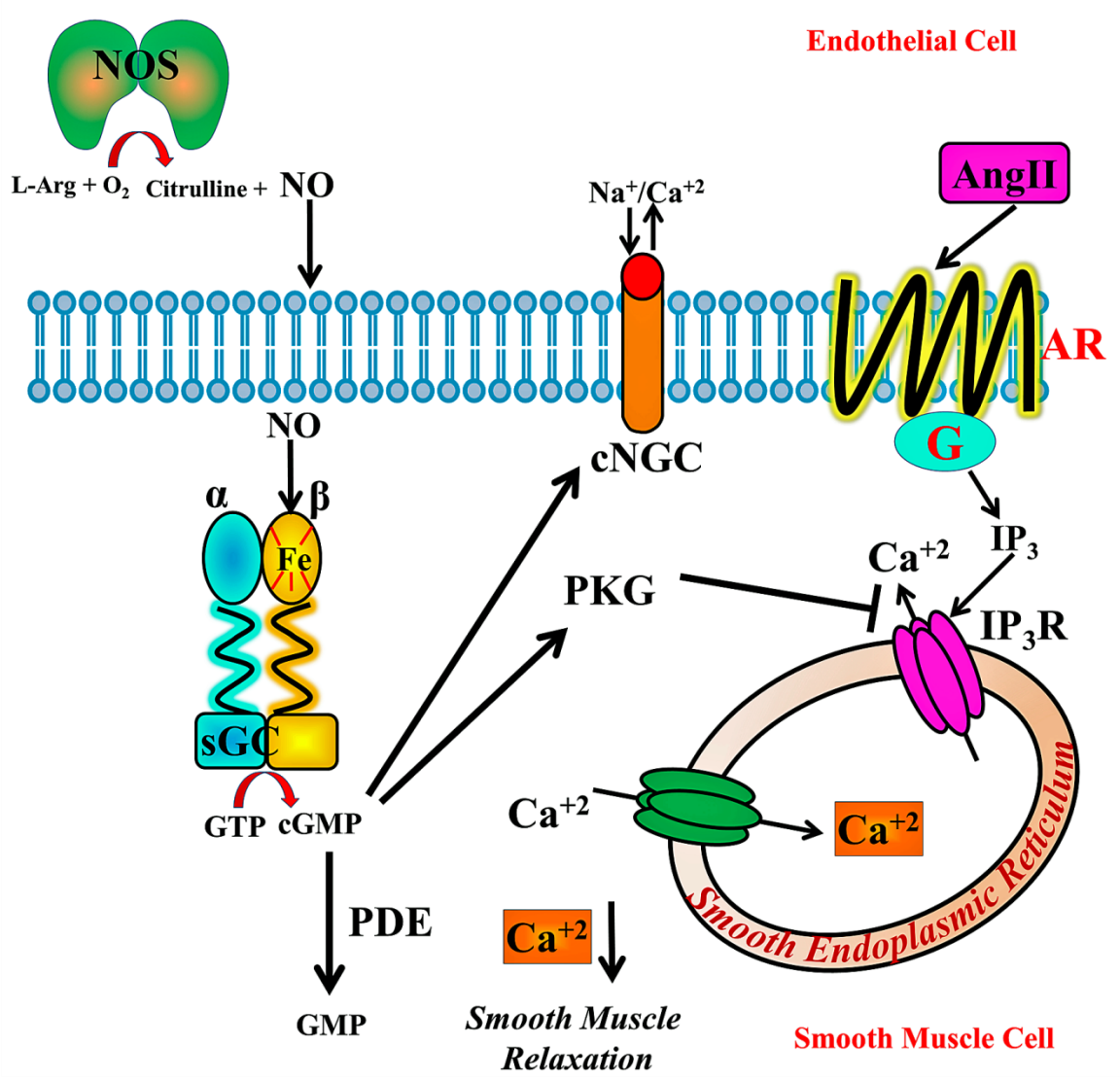

Figure 1.1 Schematic overview of the nitric oxide signal transduction pathway in smooth muscle cells. NO is synthesized by NOS in a generator cell and diffuses rapidly to bind its receptor sGC, in either the same cell or a target cell. NO binding activates sGC to convert GTP to cGMP, which targets cGMP-dependent protein kinase (PKG) and cGMP gated ion channels (CNG). In blood vessels, cGMP stimulates PKG, which phosphorylates the inositol 1,4,5-triphosphate receptor (IP_3R), causing a decrease in intracellular Ca^{+2} concentration and leading to smooth muscle relaxation and vasodilation. cGMP can be hydrolyzed by phosphodiesterase (PDE), which is allosterically regulated by cGMP.

1.3 *Soluble guanylate cyclase: The nitric oxide receptor*

The key enzyme for cyclic adenosine 3',5'-monophosphate (cAMP) production, adenylate cyclase, was discovered by Sutherland and coworkers in the late '50's (*38, 39*). Shortly thereafter, in 1963, cGMP was detected in a rat urine sample (*40*). Although the enzyme responsible for cGMP production was discovered in the late '60's, its physiological role was not known at that time (*41-44*). Detection of cGMP in both membrane and soluble fractions led to the discovery of two different proteins responsible for cGMP production in the cell, particulate and soluble guanylate cyclases (*45-47*).

Soluble guanylate cyclase (sGC) is the best characterized primary NO receptor protein and specifically binds NO. It is a ~150 kDa heterodimeric protein consisting of an α and a β subunit. The regulatory domain of the β_1 subunit, but not the α_1 subunit, binds an NO-sensitive heme, so that one protoporphyrin IX heme group is bound per $\alpha_1\beta_1$ heterodimer (*48*). Spectroscopic studies and mutagenesis studies revealed that ferrous heme is ligated through the conserved proximal histidine 105 in the β subunit (*49, 50*). Resonance Raman and EPR spectroscopic studies revealed that NO binding to the sGC heme distal pocket leads to proximal histidine bond breakage and a penta-coordinated nitrosyl-heme complex (*51-55*). NO binding also leads to activation of the catalytic domain of sGC, which carries out cyclization of guanosine triphosphate (GTP) to form cGMP. NO binding leads to ~200 fold increase in cGMP production by sGC. CO also binds to the sGC but only activates the enzyme by 2-5 fold (*56*) whereas O_2 does not bind to sGC.

1.4 *Cyclic GMP: a secondary messenger*

Six years after the identification of cAMP as an intracellular signaling molecule another purine cyclic nucleotide, cGMP, was discovered. cGMP, as a secondary messenger, binds to its target proteins to achieve its physiological effects. Three well-characterized targets of cGMP are: cGMP dependent protein kinase (PKG), cGMP gated ion channels (CNG) and cGMP regulated phosphodiesterase (PDE).

In response to cGMP binding, PKG phosphorylates specific serine or threonine residues on target proteins. The PKG Iα isoform is predominantly found in the vascular system and plays an important role in smooth muscle cell relaxation and vasodilation. Upon activation, PKG phosphorylates the IP_3 receptor thereby inhibiting Ca^{2+} transport and decreasing intracellular Ca^{2+} concentration, leading to vasodilation (*57*, *58*). Decreased intracellular Ca^{2+} leads to decreased myosin light-chain phosphorylation and vasorelaxation. In contrast, increased intracellular Ca^{2+} concentration is known to activate myosin light-chain kinase (MLCK), which phosphorylates myosin light chain (MLC), ultimately leading to vasoconstriction (*59*).

cGMP-dependent phosphodiesterases are dimeric proteins that hydrolyze the 3'-phosphodiester bond in cGMP to form GMP and control intracellular cGMP concentration (*60*). Activation of PDE5 lowers cGMP concentration leading to smooth muscle contraction while inhibition of the enzyme prolongs vasorelaxation, making PDE5 an important pharmaceutical target (*61*). cGMP production from pathways other than NO signaling (*e.g.* receptor guanylate cyclase) can regulate hyperpolarization-

activated CNG channels (HCN), leading to hyperpolarization of the plasma membrane (*62*). CNG channels also regulate Na^+ and Ca^{2+} influx and play important roles in phototransduction in rod and cone photoreceptors (*63*).

1.5 *sGC isoforms and domain architecture*

sGC is composed of two evolutionarily related homologous subunits, α and β, which are the product of a gene duplication event (*64, 65*). The most common isoforms are α_1 and β_1 subunits, which have been isolated from several tissues (*66, 67*). α_1 and β_1 subunits were first cloned separately from rat and bovine lungs (*68-71*). Only co-expressed $\alpha_1\beta_1$ heterodimers exhibit catalytic activity whereas no activity from individual subunits has been observed (*72*). Closely related isoforms of the $\alpha_1\beta_1$ heterodimer are the α_2 and β_2 isoforms. The α_2 isoform was initially cloned from human fetal brain cells and the β_2 isoform from rat kidneys (*73, 74*). α_1/α_2 subunits share roughly 46% sequence identity whereas β_1/β_2 subunits share ~41% sequence identity. The α_2 subunit, when co-expressed with the β_1 subunit, forms an active heterodimer whereas β_2 co-expression with α_1 does not exhibit activity (*73, 75*). To date, the $\alpha_1\beta_1$ isoform is the most studied and roles of other sGC isoforms are not clearly understood, although the $\alpha_2\beta_1$ complex appears to predominate in neural cells (*73*).

Heterodimeric sGC consists of an ~80 kDa α_1 subunit (690 residues in human) and an ~70 kDa β_1 subunit (619 residues in human). Both α_1 and β_1 subunits are homologous to each other with >40 % sequence similarity. The N-terminal regions are

less conserved while the C-terminal regions retain greater sequence similarity. Each subunit in sGC contains four functional domains, an N-terminal Heme-Nitric Oxide Oxygen (H-NOX) domain (*76*), a central Per-ARNT-Sim (PAS) domain (*77*), a coiled-coil domain and a C-terminal catalytic cyclase domain (*78*) (Figure 1.2). More detailed information about individual sGC domains follows in the next sections.

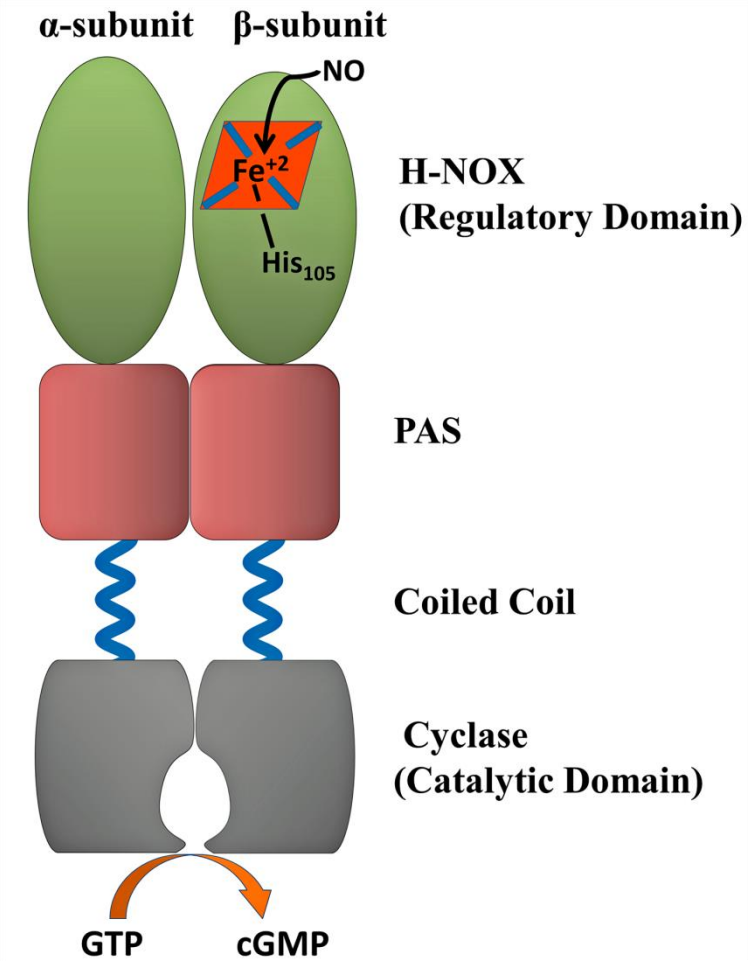

Figure 1.2 A schematic representation of soluble guanylate cyclase (sGC). Heterodimeric sGC is comprised of an α subunit and a heme-containing β subunit. Each subunit contains an N-terminal H-NOX domain, central PAS and coiled-coiled domain and a C-terminal catalytic domain. Heme in the β subunit HNOX domain is coordinated to a conserved histidine residue. NO binding to heme on the distal side leads to breakage of the His-Fe bond, inducing a conformational change in the protein, and stimulation of the cyclase activity.

1.5.1 H-NOX domain

The H-NOX domain, also known as heme nitric oxide binding (H-NOB) domain, is an ancient conserved heme-containing domain that senses and binds gaseous molecules such as NO and O_2 (*76*). Based on sequence alignment, several prokaryotic genomes have been found to contain H-NOX domains either fused to effector domains or as stand-alone proteins (*79, 80*). Structures of three prokaryotic proteins with H-NOX domains have recently appeared (*81-83*), providing insight into signaling mechanisms and suggesting a possible role for the distal pocket tyrosine residue in ligand discrimination (*84, 85*). Recently, residues important in the stabilization of the heme in the H-NOX domains have been identified as part of the highly conserved YxSxR motif (*81, 86*).

sGC contains a ferrous heme cofactor ligated to the protein at His 105 of the β-subunit H-NOX domain (Figure 1.3). During signaling, NO binding to the heme leads to formation of a pentacoordinated Fe-NO complex with dissociation of the proximal histidine bond correlated with long range conformational changes. Crystal structures of the H-NOX domain from *Nostoc sp* shows NO and CO binding induce heme pivoting and bending leading to movement of the N-terminal helices (αA-αC) (*83*). This study provides insight into the structural changes that may accompany the ligand binding to sGC. Additionally, residues between the αB-αC helices have been shown to be crucially involved in sGC activation (*87*). The structural changes due to this event are transferred to the effector cyclase domain, which in turn enhances cGMP production.

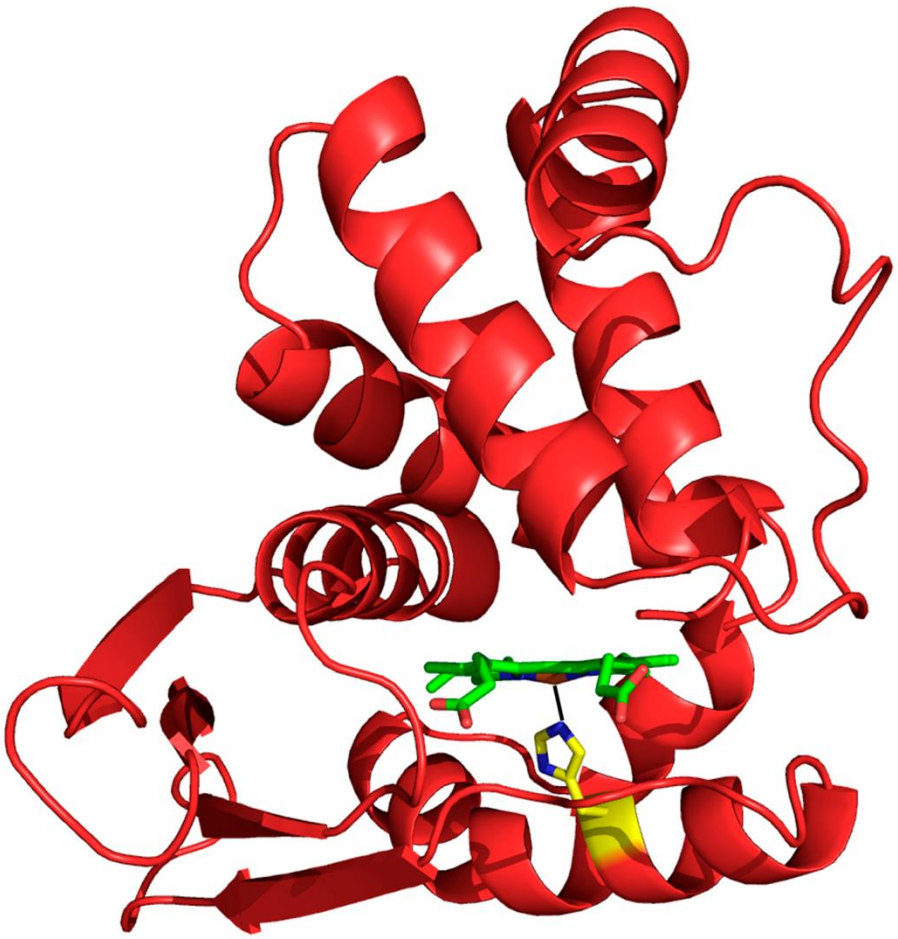

Figure 1.3 Homology model of the *Ms* sGC β_1 H-NOX domain. Shown is the proximal histidine 105 (colored in yellow), which ligates the ferrous heme (*88*).

1.5.2 PAS domain

sGC sequence alignment studies have predicted the domain at the C-terminal end of the H-NOX domain to adopt a Per-ARNT-Sim (PAS) fold (*79*). The PAS domains, also known as heme nitric oxide/oxygen binding associated (H-NOBA or H-NOXA) domains, are named after the fold initially discovered in the *Drosophila* proteins period (Per), single minded (sim), and aryl hydrocarbon receptor nuclear transporter (ARNT) (*89, 90*). Since the initial discovery of the PAS fold, it has been found in all kingdoms of life as a component of signal transduction proteins. PAS domains in general are known to function as sensory modules to sense external stimuli and regulate signaling pathways through interaction with effector domains in a diverse family of enzymes, including histidine kinases, phosphodiesterases, ion channels and transcriptional activators (*91*).

PAS domains often bind cofactors such as flavin mononucleotide in the light-oxygen-voltage-sensing domain LOV of phototropin protein in *Arabidopsis*, heme in oxygen sensor protein FixL of *Bradyrhizobium japonicum* and *p*-coumaric acid in photoactive yellow protein (*92-94*). Apart from natural ligands, PAS domains also bind various non-natural ligands (*95*). Structure activity relationship (SAR) studies by solution NMR methods have recently shown that PAS kinase can bind ligands within a hydrophobic core (*96*). Structural studies on the homologous PAS domain from signal transduction histidine kinase (*97*) and fluorescence studies on PAS-domain deletion mutants (*98, 99*) suggest that the PAS domains in sGC play an important role in hetero-dimerization. Additionally, cross-linking studies from our lab and others (*88, 100*)

suggest a potential regulatory role for the PAS domain in sGC. The crystal structure of *Ms* sGC α_1 PAS domain was determined (*101*) as part of this dissertation (see Chapter 2, Appendix I).

1.5.3 Coiled-coil domain

The linker region between the H-NOX/PAS domains and the cyclase domains adopts a conserved coiled-coil structure and has been predicted to be a part of signaling helix family (*102*). The coiled-coil domain has been previously shown to be critically important for the dimerization of sGC (*99*). Further, a crystal structure of the rat sGC β-subunit coiled-coil domain homodimer also provided insight into the residues that might be important in heterodimerization (*103*). Signaling helices are often found between two signaling domains and are known to play an important role in transferring signals from N-terminal sensory domains such as PAS, HAMP and GAF domains to C-terminal effector domains such as histidine kinases, cyclic diguanylate phosphodiesterases and diguanylate cyclases (*104*, *105*). A similar role has also been suggested for the sGC coiled-coil domain but needs further structural studies for validation.

1.5.4 Cyclase domain

The identity between the α_1 and β_1 subunits is highest in their C-terminal ~200 amino acids, and, based on their homology to the catalytic domains of adenylate cyclase, these regions are believed to come together to form a functional catalytic site that is an

obligate heterodimer (*106*). Catalytic domains from individual subunits α_1 and β_1 can be expressed and purified separately as homodimers with no catalytic activity, but when combined, the heterodimer recapitulates guanylate cyclase activity (*107*). Recent crystal structures of the catalytic domain of sGC reveal a similar fold to the homologous adenylate cyclase and provide insight into the catalytic mechanism (*108, 109*).

Active site residues are contributed by both the α_1 and β_1 subunit cyclase domains and are highly conserved across adenylate and guanylate cyclases. Only one of the two possible active sites appear to be functional. Similarly to the forskolin-binding pseudosymmetric site in adenylate cyclase, sGC also contains a pseudosymmetric site that lacks key catalytic residues (*110, 111*). sGC is believed to catalyze a two-metal-ion reaction much like that of adenylate cyclase in which an activated 3' hydroxyl of the ribose attacks the α-phosphate of guanosine triphosphate (Figure 1.4) (*112, 113*). The reaction occurs with inversion of stereochemistry, consistent with a single-displacement reaction mechanism (*114*), and divalent cations are required (*115*). Recent studies hint that the cyclase domain is maintained in a basal low-activity conformation through a direct inhibitory contact with the β_1 H-NOX domain (*107, 116, 117*). Another study indicates that other sGC domains are also required for full enzyme activity and play a potential role in modulating cyclase domain orientation (*118*). That sGC activity could be regulated through binding of nucleotides to the pseudosymmetric site has also been proposed (*119*). Despite these data, the mechanism by which signal transduction from heme domain to cyclase domain occurs upon NO binding is unknown.

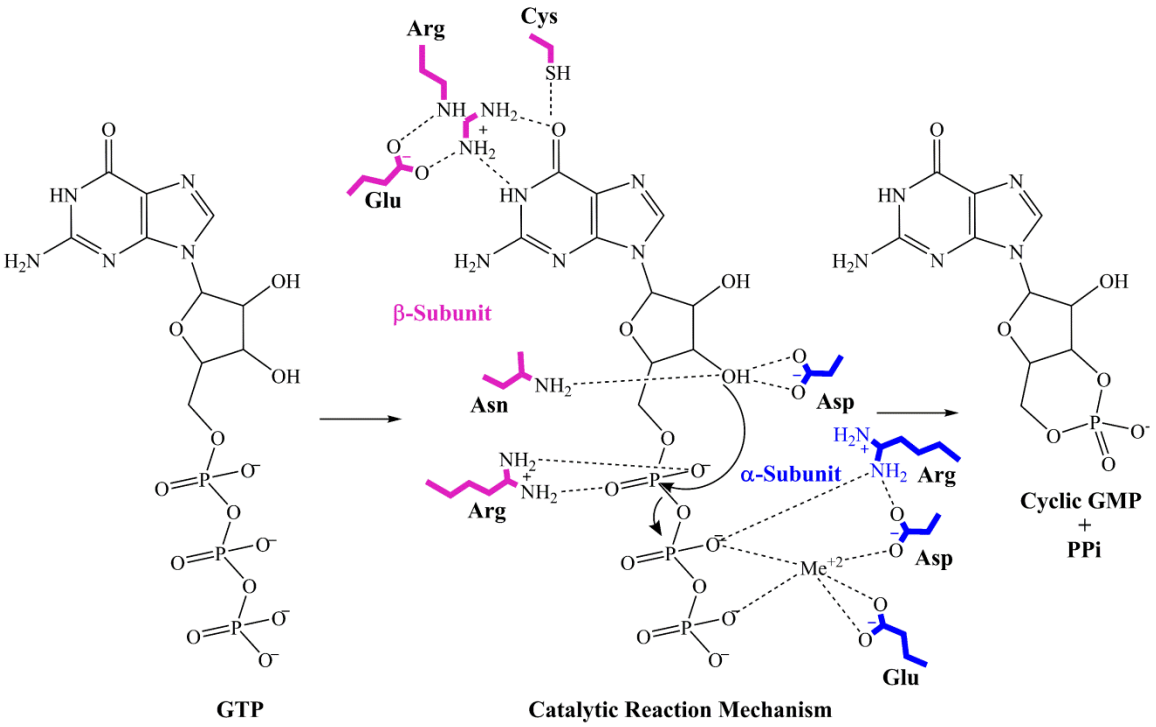

Figure 1.4 Plausible mechanism of the GTP cyclization reaction. Shown is a model for catalytic mechanism of sGC based on adenylyl cyclase (adapted from (*106*)). Active site residues are contributed by both α (colored blue) and β (colored magenta) subunits and divalent metal ion (only one metal shown in the scheme) is required for the reaction to take place. Cleavage of the α-phosphoanhydride bond through a single direct displacement reaction yields the products, cGMP and pyrophosphate (PPi).

1.6 *Allosteric stimulators and activators of sGC*

Since nitric oxide both lowers blood pressure and improves blood flow through its vasorelaxation and antiplatelet activities, NO signaling has long been a target for treating cardiovascular disease. For example, organic nitrates such as nitroglycerin, which is metabolized to release NO, have a long history in treating angina pectoris. While current treatments are successful for some patients, some do not respond and many who do develop tolerance to the compounds, which then become ineffective (*120, 121*). Efforts for discovering new treatments are increasingly focused on sGC, which is compromised in all forms of cardiovascular disease.

Several synthetic compounds have been discovered that stimulate sGC directly. YC-1 (Figure 1.5), a benzyl-indazole derivative, was first identified during pharmaceutical screening to possess antiplatelet aggregation properties (*122*). Later, it was shown that YC-1 achieves this through a direct activation of sGC in a heme-dependent but NO-independent manner (*123-125*). YC-1 by itself stimulates sGC activity by only 10-fold but acts synergistically with CO to stimulate activity to the same level as for sGC-NO (*126, 127*). The discovery of YC-1 as a novel sGC stimulator opened a promising drug discovery avenue to treat cardiovascular diseases. Since YC-1 is a weak stimulator, Bayer developed new molecules based on the YC-1 core scaffold with high potency, including compounds BAY 41-8543 and BAY 41-2272 (Figure 1.5). Although initial BAY compounds failed in early clinical trials, further modified derivative BAY 63-2521 (Riociguat) (Figure 1.5) has been approved by the Food and Drug

Administration (FDA) for the treatment of pulmonary hypertension and is currently being marketed under the commercial name 'Adempas' (*128*). Despite the success of these drugs in treatment of pulmonary hypertension, little is known about their binding site or how they stimulate activity.

sGC contains a ferrous heme in a very hydrophobic H-NOX pocket and exhibits very slow oxidation rates under normal cellular conditions. Although ferrous heme in sGC is highly stable and resistant to heme loss, upon oxidation the protein becomes unstable and undergoes rapid heme loss (*129*). Oxidized sGC is degraded in the cell and recently developed new compounds such as BAY 58-2667 (also known as Cinaciguat) are designed to rescue oxidized sGC (*130*). A recent crystal structure of cinaciguat bound to the Nostoc H-NOX domain provides insights into how this compound rescues and activates oxidized sGC by mimicking and occupying the heme site (*131*).

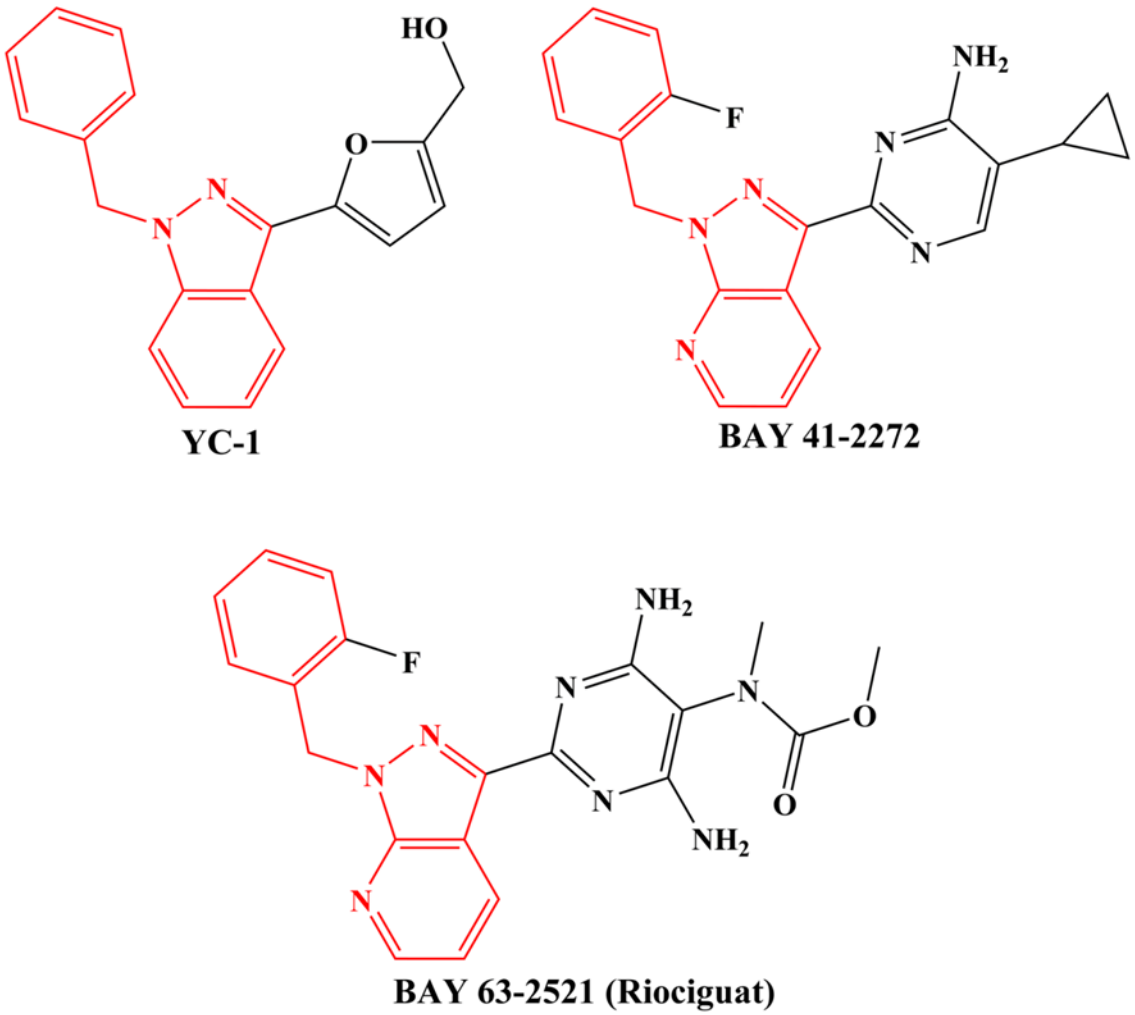

Figure 1.5 sGC stimulatory compounds. Chemical structures of sGC stimulators YC-1, BAY 41-2272 and BAY 63-2521 (Riociquat – FDA approved and marketed as Adempas). The benzyl-indazole core structure is highlighted in red and not much modification can be made in this region, whereas other positions (shown in black) can be modified to achieve varied efficacy.

1.7 *Current questions*

The role of sGC in cardiovascular physiology and blood pressure regulation is well established. For the last four decades, heme characteristics in sGC and the kinetics of ligand binding (NO and CO) to sGC heme have been extensively studied using spectroscopic methods. It has been proposed that proximal histidine bond breakage triggers structural changes in the sGC β-subunit that are propagated through the subunit interface, which in turn enhances cGMP production. Studies with NO-independent activators of sGC suggest that the enzyme can be activated in the absence of breakage of the histidine-iron bond (*100, 132-134*). Marletta and co-workers have suggested that a second non-heme binding site for NO might be involved with proximal histidine release from the sGC heme (*135*). Moreover, the number of NO molecules required for sGC activation is debated (*134, 136, 137*). Despite many studies, the molecular details involving sGC stimulation and regulation remain obscure mainly due to the difficulty in obtaining sufficient quantities of the enzyme.

Signal transduction in sGC requires the interaction of multiple domains and thus an understanding of allostery and drug stimulation can only be achieved through structures containing these same domains. The lack of structural information for sGC represents the single biggest obstacle to progress in the NO signaling field. Most of the structural information for sGC comes from homology modeling to related proteins or individual domains whose structures have been recently determined. Although these individual domain structures allow for better model building, how the domains in sGC

are organized and how they interact with each other remains unanswered. Our group has used chemical cross-linking mass spectrometry and small angle x-ray scattering (SAXS) to develop a molecular model of sGC (*88*). These studies provide an overall shape of the molecule suggesting sGC is an elongated molecule that does not appreciably change shape upon binding NO, CO or YC-1 family compounds. A recent single-particle electron microscopy structure of full-length sGC (*138*) provides new insight into sGC architecture. Hydrogen/deuterium exchange mass spectrometry (HDX-MS) has been used to map the interdomain interactions and conformational changes upon NO binding in sGC (*117, 139*). Although several interdomain interactions within sGC are becoming clear, determination of the precise nature of these interactions and critical residues involved in the signal transduction await an atomic resolution structure.

Allosteric regulators can modulate sGC activity in several ways. Both ATP and GTP alter NO-stimulated catalysis by sGC, apparently through an allosteric binding site, with ATP in particular inhibiting activity (*119, 134, 140*). Several synthetic compounds, including YC-1 and BAY 41-2272, stimulate sGC independently of NO but how they stimulate activity or where they bind is not understood. There are several conflicting reports in the literature describing different domains of sGC as the potential binding sites. Proposed binding sites include the pseudosymmetric site in the cyclase domain (*141, 142*), the α_1 H-NOX domain (*100, 143*) and the β_1 H-NOX domain (*144-147*). Understanding of the binding site of these allosteric regulators and their mechanism of action is critical for rational drug design to achieve higher efficacy.

1.8 *Explanation of the dissertation format*

This dissertation has been prepared in accordance with the format prescribed by the University of Arizona Graduate College *Manual for Electronic Theses and Dissertations* and is consistent with the formatting requirements of the Department of Chemistry and Biochemistry. I have presented my work in three chapters and three appendices. The overall key questions and its context are introduced in Chapter 1. Structure-function studies undertaken by me are attached as appendices in the publication format. Summary of important findings of the research described in each appendix is outlined in Chapter 2. The conclusion and future directions of this study are presented in Chapter 3.

My work is primarily focused on understanding the allosteric regulation of sGC and determining the atomic resolution structure of sGC. In Appendix I, I describe a 1.8 Å resolution crystal structure of the sGC α-subunit PAS domain (published in (*101*)). Appendix II contains findings describing allosteric regulation in sGC and binding studies on YC-1 family compounds. These studies narrowed the binding site for YC-1 family compounds to the β_1 HNOX and PAS domains (published in (*148*)). In Appendix III, I describe mutational studies targeting the potential YC-1 binding site and role of signaling helix in allosteric regulation.

CHAPTER II: PRESENT STUDY

The methods, results and conclusions of this study are presented in the manuscripts appended to this dissertation. Several *Manduca sexta* sGC constructs used in the study are listed in table 2.1. The following is a summary of the most important findings from each appendix.

Table 2.1 *Ms* sGC proteins used in the present study. All *Ms* sGC-NT constructs are in the pET-Duet-1 expression plasmid for dual expression of α and β subunits. *Ms* sGC α_1 PAS construct is in pETHSUL expression plasmid for expression with SUMO fusion protein. NT2 was prepared by Xiaohui Hu; NT13 and NT21 were prepared by Bradley Fritz; NT19, NT23, NT25 and β_1(1-380) were prepared by Andrzej Weichsel. *Ms* sGC α_1 PAS was prepared by myself.

***Ms* sGC Protein**	**Domain Boundaries**
Ms sGC-NT2	α_1 49−471, β_1 1−401
Ms sGC-NT13	α_1 49-450, β_1 1-380
Ms sGC-NT19	α_1 49-450, β_1 1-380-Strep
Ms sGC-NT21	α_1 272-450, β_1 1-380
Ms sGC-NT25	α_1 49-459, β_1 1-389-Strep
Ms sGC-NT23	α_1 272-459, β_1 1-389-Strep
Ms sGC β_1(1-380)	α_1 absent, β_1 1-389
Ms sGC α_1 PAS	α_1 279-404, β_1 absent

Summary of Appendix A: Crystal structure of the Alpha subunit PAS domain from soluble guanylyl cyclase.

This manuscript reports the 1.8 Å resolution crystal structure of the alpha subunit PAS domain from *Manduca sexta* soluble guanylyl cyclase. The *Ms* sGC α-PAS was expressed with small ubiquitin like modifier (SUMO) as an N-terminus fusion protein with SUMO removed during purification. Three Cys-to-Ala mutations were introduced to improve crystallizability. The structure reveals a typical PAS domain fold, but one with unique loop arrangements as compared with structures of its closest homologues. A surface helix contains residues Glu 340 and Lys 343, which cross-link with the β_1 H-NOX domain, and residue Phe 338, which, when mutated, leads to an altered heme Soret absorption band. All three lie on the same face and likely represent the interface between the α_1 PAS and β_1 H-NOX domains. Interestingly, there is a small internal cavity near where ligands typically bind to PAS domains. Although this pocket is only of sufficient size for binding a single ring, a small movement of the nearby helix at the β_1 H-NOX binding interface would make the pocket more available.

Summary of Appendix B: YC-1 Binding to the β Subunit of Soluble Guanylyl Cyclase Overcomes Allosteric Inhibition by the α Subunit.

In this study we discovered new factors in the allosteric regulation of sGC. Previous studies from our group have shown that YC-1 family compounds bind away from the catalytic domain and in the N-terminal half of the protein (*149*). Using different

constructs lacking specific domains we were able to show that both the α_1 PAS and α_1 H-NOX domains inhibit CO binding to heme in the β_1 H-NOX domain. Removal of the α_1 H-NOX domain enhances CO binding by 24-fold, and complete removal of the α_1 chain enhances CO binding by 265-fold. Interestingly, we found that the isolated β_1 subunit displays the tight CO binding only seen for the heterodimeric protein when YC-1 is bound. Binding of CO to *Ms* sGC β_1 (1−380) in the absence of YC-1 is as tight (K_d^{CO} = 0.20 μM) as binding to any of the *Ms* sGC-NT proteins in the presence of YC1. We showed that the α_1 subunit serves to keep the β_1 H-NOX domain in a conformation with weaker CO binding, while YC-1 binding allows for a heme domain conformation with stronger CO binding. Thus, binding of YC-1 appears to overcome the inhibitory effect of the α_1 subunit on the β_1 H-NOX domain.

For a system displaying linked equilibria, binding of either ligand will affect the binding of the other. We employed a multidimensional binding assay to extract the YC-1 dissociation constant through analysis of the linked equilibria between CO binding and YC-1 binding. Linked-equilibria measurements showed that CO binding to *M*s sGC-NT enhances YC-1 binding and yielded a dissociation constant of 9 μM for YC-1 binding to *Ms* sGC-NT21. Cooperativity factors determined from the analysis reflected the influence of one ligand on binding of the other, from which the dissociation constant for the binding of YC-1 to the CO-saturated protein was derived to be 0.7 μM for *Ms* sGC-NT21.

A surface plasmon resonance (SPR) spectroscopy approach was developed to clarify where YC-1 family compounds bind sGC. Avi-tagged sGC constructs were specifically biotinylated with an *E. coli* biotinylating enzyme BirA and were captured on a neutravidin coated SPR chip to measure ligand binding. We demonstrated that PF25 (more soluble YC-1 family compound) binds to both *Ms* sGC-NT21 and *Ms* sGC β_1 (1−380) but not to α_1 PAS. Moreover, PF25 binding affinity increases ~10-fold in the presence of NO. These data represent the first direct measurements of a YC-1 family compound binding to sGC and demonstrated that binding occurs on the N-terminal end of the β-subunit. Taken together, this study demonstrates that the α_1 PAS domain inhibits binding of CO, and presumably NO, to the β_1 heme domain and binding of YC-1 overcomes this inhibition. We also showed that the binding of YC-1 and CO or NO to heterodimeric sGC displays linked equilibria, with binding of one enhancing binding of the other, and that YC-1 binds to the β_1 chain, most likely in the heme domain.

Summary of Appendix C: Identification of an Allosteric Pocket in Soluble Guanylate Cyclase.

This study reports the identification of a pocket in the β_1 H-NOX domain of importance for allosteric signal transduction. The role of this pocket in allosteric regulation and YC-1 binding was characterized using mutagenesis studies. Residues lining the pocket were mutated to either phenylalanine or tryptophan in order to fill the pocket. Single mutants in *Ms* sGC-NT13 (L98F and A154F) led to decreased CO affinity

in the absence and presence of YC-1. The L98F/A154F (LA) double mutant in both *Ms* sGC-NT13 and *Ms* sGC-NT21 led to a protein with very weak CO binding affinity (K_d ~200 μM). Interestingly, YC-1 enhancement of CO binding in the double mutant proteins is now largely absent. Moreover binding affinity of YC-1 to the *Ms* sGC-NT21_LA CO complex is also ~7 fold weaker. The rate of the histidine release upon NO binding to the heme was measured for both *Ms* sGC-NT13_LA and *Ms* sGC-NT13_LA mutant proteins. Both mutant proteins showed significantly slower histidine release, with rate constants of 2.7 s^{-1} and 3.5 s^{-1}, respectively. The L98F/A154F mutation was introduced into full-length human sGC and the effect of the mutations on the cyclase activity was measured. Full length mutant sGC responded weakly to NO stimulation and exhibited higher K_m for GTP binding compared to wild type sGC. We proposed that the double mutation led to the stabilization of the heme in a low affinity conformation which binds CO and YC-1 weakly.

Additional mutations to a possible alternative YC-1 binding pocket were made, but these mutations had little effect on CO binding. The D45A mutation in the loop connecting αB and αC led to heme-free sGC. Additionally, the role of the coiled-coil domain in the signal transduction and allosteric regulation of the sGC was studied by measuring the histidine release rates in *Ms* sGC N-terminal constructs with varied lengths of the coiled-coil domain. We found that shortening the coiled-coil domain by 9 residues (α_1 450 and β_1 380) from the predicted end (α_1 459 and β_1 389) led to faster histidine

release rates (>100 s^{-1}) upon binding NO, while increasing the domain length led to slower rates.

In summary, we proposed that the coiled-coil domain plays an important regulatory role and might be directly involved in signal transduction upon NO binding. We also demonstrated that a newly-described pocket is involved in sGC allostery and is necessary for signal transduction upon NO binding.

CHAPTER III

CONCLUSIONS AND FUTURE DIRECTIONS

In my work, I undertook structural and functional studies on soluble guanylate cyclase (sGC) in order to understand the mechanism of signal transduction upon NO binding to sGC. Domain boundary optimization and fusion to the small ubiquitin related modifier (SUMO) led to successful expression and purification of the α_1 PAS domain construct. X-ray crystallographic structural studies revealed the canonical PAS fold but with an additional β strand and shortened αF helix (*101*). Residues previously cross-linked to the β_1 H-NOX domain were found on the αF helix, which has been implicated in small molecule binding and signal transduction in the PAS domains (*77, 95*). I performed the ligand binding studies on several *Ms* sGC N-terminal constructs and found that the α-subunit induces a low affinity heme conformation in the β-subunit (*148*). This inhibition could be relieved by the removal of the α-subunit or by the addition of YC-1 family compounds. I showed that the system exists as a set of linked-equilibria where binding of CO/NO enhances the binding of YC-1 family compounds and *vice versa*. Surface plasmon resonance (SPR) was used to determine binding affinity and location of YC-1 family compounds. This work confirmed that YC-1 family compounds bind near or directly to the β_1 H-NOX domain. I identified a pocket in the β_1 H-NOX domain and characterized it through mutagenesis studies for its role in the signal transduction. I found that this pocket is important in allostery and is required for the signal propagation.

Additional mutagenesis studies indicated that the β_1 H-NOX domain might harbor the binding site for YC-1 family compounds. Histidine release rate studies in various *Ms* sGC N-terminal constructs with varied coiled-coil domain length suggested that signal propagation might occur through this domain. These studies provide further insight into the mechanism of allosteric regulation in this physiologically important enzyme.

Below, I present a few open questions and suggest further studies.

3.1 Atomic structure of sGC.

Lack of structural data for full-length sGC has been a major impediment to understanding the mechanism of signal transduction and allosteric regulation. Though structures of cyclase domain and the β_1 coiled coil domain were determined recently, structures of the other N-terminal domains and full-length sGC are still elusive. Recent studies reveal that sGC is an inherently dynamic enzyme occupying multiple conformations (*138*) whereas one of the requirements for the crystallization is to obtain a single conformation of the protein. Crystallization of the individual domains has also been very challenging due to poor recombinant expression and solubility of these individual domains.

Several functional *Manduca sexta* sGC (*Ms* sGC) N-terminal constructs lacking the cyclase domain have been previously expressed in our laboratory, yielding stable

proteins (*88, 149*). These constructs also contain affinity tags, yielding better purification. Although several of these N-terminal constructs are well behaved, obtaining diffraction-quality crystals has been challenging. Domain optimization on both N- and C-termini of the α_1 PAS domain led to protein with high monodispersity and better diffracting crystals. Similar approaches for the *Ms* sGC-NT constructs are currently being employed, focusing on optimization of the coiled-coil to obtain homogeneous proteins. Although oxidation rates for the sGC heme are very slow, under crystallizing conditions oxidation might be significant and could lead to heterogeneity and hinder crystallization. Crystallization under anaerobic conditions should be tried in the future.

Recent mutagenesis studies show that the β_1 L98F/A154F mutation in the N-terminal constructs leads to heme stabilization in the low affinity conformation. Attempts should be made to crystallize the L98F/A154F mutant proteins in the N-terminal constructs. Co-crystallization in the presence of gaseous ligands or the YC-1 family compounds should be attempted as these might also stabilize the protein in a single conformation. Additionally, mutations of the cysteine residues might be helpful to avoid possible cysteine dimerization and heterogeneity under crystallization conditions. A similar case was observed during crystallization of the α-PAS domain where we were able to obtain diffraction quality crystals (1.8 Å) only after mutating all three cysteine residues. Alternatively, reductive methylation of the free lysines should be attempted to reduce surface entropy and promote crystallization (*150*). I optimized the domain boundaries for the β-subunit PAS domain by inserting a stop codon at the end of the PAS

domain and created two new constructs, P4β and P5β. Expression of P5β led to extraordinarily high yield of the protein (>200 mg of pure protein from 6L of the growth media). Preliminary crystallization led to production of small needle like crystals. These conditions should be optimized further to obtain diffraction quality crystals. Similar domain optimization should be employed for other individual sGC domains as crystallizing the heterodimeric sGC has been challenging.

My efforts led to crystallization of the *Ms* sGC-NT21 construct. Red-colored heme-containing tetragonal ($a = b = 89$ Å, $c = 172$ Å; 8 molecules per unit cell) crystals were obtained and displayed preliminary diffraction to 9 Å resolution (Figure 3.1). These crystals grow rapidly overnight and are in tetragonal space group ($P4_122$ or $P4_322$). Crystal growth and crystal freezing are being optimized to obtain improved diffraction from this promising start. Selenomethionine labeled protein was also easily crystallized under the same conditions, but unfortunately also diffracted poorly.

My efforts led to further improvements and I have also obtained new conditions for slow *Ms* sGC-NT21 crystal growth in the presence of YC-1 family compound. These new orthorhombic crystals take roughly five days to grow to ~200 micron length. Data measurement at the Stanford Synchrotron Radiation Lightsource (SSRL) recently yielded 3.5 Å data (Figure 3.1 B). Multiple datasets have been collected on these crystals and data processing show a large unit cell with dimensions $a = 157$ Å, $b = 238$ Å and $c = 181$ Å. Preliminary analysis suggests there are 4 molecules in the asymmetric part of the unit

cell. Although a multiwavelength anomalous diffraction (MAD) dataset for the iron edge was also collected, the signal appears to be low. Molecular replacement with 3.5 Å dataset appears to be a challenge at this stage since structures of all the domains are not known. A strategy is currently in place to further optimize conditions and yield better diffraction data. These studies should be extensively followed in order to obtain better resolution data and, ultimately, a crystal structure of the heterodimeric N-terminal fragment of sGC. Additionally, I have already purified and crystallized the selenomethionine labeled protein for future phasing using single wavelength and multiwavelength anomalous diffraction. A crystal structure of the N-terminal *Ms* sGC would be a product of my efforts described here and ongoing efforts of Dr. Andrzej Weischel.

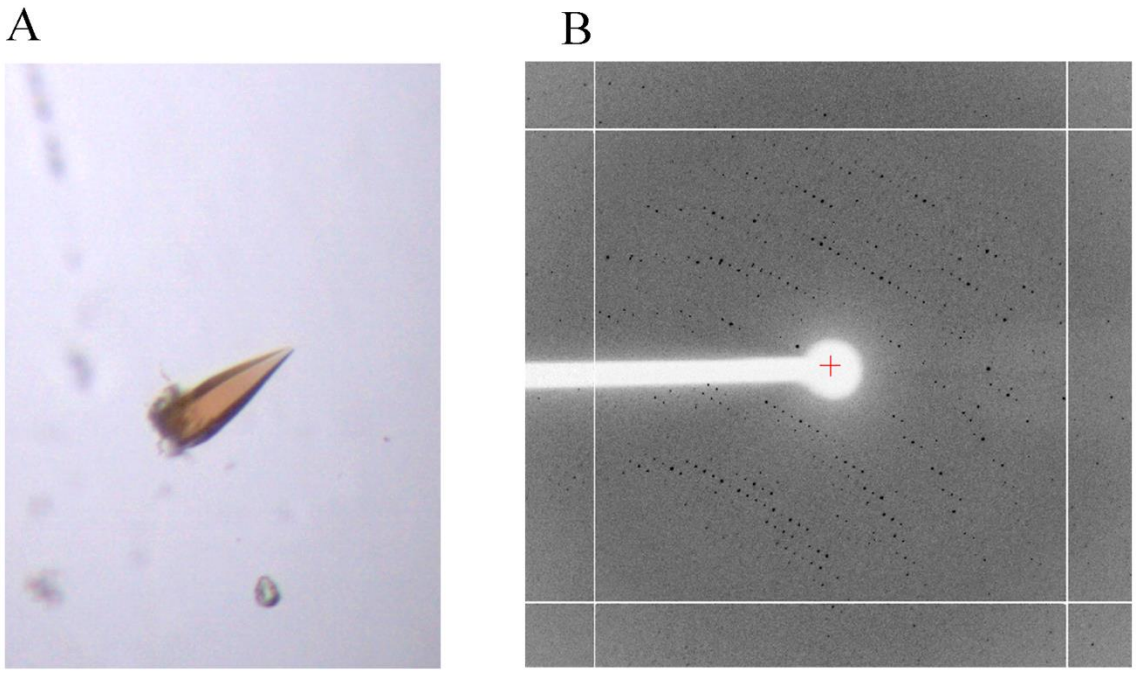

Figure 3.1 *Ms* sGC-NT21 crystals and diffraction. A. The tetragonal crystals were obtained from *Ms* sGC-NT21 at ~10-20 mg/ml and grow up to ~200 microns in length, although preliminary diffraction data collected at synchrotron radiation source yielded only 9 Å resolution. B. 3.5 Å diffraction data from *Ms* sGC-NT21 crystals in the presence of a YC-1 family stimulatory compound. *Ms* sGC-NT21 was oxidized prior to addition of the stimulatory compound and crystals appeared within five days initializing crystallization.

3.2 Location of the YC-1 family binding site and the mechanism of activation.

Locating the binding site for YC-1 family compounds has been challenging and reports of different domains as the site adds to the perplexities. Our CO binding studies indicated YC-1 binding is located somewhere on the N-terminal half of the protein and SPR studies showed the β_1 H-NOX domain as the likely binding site. The challenge of identifying the precise binding site and the specific residues involved within the β_1 H-NOX domain still remains. Mutagenesis studies to target residues around putative binding sites are currently underway and should lead to better understanding of the binding site. Additional possibilities should be probed in the β_1 H-NOX domain. Residues around the tunnel 1 (Leu 51/59, Ile 25/61/66, Val 13 and Ala 55/65) should be mutated to Phe or Trp to fill the pocket and the effect on CO binding in NT- and β-subunit constructs measured in the presence of YC-1. Additionally, the I52W mutant has been made and should be looked at for possible effects on CO binding and involvement in YC-1 binding. Further characterization of the successful mutants described in Appendix 3 should be made by carrying out the k_{on} and k_{off} measurements for CO and probably NO. Moreover, reduction potential studies should be conducted on the previously made double mutants to further understand their effect on the heme. Some of the interesting tryptophan mutants could be further pursued with FRET measurements utilizing emission of tryptophan to excite YC-1 in order to better understand the binding site.

Since SPR has been very helpful in providing direct binding evidence, these mutants should be screened for their effect on binding with this technique. An additional approach would be to attach a YC-1 compound to the SPR chip surface and flow the mutants on the surface. One end of YC-1 family compounds can be modified without losing the binding to sGC. A linker with a biotin moiety could be attached to this end of the compound and captured on a Neutravidin coated SPR chip. This could provide means to screen a large number of mutant proteins in a short duration of time. There lies a possibility that some additional contacts might be provided by other domains and should be probed.

ITC provides an excellent alternative approach for probing ligand binding affinity as it provides very sensitive and accurate measurements. Previous attempts to measure binding of YC-1 and BAY compounds to *Ms* sGC NT constructs by ITC were unsuccessful due to complications with the DMSO solvent. Since PF-25 is better behaved and displays higher solubility in aqueous buffer, performing ITC should be of high priority. As no labeling or immobilization of the samples is required, these constructs could be tested right away and should provide a direct measure of binding. Finally, these studies could provide information about the specific interactions between sGC and YC-1 compounds and conformational changes upon compound binding to the heme domain. These studies would provide a step forward for better drug design.

3.3 Role of the Coiled-Coil Domain in sGC regulation.

Whether signal propagates through the coiled coil domain or through a direct interaction between the β_1 H-NOX domain and the cyclase domain is not clear. Recent Hydrogen-Deuterium exchange mass spectrometry (HDX-MS) and electron microscopy indicated conformational changes in the coiled coil domain but details about these conformational changes still need to be elucidated (*116, 138, 139*). That the signal propagation occurs through the coiled coil domain is currently being investigated in our group. The histidine release rate upon NO binding to the heme is affected by the coiled-coil domain, indicating the domain is involved in the regulation of the β_1 H-NOX domain.

Currently, Dr. Andrzej Weischel is undertaking lanthanide-based resonance energy transfer (LRET) approaches (*151*) to probe the conformational changes in the coiled coil domain upon NO binding to the heme. The lanthanide metal binding tag (LBT) is being introduced at the C-terminus of the coiled coil domain. The emission from the lanthanide metal bound to the LBT could be absorbed by the Ni^{2+} and Co^{2+} metals bound to the His_6-tag. The LRET signal upon NO binding would provide intramolecular distances between the probes and any changes in the signal would yield information about conformational changes.

Another approach would be to insert a 13-amino acid peptide called lipoic acid ligaseA acceptor peptide (LAP) at the C-terminus of the α-subunit coiled-coil or at the N-

terminus of the α-PAS domain and a biotin ligase acceptor peptide (AP) on the β-subunit coiled-coil. The LAP sequence is specifically recognized by the *E. coli* enzyme lipoic acid ligase (LplA). LplA can ligate lipoic acid derivatives, which can then be functionalized with coumarin based fluorescent probe (*152, 153*). I have already generated the BirA ligation system for the *Ms* sGC N-terminal constructs, which could be used to ligate fluorescently labeled biotin to generate a fluorescent donor acceptor pair for a FRET assay. Detection of any conformational changes in the coiled-coil domain upon NO binding to the heme should be possible with this approach. Additionally, mutation of the coiled-coil residues at the interface should be performed to investigate the signaling mechanism.

REFERENCES

1. Ignarro, L. J., Cirino, G., Casini, A., and Napoli, C. (1999) Nitric oxide as a signaling molecule in the vascular system: An overview, *J Cardiovasc Pharm 34*, 879-886.

2. Marsh, N., and Marsh, A. (2000) A short history of nitroglycerine and nitric oxide in pharmacology and physiology, *Clin Exp Pharmacol Physiol 27*, 313-319.

3. Abraham, E. (1984) The Legacy of Nobel Alfred - The Story Behind The Nobel Prizes, *The Times Literary Supplement*, 82.

4. Arnold, W. P., Mittal, C. K., Katsuki, S., and Murad, F. (1977) Nitric-Oxide Activates Guanylate Cyclase and Increases Guanosine 3'-5'-Cyclic Monophosphate Levels in Various Tissue Preparations, *Proc Natl Acad Sci USA 74*, 3203-3207.

5. Kimura, H., Mittal, C. K., and Murad, F. (1975) Activation of guanylate cyclase with sodium azide, *Clinical Research 23*, A324-A324.

6. Kimura, H., Mittal, C. K., and Murad, F. (1975) Activation of guanylate cyclase from rat liver and other tissues by sodium azide, *J. Biol. Chem. 250*, 8016-8022.

7. Furchgott, R. F. (1983) Role of endothelium in responses of vascular smooth muscle, *Circ Res 53*, 557-573.

8. Furchgott, R. F., and Zawadzki, J. V. (1980) The obligatory role of endothelial cells in the relaxation of arterial smooth muscle by acetylcholine, *Nature 288*, 373-376.

9. Gruetter, C. A., Barry, B. K., McNamara, D. B., Gruetter, D. Y., Kadowitz, P. J., and Ignarro, L. (1979) Relaxation of bovine coronary artery and activation of

coronary arterial guanylate cyclase by nitric oxide, nitroprusside and a carcinogenic nitrosoamine, *J Cyclic Nucleotide Res 5*, 211-224.

10. Gruetter, C. A., Barry, B. K., Mcnamara, D. B., Kadowitz, P. J., and Ignarro, L. J. (1979) Nitric-Oxide, Cigarette-Smoke and Nitrosoamines Relax Coronary-Artery and Activate Soluble Guanylate Cyclase, *Fed Proc. 38*, 432-432.

11. Bredt, D. S., and Snyder, S. H. (1992) Nitric oxide, A novel neuronal messenger, *Neuron 8*, 3-11.

12. Jaffrey, S. R., and Snyder, S. H. (1995) Nitric oxide: a neural messenger, *Annu Rev Cell Dev Biol 11*, 417-440.

13. MacMicking, J., Xie, Q. W., and Nathan, C. (1997) Nitric oxide and macrophage function, *Annu Rev Immunol 15*, 323-350.

14. Foster, M. W., Hess, D. T., and Stamler, J. S. (2009) Protein S-nitrosylation in health and disease: a current perspective, *Trends Mol Med 15*, 391-404.

15. Stamler, J. S. (1994) Redox signaling: nitrosylation and related target interactions of nitric oxide, *Cell 78*, 931-936.

16. Stamler, J. S., Lamas, S., and Fang, F. C. (2001) Nitrosylation: The prototypic redox-based signaling mechanism, *Cell 106*, 675-683.

17. Collmann, C., Carlsson, M. A., Hansson, B. S., and Nighorn, A. (2004) Odorant-evoked nitric oxide signals in the antennal lobe of Manduca sexta, *J Neurosci 24*, 6070-6077.

18. Trimmer, B. A., Aprille, J. R., Dudzinski, D. M., Lagace, C. J., Lewis, S. M., Michel, T., Qazi, S., and Zayas, R. M. (2001) Nitric oxide and the control of firefly flashing, *Science 292*, 2486-2488.

19. Gusarov, I., Shatalin, K., Starodubtseva, M., and Nudler, E. (2009) Endogenous Nitric Oxide Protects Bacteria Against a Wide Spectrum of Antibiotics, *Science 325*, 1380-1384.

20. Gusarov, I., Gautier, L., Smolentseva, O., Shamovsky, I., Eremina, S., Mironov, A., and Nudler, E. (2013) Bacterial Nitric Oxide Extends the Lifespan of C. elegans, *Cell 152*, 818-830.

21. Ignarro, L. J., (Ed.) (2010) *Nitric Oxide Biology and Pathobiology*, Second ed., Academic Press, San Diego.

22. Marletta, M. A. (1993) Nitric oxide synthase structure and mechanism, *J Biol Chem 268*, 12231-12234.

23. Stuehr, D. J. (1999) Mammalian nitric oxide synthases, *Biochim Biophys Acta 1411*, 217-230.

24. Alderton, W. K., Cooper, C. E., and Knowles, R. G. (2001) Nitric oxide synthases: structure, function and inhibition, *Biochem J 357*, 593-615.

25. Li, H., and Poulos, T. L. (2005) Structure-function studies on nitric oxide synthases, *J. Inorg. Biochem. 99*, 293-305.

26. Fleming, I. (2008) Biology of Nitric Oxide Synthases, *Handbook of Physiology: Microcirculation, 2nd Edition*, 56-80.

27. Lamas, S., Marsden, P. A., Li, G. K., Tempst, P., and Michel, T. (1992) Endothelial nitric oxide synthase: molecular cloning and characterization of a distinct constitutive enzyme isoform, *Proc Natl Acad Sci U S A 89*, 6348-6352.

28. Bredt, D. S., Hwang, P. M., Glatt, C. E., Lowenstein, C., Reed, R. R., and Snyder, S. H. (1991) Cloned and expressed nitric oxide synthase structurally resembles cytochrome P-450 reductase, *Nature 351*, 714-718.

29. Bredt, D. S., Hwang, P. M., and Snyder, S. H. (1990) *Localization of nitric oxide synthase indicating a neural role for nitric oxide*, *Nature 347*, 768-770.

30. Xie, Q. W., Cho, H. J., Calaycay, J., Mumford, R. A., Swiderek, K. M., Lee, T. D., Ding, A., Troso, T., and Nathan, C. (1992) Cloning and characterization of inducible nitric oxide synthase from mouse macrophages, *Science 256*, 225-228.

31. Brookes, P. S. (2004) Mitochondrial nitric oxide synthase, *Mitochondrion 3*, 187-204.

32. Elfering, S. L., Sarkela, T. M., and Giulivi, C. (2002) Biochemistry of mitochondrial nitric-oxide synthase, *J. Biol. Chem. 277*, 38079-38086.

33. Ghafourifar, P., and Cadenas, E. (2005) Mitochondrial nitric oxide synthase, *Trends Pharmacol Sci 26*, 190-195.

34. Lancaster, J. R., Jr. (1994) Simulation of the diffusion and reaction of endogenously produced nitric oxide, *Proc. Natl. Acad. Sci. USA 91*, 8137-8141.

35. Lancaster, J. R. (1997) A tutorial on the diffusibility and reactivity of free nitric oxide, *Nitric Oxide-Biology and Chemistry 1*, 18-30.

36. Subczynski, W. K., Lomnicka, M., and Hyde, J. S. (1996) Permeability of nitric oxide through lipid bilayer membranes, *Free Radical Res 24*, 343-349.

37. Beckman, J. S., and Koppenol, W. H. (1996) Nitric oxide, superoxide, and peroxynitrite: the good, the bad, and ugly, *Am J Physiol 271*, C1424-1437.

38. Hardman, J. G., Robison, G. A., and Sutherland, E. W. (1971) Cyclic nucleotides, *Annu Rev Physiol 33*, 311-336.

39. Rall, T. W., and Sutherland, E. W. (1958) Formation of a cyclic adenine ribonucleotide by tissue particles, *J. Biol. Chem. 232*, 1065-1076.

40. Ashman, D. F., Lipton, R., Melicow, M. M., and Price, T. D. (1963) Isolation of adenosine 3', 5'-monophosphate and guanosine 3', 5'-monophosphate from rat urine, *Biochem Biophys Res Commun 11*, 330-334.

41. Hardman, J. G., Beavo, J. A., Gray, J. P., Chrisman, T. D., Patterson, W. D., and Sutherland, E. W. (1971) The formation and metabolism of cyclic GMP, *Ann N Y Acad Sci 185*, 27-35.

42. Hardman, J. G., and Sutherland, E. W., (1969) *Guanyl Cyclase, an Enzyme Catalyzing Formation of Guanosine 3',5'-Monophosphate from Guanosine Triphosphate, J. Biol. Chem. 244*, 6363-6370.

43. Ishikawa, E., Ishikawa, S., Davis, J. W., and Sutherland, E. W. (1969) Determination of guanosine 3',5'-monophosphate in tissues and of guanyl cyclase in rat intestine, *J. Biol. Chem. 244*, 6371-6376.

44. White, A. A., and Aurbach, G. D. (1969) Detection of guanyl cyclase in mammalian tissues, *Biochim Biophys Acta 191*, 686-697.

45. Chrisman, T. D., Garbers, D. L., Parks, M. A., and Hardman, J. G. (1975) Characterization of particulate and soluble guanylate cyclases from rat lung, *J. Biol. Chem. 250*, 374-381.

46. Garbers, D. L., and Gray, J. P. (1974) Guanylate cyclase from sperm of the sea urchin, Strongylocentrotus purpuratus, *Methods in enzymology 38*, 196-199.

47. Kimura, H., and Murad, F. (1974) Evidence for two different forms of guanylate cyclase in rat heart, *J. Biol. Chem. 249*, 6910-6916.

48. Foerster, J., Harteneck, C., Malkewitz, J., Schultz, G., and Koesling, D. (1996) A functional heme-binding domain of soluble guanylyl cyclase requires intact N-termini of a1 and b1 subunits, *Eur. J. Biochem. 240*, 380-386.

49. Wedel, B., Humbert, P., Harteneck, C., Foerster, J., Malkewitz, J., Böhme, E., Schultz, G., and Koesling, D. (1994) Mutation of His-105 in the b1 subunit yields a nitric oxide-insensitive form of soluble guanylate cyclase, *Proc. Natl. Acad. Sci. USA 91*, 2592-2596.

50. Zhao, Y., Schelvis, J. P. M., Babcock, G. T., and Marletta, M. A. (1998) Identification of histidine 105 in the b1 subunit of soluble guanylate cyclase as the heme proximal ligand, *Biochemistry 37*, 4502-4509.

51. Fan, B., Gupta, G., Danziger, R. S., Friedman, J. M., and Rousseau, D. L. (1998) Resonance Raman characterization of soluble guanylate cyclase expressed from baculovirus, *Biochemistry 37*, 1178-1184.

52. Dierks, E. A., Hu, S., Vogel, K. M., Yu, A. E., Spiro, T. G., and Burstyn, J. N. (1997) Demonstration of the role of scission of the proximal histidine-iron bond in the activation of soluble guanylyl cyclase though metalloporphyrin substitution studies, *J Am Chem Soc 119*, 7316-7323.

53. Yu, A. E., Hu, S. Z., Spiro, T. G., and Burstyn, J. N. (1994) Resonance Raman-Spectroscopy of Soluble Guanylyl Cyclase Reveals Displacement of Distal and Proximal Heme Ligands by No, *J Am Chem Soc 116*, 4117-4118.

54. Stone, J. R., Sands, R. H., Dunham, W. R., and Marletta, M. A. (1995) Electron paramagnetic resonance spectral evidence for the formation of a pentacoordinated

nitrosyl-heme complex on soluble guanylate cyclase, *Biochemic. Biophys. Res. Commun. 207*, 572-577.

55. Deinum, G., Stone, J. R., Babcock, G. T., and Marletta, M. A. (1996) Binding of nitric oxide and carbon monoxide to soluble guanylate cyclase as observed with resonance Raman spectroscopy, *Biochemistry 35*, 1540-1547.

56. Stone, J. R., and Marletta, M. A. (1994) Soluble guanylate cyclase from bovine lung: Activation with nitric oxide and carbon monoxide and spectral characterization of the ferrous and ferric states, *Biochemistry 33*, 5636-5640.

57. Fukao, M., Mason, H. S., Britton, F. C., Kenyon, J. L., Horowitz, B., and Keef, K. D. (1999) Cyclic GMP-dependent protein kinase activates cloned BKCa channels expressed in mammalian cells by direct phosphorylation at serine 1072, *J. Biol. Chem. 274*, 10927-10935.

58. Komalavilas, P., and Lincoln, T. M. (1994) Phosphorylation of the inositol 1,4,5-trisphosphate receptor by cyclic GMP-dependent protein kinase, *J. Biol. Chem. 269*, 8701-8707.

59. Hofmann, F. (2005) The biology of cyclic GMP-dependent protein kinases, *J. Biol. Chem. 280*, 1-4.

60. Beavo, J. A. (1995) Cyclic nucleotide phosphodiesterases: functional implications of multiple isoforms, *Physiol Rev. 75*, 725-748.

61. Rybalkin, S. D., Yan, C., Bornfeldt, K. E., and Beavo, J. A. (2003) Cyclic GMP phosphodiesterases and regulation of smooth muscle function, *Circ. Res. 93*, 280-291.

62. Ludwig, A., Zong, X. G., Jeglitsch, M., Hofmann, F., and Biel, M. (1998) A family of hyperpolarization-activated mammalian cation channels, *Nature 393*, 587-591.

63. Biel, M., Seeliger, M., Pfeifer, A., Kohler, K., Gerstner, A., Ludwig, A., Jaissle, G., Fauser, S., Zrenner, E., and Hofmann, F. (1999) Selective loss of cone function in mice lacking the cyclic nucleotide-gated channel CNG3, *Proc Natl Acad Sci U S A 96*, 7553-7557.

64. Fitzpatrick, D. A., O'Halloran, D. M., and Burnell, A. M. (2006) Multiple lineage specific expansions within the guanylyl cyclase gene family, *BMC Evolutionary Biology 6*, 26.

65. Schaap, P. (2005) Guanylyl cyclases across the tree of life, *Front Biosci 10*, 1485-U1485.

66. Braughler, J. M., Mittal, C. K., and Murad, F. (1979) Purification of soluble guanylate cyclase from rat liver, *Proc Natl Acad Sci U S A 76*, 219-222.

67. Budworth, J., Meillerais, S., Charles, I., and Powell, K. (1999) Tissue distribution of the human soluble guanylate cyclases, *Biochem Biophys Res Commun 263*, 696-701.

68. Koesling, D., Harteneck, C., Humbert, P., Bosserhoff, A., Frank, R., Schultz, G., and Bohme, E. (1990) The Primary Structure of the Larger Subunit of Soluble Guanylyl Cyclase from Bovine Lung - Homology between the 2 Subunits of the Enzyme, *FEBS Lett 266*, 128-132.

69. Koesling, D., Herz, J., Gausepohl, H., Niroomand, F., Hinsch, K. D., Mulsch, A., Bohme, E., Schultz, G., and Frank, R. (1988) The primary structure of the 70 kDa subunit of bovine soluble guanylate cyclase, *FEBS Lett 239*, 29-34.

70. Nakane, M., Arai, K., Saheki, S., Kuno, T., Buechler, W., and Murad, F. (1990) Molecular cloning and expression of cDNAs coding for soluble guanylate cyclase from rat lung, *J. Biol. Chem. 265*, 16841-16845.

71. Nakane, M., Saheki, S., Kuno, T., Ishii, K., and Murad, F. (1988) Molecular cloning of a cDNA coding for 70 kilodalton subunit of soluble guanylate cyclase from rat lung, *Biochem Biophys Res Commun 157*, 1139-1147.

72. Buechler, W. A., Nakane, M., and Murad, F. (1991) Expression of soluble guanylate cyclase activity requires both enzyme subunits, *Biochem Biophys Res Commun 174*, 351-357.

73. Harteneck, C., Wedel, B., Koesling, D., Malkewitz, J., Bohme, E., and Schultz, G. (1991) Molecular cloning and expression of a new alpha-subunit of soluble guanylyl cyclase. Interchangeability of the alpha-subunits of the enzyme, *FEBS Lett 292*, 217-222.

74. Yuen, P. S. T., Potter, L. R., and Garbers, D. L. (1990) A New Form of Guanylyl Cyclase Is Preferentially Expressed in Rat-Kidney, *Biochemistry 29*, 10872-10878.

75. Koglin, M., Vehse, K., Budaeus, L., Scholz, H., and Behrends, S. (2001) Nitric oxide activates the beta 2 subunit of soluble guanylyl cyclase in the absence of a second subunit, *J. Biol. Chem. 276*, 30737-30743.

76. Cary, S. P., Winger, J. A., Derbyshire, E. R., and Marletta, M. A. (2006) Nitric oxide signaling: no longer simply on or off, *Trends Biochem. Sci. 31*, 231-239.

77. Moglich, A., Ayers, R. A., and Moffat, K. (2009) Structure and Signaling Mechanism of Per-ARNT-Sim Domains, *Structure 17*, 1282-1294.

78. Derbyshire, E. R., and Marletta, M. A. (2012) Structure and regulation of soluble guanylate cyclase, *Annu. Rev. Biochem. 81*, 533-559.

79. Iyer, L. M., Anantharaman, V., and Aravind, L. (2003) Ancient conserved domains shared by animal soluble guanylyl cyclases and bacterial signaling proteins, *BMC Genomics 4*.

80. Karow, D. S., Pan, D. H., Tran, R., Pellicena, P., Presley, A., Mathies, R. A., and Marletta, M. A. (2004) Spectroscopic characterization of the soluble guanylate cyclase-like heme domains from Vibrio cholerae and Thermoanaerobacter tengcongensis, *Biochemistry 43*, 10203-10211.

81. Pellicena, P., Karow, D. S., Boon, E. M., Marletta, M. A., and Kuriyan, J. (2004) Crystal structure of an oxygen-binding heme domain related to soluble guanylate cyclases, *Proc. Natl. Acad. Sci. USA 101*, 12854-12859.

82. Nioche, P., Berka, V., Vipond, J., Minton, N., Tsai, A. L., and Raman, C. S. (2004) Femtomolar sensitivity of a NO sensor from Clostridium botulinum, *Science 306*, 1550-1553.

83. Ma, X., Sayed, N., Beuve, A., and van den Akker, F. (2007) NO and CO differentially activate soluble guanylyl cyclase via a heme pivot-bend mechanism, *EMBO J. 26*, 578-588.

84. Boon, E. M., Huang, S. H., and Marletta, M. A. (2005) A molecular basis for NO selectivity in soluble guanylate cyclase, *Nat Chem Biol 1*, 53-59.

85. Boon, E. M., and Marletta, M. A. (2005) Ligand discrimination in soluble guanylate cyclase and the H-NOX family of heme sensor proteins, *Curr Opin Chem Biol 9*, 441-446.

86. Schmidt, P. M., Rothkegel, C., Wunder, F., Schroder, H., and Stasch, J. P. (2005) Residues stabilizing the heme moiety of the nitric oxide sensor soluble guanylate cyclase, *Eur J Pharmacol 513*, 67-74.

87. Rothkegel, C., Schmidt, P. M., Stoll, F., Schroeder, H., Schmidt, H. H. H. W., and Stasch, J.-P. (2006) Identification of residues crucially involved in soluble guanylate cyclase activation, *FEBS Lett 580*, 4205-4213.

88. Fritz, B. G., Roberts, S. A., Ahmed, A., Breci, L., Li, W., Weichsel, A., Brailey, J. L., Wysocki, V. H., Tama, F., and Montfort, W. R. (2013) Molecular Model of a Soluble Guanylyl Cyclase Fragment Determined by Small-Angle X-ray Scattering and Chemical Cross-Linking, *Biochemistry 52*, 1568-1582.

89. Hoffman, E. C., Reyes, H., Chu, F. F., Sander, F., Conley, L. H., Brooks, B. A., and Hankinson, O. (1991) Cloning of a factor required for activity of the Ah (dioxin) receptor, *Science 252*, 954-958.

90. Nambu, J. R., Lewis, J. O., Wharton, K. A., and Crews, S. T. (1991) The Drosophila Single-Minded Gene Encodes a Helix-Loop-Helix Protein That Acts as a Master Regulator of Cns Midline Development, *Cell 67*, 1157-1167.

91. Taylor, B. L., and Zhulin, I. B. (1999) PAS domains: internal sensors of oxygen, redox potential, and light, *Microbiol Mol Biol Rev 63*, 479-506.

92. Nakasako, M., Zikihara, K., Matsuoka, D., Katsura, H., and Tokutomi, S. (2008) Structural basis of the LOV1 dimerization of Arabidopsis phototropins 1 and 2, *J Mol Biol 381*, 718-733.

93. Key, J., Hefti, M., Purcell, E. B., and Moffat, K. (2007) Structure of the redox sensor domain of Azotobacter vinelandii NifL at atomic resolution: Signaling, dimerization, and mechanism, *Biochemistry 46*, 3614-3623.

94. Borgstahl, G. E. O., Williams, D. R., and Getzoff, E. D. (1995) 1.4 Angstrom structure of photoactive yellow protein, a cytosolic photoreceptor - unusual fold, active-site, and chromophore, *Biochemistry 34*, 6278-6287.

95. Scheuermann, T. H., Tomchick, D. R., Machius, M., Guo, Y., Bruick, R. K., and Gardner, K. H. (2009) Artificial ligand binding within the HIF2alpha PAS-B domain of the HIF2 transcription factor, *Proc Natl Acad Sci U S A 106*, 450-455.

96. Amezcua, C. A., Harper, S. M., Rutter, J., and Gardner, K. H. (2002) Structure and interactions of PAS kinase N-terminal PAS domain: Model for intramolecular kinase regulation, *Structure 10*, 1349-1361.

97. Ma, X., Sayed, N., Baskaran, P., Beuve, A., and van den Akker, F. (2008) PAS-mediated dimerization of soluble guanylyl cyclase revealed by signal transduction histidine kinase domain crystal structure, *J. Biol. Chem. 283*, 1167-1178.

98. Rothkegel, C., Schmidt, P. M., Atkins, D. J., Hoffmann, L. S., Schmidt, H., Schroder, H., and Stasch, J. P. (2007) Dimerization region of soluble guanylate cyclase characterized by bimolecular fluorescence complementation in vivo, *Mol Pharmacol 72*, 1181-1190.

99. Zhou, Z., Gross, S., Roussos, C., Meurer, S., Muller-Esterl, W., and Papapetropoulos, A. (2004) Structural and functional characterization of the dimerization region of soluble guanylyl cyclase, *J. Biol. Chem. 279*, 24935-24943.

100. Stasch, J.-P., Becker, E. M., Alonso-Alija, C., Apeler, H., Gerzer, R., Minuth, T., Perzborn, E., Pleiss, U., Schröder, H., Schroeder, W., Stahl, E., Steinke, W., Straub, A., and Schramm, M. (2001) NO-independent regulatory site on soluble guanylate cyclase, *Nature 410*, 212-215.

101. Purohit, R., Weichsel, A., and Montfort, W. R. (2013) Crystal structure of the Alpha subunit PAS domain from soluble guanylyl cyclase, *Protein Science 22*, 1439-1444.

102. Anantharaman, V., Balaji, S., and Aravind, L. (2006) The signaling helix: a common functional theme in diverse signaling proteins, *Biol Direct 1*.

103. Ma, X., Beuve, A., and van den Akker, F. (2010) Crystal structure of the signaling helix coiled-coil domain of the beta1 subunit of the soluble guanylyl cyclase, *BMC Struct. Biol. 10*, 2.

104. Brooks, A. J., Dai, W., O'Mara, M. L., Abankwa, D., Chhabra, Y., Pelekanos, R. A., Gardon, O., Tunny, K. A., Blucher, K. M., Morton, C. J., Parker, M. W., Sierecki, E., Gambin, Y., Gomez, G. A., Alexandrov, K., Wilson, I. A., Doxastakis, M., Mark, A. E., and Waters, M. J. (2014) Mechanism of Activation of Protein Kinase JAK2 by the Growth Hormone Receptor, *Science 344*, 710-+.

105. Tao, W., Malone, C. L., Ault, A. D., Deschenes, R. J., and Fassler, J. S. (2002) A cytoplasmic coiled-coil domain is required for histidine kinase activity of the yeast osmosensor, SLN1, *Mol Microbiol 43*, 459-473.

106. Liu, Y., Ruoho, A. E., Rao, V. D., and Hurley, J. H. (1997) Catalytic mechanism of the adenylyl and guanylyl cyclases: Modeling and mutational analysis, *Proc. Natl. Acad. Sci. USA 94*, 13414-13419.

107. Winger, J. A., and Marletta, M. A. (2005) Expression and characterization of the catalytic domains of soluble guanylate cyclase: interaction with the heme domain, *Biochemistry 44*, 4083-4090.

108. Allerston, C. K., von Delft, F., and Gileadi, O. (2013) Crystal Structures of the Catalytic Domain of Human Soluble Guanylate Cyclase, *Plos One 8*.

109. Winger, J. A., Derbyshire, E. R., Lamers, M. H., Marletta, M. A., and Kuriyan, J. (2008) The crystal structure of the catalytic domain of a eukaryotic guanylate cyclase, *BMC Struct. Biol. 8*.

110. Hurley, J. H. (1998) The adenylyl and guanylyl cyclase superfamily, *Curr Opin Struct Biol 8*, 770-777.

111. Tesmer, J. J. G., Sunahara, R. K., Gilman, A. G., and Sprang, S. R. (1997) Crystal structure of the catalytic domains of adenylyl cyclase in a complex with G(s alpha).GTP gamma S, *Science 278*, 1907-1916.

112. Hurley, J. H. (1999) Structure, mechanism, and regulation of mammalian adenylyl cyclase, *J. Biol. Chem. 274*, 7599-7602.

113. Tesmer, J. J. G., Sunahara, R. K., Johnson, R. A., Gosselin, G., Gilman, A. G., and Sprang, S. R. (1999) Two-metal-ion catalysis in adenylyl cylase, *Science 285*, 756-760.

114. Senter, P. D., Eckstein, F., Mulsch, A., and Bohme, E. (1983) The stereochemical course of the reaction catalyzed by soluble bovine lung guanylate cyclase, *J. Biol. Chem. 258*, 6741-6745.

115. Ohlstein, E. H., Wood, K. S., and Ignarro, L. J. (1982) Purification and properties of heme-deficient hepatic soluble guanylate cyclase: Effects of heme and other cofactors on enzyme activation by NO, NO-heme, and protoporphyrin IX, *Arch. Biochem. Biophys. 218*, 187-198.

116. Busker, M., Neidhardt, I., and Behrends, S. (2014) Nitric oxide activation of guanylate cyclase pushes the alpha1 signaling helix and the beta1 heme-binding domain closer to the substrate-binding site, *J. Biol. Chem. 289*, 476-484.

117. Underbakke, E. S., Iavarone, A. T., and Marletta, M. A. (2013) Higher-order interactions bridge the nitric oxide receptor and catalytic domains of soluble guanylate cyclase, *Proc Natl Acad Sci U S A 110*, 6777-6782.

118. Seeger, F., Quintyn, R., Tanimoto, A., Williams, G. J., Tainer, J. A., Wysocki, V. H., and Garcin, E. D. (2014) Interfacial Residues Promote an Optimal Alignment of the Catalytic Center in Human Soluble Guanylate Cyclase: Heterodimerization Is Required but Not Sufficient for Activity, *Biochemistry 53*, 2153-2165.

119. Chang, F. J., Lemme, S., Sun, Q., Sunahara, R. K., and Beuve, A. (2005) Nitric oxide-dependent allosteric inhibitory role of a second nucleotide binding site in soluble guanylyl cyclase, *J. Biol. Chem. 280*, 11513-11519.

120. Gori, T., and Parker, J. D. (2002) Nitrate tolerance - A unifying hypothesis, *Circulation 106*, 2510-2513.

121. Sage, P. R., de la Lande, I. S., Stafford, I., Bennett, C. L., Phillipov, G., Stubberfield, J., and Horowitz, J. D. (2000) Nitroglycerin tolerance in human vessels - Evidence for impaired nitroglycerin bioconversion, *Circulation 102*, 2810-2815.

122. Ko, F. N., Wu, C. C., Kuo, S. C., Lee, F. Y., and Teng, C. M. (1994) YC-1, a novel activator of platelet guanylate-cyclase, *Blood 84*, 4226-4233.

123. Evgenov, O. V., Pacher, P., Schmidt, P. M., Hasko, G., Schmidt, H. H., and Stasch, J. P. (2006) NO-independent stimulators and activators of soluble guanylate cyclase: discovery and therapeutic potential, *Nature reviews. Drug discovery 5*, 755-768.

124. Friebe, A., and Koesling, D. (1998) Mechanism of YC-1-induced activation of soluble guanylyl cyclase, *Mol Pharmacol 53*, 123-127.

125. Wu, C. C., Ko, F. N., Kuo, S. C., Lee, F. Y., and Teng, C. M. (1995) Yc-1 Inhibited Human Platelet-Aggregation through No-Independent Activation of Soluble Guanylate-Cyclase, *Brit J Pharmacol 116*, 1973-1978.

126. Friebe, A., Schultz, G., and Koesling, D. (1996) Sensitizing soluble guanylyl cyclase to become a highly CO-sensitive enzyme, *EMBO Journal 15*, 6863-6868.

127. Stone, J. R., and Marletta, M. A. (1998) Synergistic activation of soluble guanylate cyclase by YC-1 and carbon monoxide: Implications for the role of cleavage of the iron-histidine bond during activation by nitric oxide, *Chem. Biol. 5*, 255-261.

128. Mittendorf, J., Weigand, S., Alonso-Alija, C., Bischoff, E., Feurer, A., Gerisch, M., Kern, A., Knorr, A., Lang, D., Muenter, K., Radtke, M., Schirok, H., Schlemmer, K. H., Stahl, E., Straub, A., Wunder, F., and Stasch, J. P. (2009) Discovery of riociguat (BAY 63-2521): a potent, oral stimulator of soluble guanylate cyclase for the treatment of pulmonary hypertension, *ChemMedChem 4*, 853-865.

129. Fritz, B. G., Hu, X., Brailey, J. L., Berry, R. E., Walker, F. A., and Montfort, W. R. (2011) Oxidation and loss of heme in soluble guanylyl cyclase from Manduca sexta, *Biochemistry 50*, 5813-5815.

130. Meurer, S., Pioch, S., Pabst, T., Opitz, N., Schmidt, P. M., Beckhaus, T., Wagner, K., Matt, S., Gegenbauer, K., Geschka, S., Karas, M., Stasch, J. P., Schmidt, H. H., and Muller-Esterl, W. (2009) Nitric oxide-independent vasodilator rescues heme-oxidized soluble guanylate cyclase from proteasomal degradation, *Circ. Res. 105*, 33-41.

131. Martin, F., Baskaran, P., Ma, X., Dunten, P. W., Schaefer, M., Stasch, J. P., Beuve, A., and van den Akker, F. (2010) Structure of cinaciguat (BAY 58-2667)

bound to Nostoc H-NOX domain reveals insights into heme-mimetic activation of the soluble guanylyl cyclase, *J. Biol. Chem. 285*, 22651-22657.

132. Denninger, J. W., and Marletta, M. A. (1999) Guanylate cyclase and the •NO/cGMP signaling pathway, *Biochim. Biophys. Acta 1411*, 334-350.

133. Hering, K. W., Artz, J. D., Pearson, W. H., and Marletta, M. A. (2006) The design and synthesis of YC-1 analogues as probes for soluble guanylate cyclase, *Bioorg. Med. Chem. Lett. 16*, 618-621.

134. Cary, S. P., Winger, J. A., and Marletta, M. A. (2005) Tonic and acute nitric oxide signaling through soluble guanylate cyclase is mediated by nonheme nitric oxide, ATP, and GTP, *Proc. Natl. Acad. Sci. USA 102*, 13064-13069.

135. Zhao, Y., Brandish, P. E., Ballou, D. P., and Marletta, M. A. (1999) A molecular basis for nitric oxide sensing by soluble guanylate cyclase, *Proc. Natl. Acad. Sci. USA 96*, 14753-14758.

136. Martin, E., Berka, V., Sharina, I., and Tsai, A. L. (2012) Mechanism of binding of NO to soluble guanylyl cyclase: implication for the second NO binding to the heme proximal site, *Biochemistry 51*, 2737-2746.

137. Tsai, A. L., Berka, V., Sharina, I., and Martin, E. (2011) Dynamic ligand exchange in soluble guanylyl cyclase (sGC): implications for sGC regulation and desensitization, *J. Biol. Chem. 286*, 43182-43192.

138. Campbell, M. G., Underbakke, E. S., Potter, C. S., Carragher, B., and Marletta, M. A. (2014) Single-particle EM reveals the higher-order domain architecture of soluble guanylate cyclase, *Proc Natl Acad Sci U S A 111*, 2960-2965.

139. Underbakke, E. S., Iavarone, A. T., Chalmers, M. J., Pascal, B. D., Novick, S., Griffin, P. R., and Marletta, M. A. (2014) Nitric Oxide-Induced Conformational Changes in Soluble Guanylate Cyclase, *Structure 22*, 602-611.

140. Derbyshire, E. R., Fernhoff, N. B., Deng, S., and Marletta, M. A. (2009) Nucleotide Regulation of Soluble Guanylate Cyclase Substrate Specificity, *Biochemistry 48*, 7519-7524.

141. Lamothe, M., Chang, F. J., Balashova, N., Shirokov, R., and Beuve, A. (2004) Functional characterization of nitric oxide and YC-1 activation of soluble guanylyl cyclase: Structural implication for the YC-1 binding site?, *Biochemistry 43*, 3039-3048.

142. Yazawa, S., Tsuchiya, H., Hori, H., and Makino, R. (2006) Functional characterization of two nucleotide-binding sites in soluble guanylate cyclase, *J. Biol. Chem. 281*, 21763-21770.

143. Hu, X., Murata, L. B., Weichsel, A., Brailey, J. L., Roberts, S. A., Nighorn, A., and Montfort, W. R. (2008) Allostery in recombinant soluble guanylyl cyclase from Manduca sexta, *J. Biol. Chem. 283*, 20968-20977.

144. Ibrahim, M., Derbyshire, E. R., Marletta, M. A., and Spiro, T. G. (2010) Probing soluble guanylate cyclase activation by CO and YC-1 using resonance Raman spectroscopy, *Biochemistry 49*, 3815-3823.

145. Ibrahim, M., Derbyshire, E. R., Soldatova, A. V., Marletta, M. A., and Spiro, T. G. (2010) Soluble guanylate cyclase is activated differently by excess NO and by YC-1: resonance Raman spectroscopic evidence, *Biochemistry 49*, 4864-4871.

146. Martin, E., Czarnecki, K., Jayaraman, V., Murad, F., and Kincaid, J. (2005) Resonance Raman and infrared spectroscopic studies of high-output forms of human soluble guanylyl cyclase, *J Am Chem Soc 127*, 4625-4631.

147. Yoo, B. K., Lamarre, I., Rappaport, F., Nioche, P., Raman, C. S., Martin, J. L., and Negrerie, M. (2012) Picosecond to Second Dynamics Reveals a Structural Transition in Clostridium botulinum NO-Sensor Triggered by the Activator BAY-41-2272, *ACS Chem. Biol. 7, 2046-2054.*

148. Purohit, R., Fritz, B. G., The, J., Issaian, A., Weichsel, A., David, C. L., Campbell, E., Hausrath, A. C., Rassouli-Taylor, L., Garcin, E. D., Gage, M. J., and Montfort, W. R. (2014) YC-1 Binding to the beta Subunit of Soluble Guanylyl Cyclase Overcomes Allosteric Inhibition by the alpha Subunit, *Biochemistry 53*, 101-114.

149. Hu, X., Murata, L. B., Weichsel, A., Brailey, J. L., Roberts, S. A., Nighorn, A., and Montfort, W. R. (2008) Allostery in recombinant soluble guanylyl cyclase from Manduca sexta, *J. Biol. Chem. 283*, 20968-20977.

150. Kim, Y., Quartey, P., Li, H., Volkart, L., Hatzos, C., Chang, C., Nocek, B., Cuff, M., Osipiuk, J., Tan, K., Fan, Y., Bigelow, L., Maltseva, N., Wu, R., Borovilos, M., Duggan, E., Zhou, M., Binkowski, T. A., Zhang, R.-G., and Joachimiak, A. (2008) Large-scale evaluation of protein reductive methylation for improving protein crystallization, *Nature Methods 5*, 853-854.

151. Sandtner, W., Bezanilla, F., and Correa, A. M. (2007) In vivo measurement of intramolecular distances using genetically encoded reporters, *Biophys J 93*, L45-L47.

152. Fernandez-Suarez, M., Baruah, H., Martinez-Hernandez, L., Xie, K. T., Baskin, J. M., Bertozzi, C. R., and Ting, A. Y. (2007) Redirecting lipoic acid ligase for cell

surface protein labeling with small-molecule probes, *Nature Biotech. 25*, 1483-1487.

153. Uttamapinant, C., White, K. A., Baruah, H., Thompson, S., Fernandez-Suarez, M., Puthenveetil, S., and Ting, A. Y. (2010) A fluorophore ligase for site-specific protein labeling inside living cells, *Proc Natl Acad Sci U S A 107*, 10914-10919.

APPENDIX A

CRYSTAL STRUCTURE OF THE ALPHA SUBUNIT PAS DOMAIN FROM SOLUBLE GUANYLYL CYCLASE

JOHN WILEY AND SONS LICENSE TERMS AND CONDITIONS

Apr 03, 2014

This is a License Agreement between Rahul Purohit ("You") and John Wiley and Sons ("John Wiley and Sons") provided by Copyright Clearance Center ("CCC"). The license consists of your order details, the terms and conditions provided by John Wiley and Sons, and the payment terms and conditions.

License Number	3361201211379
License date	Apr 03, 2014
Licensed content publisher	John Wiley and Sons
Licensed content publication	Protein Science
Licensed content title	Crystal structure of the Alpha subunit PAS domain from soluble guanylyl cyclase
Licensed copyright line	© 2013 The Protein Society
Licensed content author	Rahul Purohit, Andrzej Weichsel, William R. Montfort
Licensed content date	Sep 6, 2013
Start page	1439
End page	1444
Type of use	Dissertation/Thesis
Requestor type	Author of this Wiley article
Format	Print and electronic
Portion	Full article
Will you be translating?	No
Title of your thesis / dissertation	THE MECHANISM OF ALLOSTERIC REGULATION IN SOLUBLE GUANYLATE CYCLASE
Expected completion date	Aug 2014
Expected size (number of pages)	180
Total	0.00 USD

Terms and Conditions

Terms and Conditions are not available at this time.

Contributions: Cloning, protein purification, crystallization experiments were solely performed by me. Dr. Andrzej Weichsel assisted in the X-ray diffraction data collection, processing and refinement of the crystal structure. Dr. William R. Montfort provided guidance for the project and edited the manuscript.

THE PROTEIN SOCIETY

PROTEIN STRUCTURE REPORT

Crystal structure of the Alpha subunit PAS domain from soluble guanylyl cyclase

Rahul Purohit, Andrzej Weichsel, and William R. Montfort*

Department of Chemistry and Biochemistry, University of Arizona, Tucson, Arizona 85721

Received 7 June 2013; Revised 31 March 2013; Accepted 5 August 2013
DOI: 10.1002/pro.2331
Published online 12 August 2013 proteinscience.org

Abstract: Soluble guanylate cyclase (sGC) is a heterodimeric heme protein of ~150 kDa and the primary nitric oxide receptor. Binding of NO stimulates cyclase activity, leading to regulation of cardiovascular physiology and providing attractive opportunities for drug discovery. How sGC is stimulated and where candidate drugs bind remains unknown. The α and β sGC chains are each composed of Heme-Nitric Oxide Oxygen (H-NOX), Per-ARNT-Sim (PAS), coiled-coil and cyclase domains. Here, we present the crystal structure of the α_1 PAS domain to 1.8 Å resolution. The structure reveals the binding surfaces of importance to heterodimer function, particularly with respect to regulating NO binding to heme in the β_1 H-NOX domain. It also reveals a small internal cavity that may serve to bind ligands or participate in signal transduction.

Keywords: nitric oxide; soluble guanylate cyclase; per-ARNT-sim domain; YC-1; X-ray crystallography; *Manduca sexta*

Introduction

Nitric oxide (NO) is produced in most mammalian cells and serves to regulate blood pressure, wound healing, memory formation, and numerous other physiological processes.[1] The NO receptor is soluble guanylyl/guanylate cyclase (sGC), a large heterodimeric heme protein that is increasingly targeted for drug discovery in the treatment of cardiovascular disease.[2] Two classes of compounds targeting sGC are now in clinical trial, one that stimulates the heme-containing protein (BAY 63-2521/riociguat),[3,4] and another that functions to replace heme after loss due to oxidation (BAY 58-2667/cinaciguat and HMR1766/ataciguat).[5,6] How NO or drug binding leads to cyclase stimulation and signal transduction in sGC is poorly understood.

sGC is composed of two homologous subunits, α and β. Multiple isoforms of each subunit have been identified; however, the most common isoform is the α_1/β_1 heterodimer.[7] Each sGC subunit consists of four domains, an N-terminal Heme-Nitric Oxide Oxygen (H-NOX) domain[8] (also called a SONO domain),[9] a central Per-ARNT-Sim (PAS) domain,[10] a coiled-coil domain and a C-terminal catalytic cyclase domain.[11] NO binding to the heme in the

Abbreviations: H-NOX domain, heme-nitric oxide/oxygen binding domain; PAS domain, Per-ARNT-Sim domain; SAXS, small angle X-ray scattering; sGC, soluble guanylyl cyclase; *Ms* sGC, *Manduca sexta* sGC; *Ms* sGC-NT, *Manduca sexta* sGC lacking the catalytic domains.

Grant sponsor: National Institutes of Health; Grant numbers: HL062969 and U54 CA143924 (to WRM) and S10 RR025485-01A1 (to AW). Grant sponsor: American Heart Association; Grant number: 11PRE7610113 (to RP).

*Correspondence to: William R. Montfort, Department of Chemistry and Biochemistry, The University of Arizona, 1041 E. Lowell St., Tucson, AZ 85721. E-mail: montfort@email.arizona.edu

β_1-subunit leads to the formation of a pentacoordinated Fe–NO complex, stimulation of cyclase activity and production cGMP from GTP. Structural insight into the allostery underlying stimulation is lacking. Structures of individual sGC domains such as the β_1 coiled-coil homodimer[12] and the α_1/β_1 heterodimeric cyclase domain[13] have recently been determined, as have bacterial homologues of the H-NOX and PAS domains.[9,14–16] Yet an understanding of how these domains are arranged in the functional NO sensor remains unknown.

To fill this gap, we have developed sGC from *Manduca sexta* (tobacco hornworm) for biophysical and biochemical characterization.[17–20] *Manduca sexta* sGC (*Ms* sGC) is highly homologous to its mammalian counterparts and responds well to YC-1, the parent compound for riociguat. Using homology modeling, small angle X-ray scattering (SAXS) and chemical cross-linking, we previously determined that *Ms* sGC lacking the cyclase domains (*Ms* sGC-NT) is an elongated molecule with a central parallel coiled-coil.[20] In this model, the α_1 subunit PAS domain directly contacts the heme-containing β_1 subunit H-NOX domain[20] and inhibits NO and CO binding.[1] Here, we present the 1.8 Å crystal structure of the *Ms* sGC α_1 PAS domain, which reveals the H-NOX binding surface and a small internal cavity.

Table I. *Crystallographic Data*

Data measurement	
PDB entry	4GJ4
Wavelength (Å)	0.97950
Space group	H32
Unit cell parameters	$a = b = 95.42$ Å, $c = 317.69$ Å, $\alpha = \beta = 90°$, $\gamma = 120°$
Resolution (Å)[a]	23.7–1.8 (1.86–1.80)
Total reflections	455433 (43841)
Unique reflections	52047 (5122)
Completeness (%)	100.0 (100.0)
Mean I/σ_I	11.3 (1.9)
Redundancy	8.75 (8.56)
R_{merge} (%)	5.5 (69.1)
Refinement	
R_{work} (%)	19.6 (39.8)
R_{free} (%)[b]	24.2 (42.1)
RMS deviation	
Bond lengths (Å)	0.012
Bond angles (°)	1.55
No. of solvent molecules	176
Ramachandran plot	
Most favored (%)	89.9
Allowed (%)	10.1

[a] Overall (outermost shell).
[b] Five percent of data not used in refinement.

Results

Crystal structure of the α_1 PAS domain

Ms sGC α_1 PAS protein was obtained from an *Escherichia coli* expression vector as a SUMO-tagged fusion protein. SUMO cleavage and purification yielded 2–3 mg of highly pure α_1 PAS protein per liter of cell culture. Crystals of the wild-type α_1 PAS domain (residues 279–404) were initially small and could not be improved, possibly due to a requirement for cysteine modification by the arsenic in the cacodylate-containing crystallization buffer.[21–23] To overcome this, we made the triple cysteine mutant C285A, C352A, C374A. This protein crystallized under new conditions, yielding larger crystals with a rhombic dodecahedron morphology and diffraction to 1.8 Å resolution (Table I). Structure solution was by molecular replacement, using the *Nostoc punctiforme* signal transduction histidine kinase (*Np* STHK) PAS domain structure (PDB entry 2P04).[15] Four nearly-identical copies of the α_1 PAS domain were present in the asymmetric unit and were generally well ordered except for the loop between beta strands 4 and 5 (residues 357–361; also called Gβ and Hβ, Fig. 1) and the C-termini. All four C-termini were disordered and not included in the final refined models. In the final model, chains A and C included residues 279–391, chain B included residues 279–390 and chain D included residues 279–395.

The *Ms* sGC α_1 PAS domain contains a typical PAS fold but one that is modified near the site where ligands often bind in PAS-containing proteins (Fig. 1).[10] The core PAS fold consists of a five-stranded antiparallel beta-sheet with strands arranged in the sequence with order 2-1-5-4-3.[10] The segment connecting strand 1 (also called Bβ, Fig. 1) to strand 5 (Gβ) is quite variable both in length and structure among PAS proteins and often provides a ligand-binding surface. Ligands commonly bind in a pocket formed between the beta 1–5 connecting strand and the interior face of the curved beta sheet. An N-terminal flanking helix is generally also present in PAS-containing proteins.

In α_1 PAS, the beta 1–5 connecting strand displays a unique structure as compared with other PAS domains. In most PAS proteins, this segment includes four helices, generally referred to as Cα, Dα, Eα, and Fα. All four helices are present in *Ms* sGC α_1 PAS; however, the residues that form the first half of Fα in a typical PAS domain are seen to form a new beta strand in α_1 PAS (referred to as Fβ in Fig. 1), yielding an overall 6-stranded beta sheet

[1]Rahul Purohit, Bradley Fritz, Juliana The, Aaron Issaian, Andrzej Weichsel, Cynthia David, Eric Campbell, Andrew C. Hausrath, Leida Rassouli-Taylor, Elsa D. Garcin, Matthew J. Gage, and William R. Montfort, *YC-1 Binding to the Beta Subunit of Soluble Guanylyl Cyclase Overcomes Allosteric Inhibition by the Alpha Subunit, in revision.*

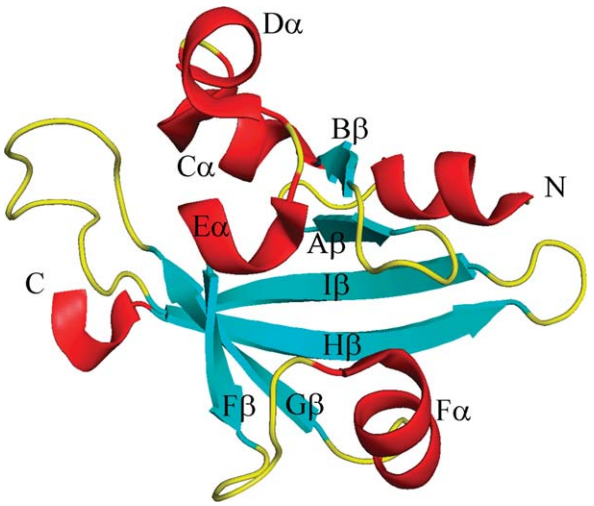

Figure 1. Ribbon diagram of *Ms* sGC α_1 PAS highlighting secondary structure elements. Helix Fα, which splits into a β strand and α helix as compared with canonical PAS domains, is shown as Fβ and Fα.

with topology 2-1-6-5-4-3. The remaining portion of Fα is in a different orientation than typically observed in PAS domains and makes a critical contact with the β_1 H-NOX domain, based on cross-linking studies.[20] The helix includes residues Glu 340 and Lys 343, each of which can be cross-linked to β_1 H-NOX residue Lys 170,[20] indicating that the α_1 PAS and β_1 H-NOX domains are in direct contact in sGC.

Of additional interest is an internal cavity found directly behind the Fα helix in the α_1 PAS structure (Fig. 2). This cavity is in a similar position to the ligand-binding site in other PAS domains, overlapping, for example, with the positions for heme in FixL[24,25] and flavin in the FMN containing LOV domains.[26,27] The cavity size is ~36 Å,^{3} about two-thirds the size of a benzene ring. While it is tempting to suggest this cavity represents a ligand or protein binding site, a substantial rearrangement in the Fα helix would be required to accommodate anything larger than 3–4 atoms. Nonetheless, large rearrangements are known to occur in other PAS domains leading to ligand binding (see, for example, references[28,29]) and the cavity found in *Ms* sGC α_1 PAS may yet have a ligand-binding function. YC-1 appears, however, not to bind to α_1 PAS, but rather to bind to the β_1 H-NOX domain (see footnote *).

The four copies of α_1 PAS in the asymmetric unit are quite similar, displaying similar internal cavity volumes and pairwise RMS deviations in Cα positions of 0.4–0.6 Å. Superpositioning of *Ms* sGC α_1 PAS with *Np* STHK, which was used for molecular replacement, leads to an RMSD of 1.4 Å for 93 core residues (29% identity) when aligned using secondary structure matching (SSM).[30] Superimposing *Ms* sGC α_1 PAS with heme-containing FixL (PDB entry 1EW0)[25] and FAD-containing PAS1 of NIFL (PDB entry 2GJ3)[26] reveal RMSD values of 2.7 Å for 87 core residues (10% identity) and 2.7 Å for 86 core residues (11% identity), respectively. The key difference between the FixL and NIFL PAS1 structures is the position of the Fα helix.

Discussion

The α_1 PAS crystal structure provides constraints for understanding domain arrangement in sGC. The overall fold is typical for PAS domains but displays a unique arrangement for the most variable region in the family, the segment connecting beta sheet strands 1 and 5. In this segment, the Fα helix is split into a sixth beta strand and a shorter helix with a new orientation with respect to most other PAS domains, but similar to that of *Np* STHK.[15]

In *Ms* sGC-NT, a parallel coiled-coil provides a platform on which the other domains assemble.

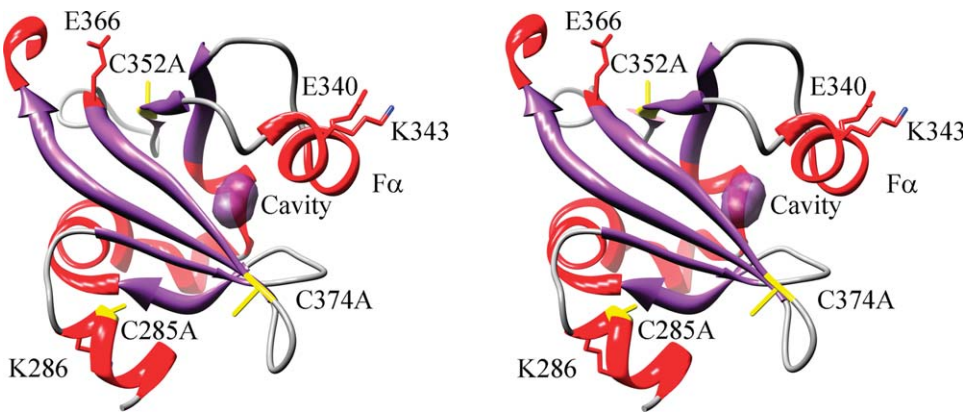

Figure 2. Ribbon drawing of *Ms* sGC α_1 emphasizing the small internal pocket and inter-domain contact residues (cross-eyed stereo view). The small internal pocket found in the structure is highlighted in purple and the C285A, C352A, C374A mutations are shown in yellow. Also shown are residues Glu 340 and Lys 343, which can be cross-linked to the β_1 H-NOX domain; residue Lys 286, which can be cross-linked to the β_1 PAS domain; and residue Glu 366, which can be cross-linked to the β_1 coiled-coil.

Direct cross-links between the α_1 PAS Fα helix and the β_1 H-NOX domain near the heme pocket suggest the two domains are in direct contact, providing a means for allosteric regulation of the protein. Both domains also cross-link with the coiled-coil domain. Our working hypothesis is that YC-1 binding disrupts the α_1 PAS/β_1 H-NOX interaction, leading to a closed H-NOX domain and tighter CO and NO binding.

PAS domains often form homo- or hetero-oligomers as part of their function[10] and the possibility that sGC forms an α_1/β_1 PAS dimer has been previously proposed. The most compelling data are based on the oligomer formed by *Np* STHK, which shares sequence homology with the sGC PAS domains.[15] *Np* STHK forms a homodimer involving a hydrophobic patch near the N-terminus and a strand swap that allows Leu 8 from one chain to cover the hydrophobic patch of the other chain in the dimer. Several hydrogen bonds help stabilize the dimer while removal of the first seven residues in the protein abolishes the dimer. Intriguingly, the rat β_1 PAS domain also dimerizes. In contrast, our construct for *Ms* α_1 PAS runs as a monomer over a sizing column and appears to be monomeric in solution. The protein crystallizes as a rhombic dodecahedron, but this arrangement is likely an artifact of crystallization and of no physiological significance. The N-terminal hydrophobic patch at the heart of the *Np* STHK dimer interface is also found in *Ms* α_1 PAS; however, it does not lead to a dimer interface. Our structure is six residues shorter at the N-terminus than that for the rat β_1 PAS construct and, conceivably, this could alter dimer formation much as it did in *Np* STHK. Nonetheless, our cross-linking data for *Ms* sGC-NT include a link between α_1 Lys 286 and β_1 Glu 196, located at the N-termini of the two PAS domains, indicating the two PAS domains are in contact in the intact heterodimer.[20]

The *Ms* sGC α_1 PAS structure also displays a small internal cavity behind the Fα helix (Fig. 2). Our binding data indicate YC-1 does not bind to this domain but do not rule out another role for this pocket in ligand binding. For ligand binding to occur, the beta 1–5 connecting segment, which includes the Fα helix, would need to rearrange, allowing the pocket to open up. There is precedent for such rearrangements in PAS domain proteins. For example, human PAS kinase has a dynamic Fα helix in the PAS A domain that allows for small molecule entry into the hydrophobic protein core, near to where the internal cavity lies in sGC α_1 PAS.[28] Importantly, the ligand-binding pocket is collapsed in the apo protein and only forms upon ligand binding. A second example is that of histidine kinase CitA, which uses a PAS domain for sensing citrate.[29] In CitA, the beta 1–5 connecting segment is poorly ordered in the absence of citrate binding, but becomes well ordered in the complex with citrate bound in the protein interior. The loop connecting beta strands 4 and 5 also rearranges upon citrate binding, shifting inward. In *Ms* sGC α_1 PAS, the beta 4–5 loop is poorly ordered and could serve a similar role in ligand binding or in signal transduction.

Materials and Methods

Ms sGC α_1 PAS expression and purification

All chemicals were obtained from Sigma-Aldrich, restriction enzymes from New England Biolabs, and purification columns from GE Healthcare unless otherwise indicated. *Ms* sGC α_1 PAS with a N-terminal His-tagged SUMO fusion was cloned into the pETH-SUL vector,[31] expressed in *E. coli* strain BL21 (DE3) pLysS, and purified after cleavage of the SUMO tag with SUMO hydrolase, as described elsewhere (see footnote *). The final material was concentrated to 10–15 mg/mL using a Vivaspin concentrator (Sartorius Stedim Biotech) and stored at –80°C. A final yield 2–3 mg of highly pure protein was obtained per liter of cell culture.

Crystallization

Initial crystallization conditions for *Ms* sGC α_1 PAS were found using a PHOENIX protein crystallization robot (Art Robbins Instruments) and commercially available screens (Hampton Research and Qiagen). Crystals formed in a 96-well Intelli-Plate using sitting drop vapor diffusion at 4°C and precipitants of 1.4–1.6 *M* ammonium sulfate, 50 m*M* sodium cacodylate (pH 5.5–6.5) and 15 m*M* magnesium acetate tetrahydrate. Protein at 10–15 mg/mL was mixed with precipitant at ratios of 1:1 and 1:2. Cubic crystals appeared within 24–48 h after plate setup but failed to grow beyond 100 μm in size. Diffraction quality hexagonal crystals for *Ms* sGC P35α (cysteine triple mutant) were obtained by hanging drop vapor diffusion at 4°C using a precipitant solution of 1.5 *M* lithium sulfate, 0.1 *M* Hepes (pH 7.5). Small crystals were also observed from 4.3 *M* NaCl, 0.1 *M* Hepes (pH 7.5) and from 25% PEG 3350, 0.2 *M* NaCl, 0.1 *M* Hepes (pH 7.5). Total of 90% saturated lithium sulfate was used as the cryoprotectant and crystals were flash frozen in liquid nitrogen.

Data collection, structure solution, and refinement

X-ray diffraction data for *Ms* sGC α_1 PAS (wild type) cubic crystals were measured remotely on SSRL beamline 9–2 (Stanford) using a MAR325 detector at T = 100 K and λ = 0.97950 Å. The data were processed in space group $P2_13$ to 3.7 Å resolution using CrystalClear.[32] The unit cell parameters were $a = b = c$ = 143.26 Å, and $\alpha = \beta = \gamma = 90°$.

Diffraction data for hexagonal crystals of *Ms* sGC α_1 PAS (triple mutant) were also measured remotely on SSRL beamline 7-1 (Stanford) using a MAR325 detector at T = 100 K, λ = 0.97950 Å and were processed to 1.8 Å with CrystalClear in hexagonal space group H32 (Table I). There were four molecules in the asymmetric unit. The structure was determined using molecular replacement as implemented in MrBUMP[33,34] and search models generated from the structure of the *Nostoc punctiforme* signal transduction histidine kinase HNOXA domain (PDB entries 2P04 and 2P08),[15] which yielded an ensemble model. Model building and refinement were performed using programs COOT and REFMAC5.[35,36] Figures were prepared using PyMOL (W. L. DeLano, http://www.pymol.org) and UCSF Chimera.[37] Model quality was evaluated with PROCHECK.[38] Cavity volume was computed using CASTp.[39]

Atomic Coordinates

The atomic coordinates and structure factors have been deposited with the Protein Data Bank (PDB entry 4GJ4).

Acknowledgments

Portions of this research were carried out at the Stanford Synchrotron Radiation Lightsource, a national user facility operated by Stanford University on behalf of the USA Department of Energy, Office of Basic Energy Sciences. The SSRL Structural Molecular Biology Program is supported by the Department of Energy, Office of Biological and Environmental Research, and by the National Institutes of Health, National Center for Research Resources, Biomedical Technology Program, and the National Institute of General Medical Sciences. Molecular graphics and analyses were performed with the UCSF Chimera package. Chimera is developed by the Resource for Biocomputing, Visualization, and Informatics at the University of California, San Francisco (supported by NIGMS P41-GM103311).

References

1. Ignarro LJ, editor (2010) Nitric Oxide Biology and Pathobiology. Second ed. San Diego: Academic Press.
2. Evgenov OV, Pacher P, Schmidt PM, Hasko G, Schmidt HH, Stasch JP (2006) NO-independent stimulators and activators of soluble guanylate cyclase: discovery and therapeutic potential. Nat Rev Drug Discov 5:755–768.
3. Belik J (2009) Riociguat, an oral soluble guanylate cyclase stimulator for the treatment of pulmonary hypertension. Curr Opin Investig Drugs 10:971–979.
4. Mittendorf J, Weigand S, Alonso-Alija C, Bischoff E, Feurer A, Gerisch M, Kern A, Knorr A, Lang D, Muenter K, Radtke M and others (2009) Discovery of riociguat (BAY 63-2521): a potent, oral stimulator of soluble guanylate cyclase for the treatment of pulmonary hypertension. ChemMedChem 4:853–865.
5. Schmidt PM, Schramm M, Schroder H, Wunder F, Stasch JP (2004) Identification of residues crucially involved in the binding of the heme moiety of soluble guanylate cyclase. J Biol Chem 279:3025–3032.
6. Schindler U, Strobel H, Schonafinger K, Linz W, Lohn M, Martorana PA, Rutten H, Schindler PW, Busch AE, Sohn M, Topfer A and others (2006) Biochemistry and pharmacology of novel anthranilic acid derivatives activating heme-oxidized soluble guanylyl cyclase. Mol Pharmacol 69:1260–1268.
7. Derbyshire ER, Marletta MA (2012) Structure and regulation of soluble guanylate cyclase. Annu Rev Biochem 81:533–559.
8. Cary SP, Winger JA, Derbyshire ER, Marletta MA (2006) Nitric oxide signaling: no longer simply on or off. Trends Biochem Sci 31:231–239.
9. Nioche P, Berka V, Vipond J, Minton N, Tsai AL, Raman CS (2004) Femtomolar sensitivity of a NO sensor from Clostridium botulinum. Science 306:1550–1553.
10. Moglich A, Ayers RA, Moffat K (2009) Structure and signaling mechanism of Per-ARNT-Sim domains. Structure 17:1282–1294.
11. Liu Y, Ruoho AE, Rao VD, Hurley JH (1997) Catalytic mechanism of the adenylyl and guanylyl cyclases: modeling and mutational analysis. Proc Natl Acad Sci USA 94:13414–13419.
12. Ma X, Beuve A, van den Akker F (2010) Crystal structure of the signaling helix coiled-coil domain of the beta1 subunit of the soluble guanylyl cyclase. BMC Struct Biol 10:2.
13. Allerston CK, von Delft F, Gileadi O (2013) Crystal structures of the catalytic domain of human soluble guanylate cyclase. PLoS One 8:e57644.
14. Pellicena P, Karow DS, Boon EM, Marletta MA, Kuriyan J (2004) Crystal structure of an oxygen-binding heme domain related to soluble guanylate cyclases. Proc Natl Acad Sci USA 101:12854–12859.
15. Ma X, Sayed N, Baskaran P, Beuve A, van den Akker F (2008) PAS-mediated dimerization of soluble guanylyl cyclase revealed by signal transduction histidine kinase domain crystal structure. J Biol Chem 283: 1167–1178.
16. Ma X, Sayed N, Beuve A, van den Akker F (2007) NO and CO differentially activate soluble guanylyl cyclase via a heme pivot-bend mechanism. EMBO J 26:578–588.
17. Hu X, Feng C, Hazzard JT, Tollin G, Montfort WR (2008) Binding of YC-1 or BAY 41-2272 to soluble guanylyl cyclase induces a geminate phase in CO photolysis. J Am Chem Soc 130:15748–15749.
18. Hu X, Murata LB, Weichsel A, Brailey JL, Roberts SA, Nighorn A, Montfort WR (2008) Allostery in recombinant soluble guanylyl cyclase from Manduca sexta. J Biol Chem 283:20968–20977.
19. Fritz BG, Hu X, Brailey JL, Berry RE, Walker FA, Montfort WR (2011) Oxidation and loss of heme in soluble guanylyl cyclase from Manduca sexta. Biochemistry 50:5813–5815.
20. Fritz BG, Roberts SA, Ahmed A, Breci L, Li W, Weichsel A, Brailey JL, Wysocki VH, Tama F, Montfort WR (2013) Molecular model of a soluble guanylyl cyclase fragment determined by small-angle x-ray scattering and chemical cross-linking. Biochemistry 52: 1568–1582.
21. Jacobson KB, Murphy JB, Das Sarma B (1972) Reaction of cacodylic acid with organic thiols. FEBS Lett 22:80–82.
22. Maignan S, Guilloteau JP, Zhou-Liu Q, Clement-Mella C, Mikol V (1998) Crystal structures of the catalytic domain of HIV-1 integrase free and complexed with its

metal cofactor: high level of similarity of the active site with other viral integrases. J Mol Biol 282:359–368.
23. Winger JA, Derbyshire ER, Lamers MH, Marletta MA, Kuriyan J (2008) The crystal structure of the catalytic domain of a eukaryotic guanylate cyclase. BMC Struct Biol 8:42.
24. Gong W, Hao B, Mansy SS, Gonzalez G, Gilles-Gonzalez MA, Chan MK (1998) Structure of a biological oxygen sensor: a new mechanism for heme- driven signal transduction. Proc Natl Acad Sci USA 95:15177–15182.
25. Miyatake H, Mukai M, Park SY, Adachi S, Tamura K, Nakamura H, Nakamura K, Tsuchiya T, Iizuka T, Shiro Y (2000) Sensory mechanism of oxygen sensor FixL from Rhizobium meliloti: crystallographic, mutagenesis and resonance Raman spectroscopic studies. J Mol Biol 301:415–431.
26. Key J, Hefti M, Purcell EB, Moffat K (2007) Structure of the redox sensor domain of Azotobacter vinelandii NifL at atomic resolution: signaling, dimerization, and mechanism. Biochemistry 46:3614–3623.
27. Crosson S, Moffat K (2001) Structure of a flavin-binding plant photoreceptor domain: insights into light-mediated signal transduction. Proc Natl Acad Sci USA 98:2995–3000.
28. Amezcua CA, Harper SM, Rutter J, Gardner KH (2002) Structure and interactions of PAS kinase N-terminal PAS domain: model for intramolecular kinase regulation. Structure 10:1349–1361.
29. Sevvana M, Vijayan V, Zweckstetter M, Reinelt S, Madden DR, Herbst-Irmer R, Sheldrick GM, Bott M, Griesinger C, Becker S (2008) A ligand-induced switch in the periplasmic domain of sensor histidine kinase CitA. J Mol Biol 377:512–523.
30. Krissinel E, Henrick K (2004) Secondary-structure matching (SSM), a new tool for fast protein structure alignment in three dimensions. Acta Crystallogr D Biol Crystallogr 60:2256–2268.
31. Weeks SD, Drinker M, Loll PJ (2007) Ligation independent cloning vectors for expression of SUMO fusions. Protein Expr Purif 53:40–50.
32. Pflugrath JW (1999) The finer things in X-ray diffraction data collection. Acta Crystallogr D55:1718–1725.
33. Keegan RM, Long F, Fazio VJ, Winn MD, Murshudov GN, Vagin AA (2011) Evaluating the solution from MrBUMP and BALBES. Acta Crystallogr D Biol Crystallogr 67:313–323.
34. Keegan RM, Winn MD (2008) MrBUMP: an automated pipeline for molecular replacement. Acta Crystallogr D Biol Crystallogr 64:119–124.
35. Emsley P, Lohkamp B, Scott WG, Cowtan K (2010) Features and development of Coot. Acta Crystallogr D Biol Crystallogr 66:486–501.
36. Murshudov GN, Skubak P, Lebedev AA, Pannu NS, Steiner RA, Nicholls RA, Winn MD, Long F, Vagin AA (2011) REFMAC5 for the refinement of macromolecular crystal structures. Acta Crystallogr D Biol Crystallogr 67:355–367.
37. Pettersen EF, Goddard TD, Huang CC, Couch GS, Greenblatt DM, Meng EC, Ferrin TE (2004) UCSF Chimera – a visualization system for exploratory research and analysis. J Comput Chem 25:1605–1612.
38. Laskowski RA, MacArthur MW, Moss DS, Thorton JM (1993) PROCHECK: A program to check the stereochemical quality of protein structures. J Appl Crystal 26:283–291.
39. Dundas J, Ouyang Z, Tseng J, Binkowski A, Turpaz Y, Liang J (2006) CASTp: computed atlas of surface topography of proteins with structural and topographical mapping of functionally annotated residues. Nucleic Acids Res 34:W116–W118.

APPENDIX B

YC-1 BINDING TO THE β SUBUNIT OF SOLUBLE GUANYLYL CYCLASE OVERCOMES ALLOSTERIC INHIBITION BY THE α SUBUNIT

Contributions: Expression and purification of all proteins except *Bt* sGC β_1(1−197), *Bt* sGC β_1(1−359), BirA and TEV protease were solely my work. Dr. Andrzej Weichsel and Jacquie Brailey constructed *Ms* sGC BNT2 vector. Dr. Bradley Fritz constructed *Ms* sGC NT21, *Ms* sGC NT13 and *Ms* sGC PAS-Coiled Coil (β_1 199-380) vectors. Dr. Juliana The prepared original pETDuet1 *Ms* sGC CT1 (α_1 residues 272−699 and β_1 residues 199−600). Dr. Elsa D. Garcin and Leida Rassouli-Taylor constructed vector for both Bt sGC β_1(1−197) and Bt sGC β_1(1−359), expressed and purified. I constructed the *Ms* sGC α_1 PAS vector in pETSUL and *Ms* sGC β1 PAS expression vectors. Aaron Issaian constructed, expressed and purified BirA vector and also purified TEV protease. Dr. Matthew J. Gage and Eric Campbell (NAU) performed fluorescence anisotropy experiments. Dr. Cynthia L. David helped in performing surface plasmon resonance (SPR) experiments. I performed all CO binding measurements and YC-1 family compounds binding measurements. Dr. Andrew C. Hausrath wrote the MATLAB code for the linked equilibria analyses. Dr. William R. Montfort and myself prepared the manuscript. Dr. William R. Montfort provided oversight for the project and edited the manuscript.

BIOCHEMISTRY
including biophysical chemistry & molecular biology

Article

pubs.acs.org/biochemistry

YC-1 Binding to the β Subunit of Soluble Guanylyl Cyclase Overcomes Allosteric Inhibition by the α Subunit

Rahul Purohit,[†] Bradley G. Fritz,[†] Juliana The,[†] Aaron Issaian,[†] Andrzej Weichsel,[†] Cynthia L. David,[‡] Eric Campbell,[∥] Andrew C. Hausrath,[†] Leida Rassouli-Taylor,[§] Elsa D. Garcin,[§] Matthew J. Gage,[∥] and William R. Montfort*,[†]

[†]Department of Chemistry and Biochemistry, The University of Arizona, Tucson, Arizona 85721, United States
[‡]Center for Toxicology, College of Pharmacy, The University of Arizona, Tucson, Arizona 85721, United States
[§]Department of Chemistry and Biochemistry, University of Maryland, Baltimore County, Baltimore, Maryland 21250, United States
[∥]Department of Chemistry and Biochemistry, Northern Arizona University, Flagstaff, Arizona 86011, United States

ABSTRACT: Soluble guanylate cyclase (sGC) is a heterodimeric heme protein and the primary nitric oxide receptor. NO binding stimulates cyclase activity, leading to regulation of cardiovascular physiology and making sGC an attractive target for drug discovery. YC-1 and related compounds stimulate sGC both independently and synergistically with NO and CO binding; however, where the compounds bind and how they work remain unknown. Using linked equilibrium binding measurements, surface plasmon resonance, and domain truncations in *Manduca sexta* and bovine sGC, we demonstrate that YC-1 binds near or directly to the heme-containing domain of the β subunit. In the absence of CO, YC-1 binds with a K_d of 9−21 μM, depending on the construct. In the presence of CO, these values decrease to 0.6−1.1 μM. Pfizer compound 25 bound ∼10-fold weaker than YC-1 in the absence of CO, whereas compound BAY 41-2272 bound particularly tightly in the presence of CO (K_d = 30−90 nM). Additionally, we found that CO binds much more weakly to heterodimeric sGC proteins (K_d = 50−100 μM) than to the isolated heme domain (K_d = 0.2 μM for *Manduca* β H-NOX/PAS). YC-1 greatly enhanced binding of CO to heterodimeric sGC, as expected (K_d ∼ 1 μM). These data indicate the α subunit induces a heme pocket conformation with a lower affinity for CO and NO. YC-1 family compounds bind near the heme domain, overcoming the α subunit effect and inducing a heme pocket conformation with high affinity. We propose this high-affinity conformation is required for the full-length protein to achieve high catalytic activity.

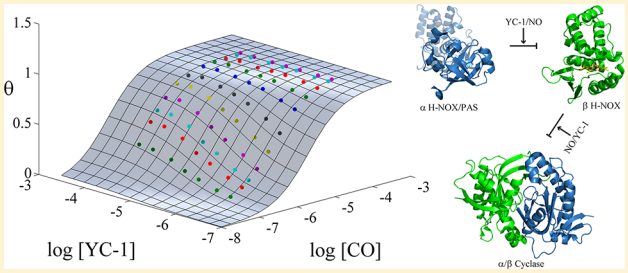

Nitric oxide (NO) regulates a phenomenal array of physiological processes, including blood pressure homeostasis, wound healing, memory formation, sexual response, and the fighting of infectious disease.[1] Impairment in NO signaling can lead to hypertension and atherosclerosis and contribute to heart attack and stroke.[2,3] NO is produced by a class of enzymes called nitric oxide synthases (NOSs) through the oxidation of L-arginine to L-citrulline.[4,5] The primary receptor for NO is soluble guanylyl/guanylate cyclase (sGC), a heterodimeric heme protein of ∼150 kDa that responds to binding of NO to heme through enhanced cyclase activity, producing cGMP and a signaling cascade. Treatment of cardiovascular disease by stimulating the nitric oxide pathway has long been a treatment goal, beginning more than 150 years ago with the administration of amyl nitrite[6] and nitroglycerin[7] to relieve symptoms of angina pectoris, although the mode of action of these compounds (release of NO) was not discovered until many years later. More recently, sGC, the NO receptor, has been heavily targeted for drug discovery.

sGC is composed of two homologous subunits, α and β. Multiple isoforms of each subunit have been identified; however, the most common isoform is the α_1/β_1 heterodimer (reviewed in ref 8). Each sGC subunit consists of four domains, an N-terminal heme-nitric oxide oxygen (H-NOX) domain[9] (also called a SONO domain[10]), a central Per-Arnt-Sim (PAS) domain,[11] a coiled-coil domain, and a C-terminal catalytic cyclase domain.[12] There is a single heme moiety in the heterodimer, associated with the β_1 H-NOX domain. The equivalent domain in the α_1 subunit has lost the ability to bind heme but appears to have retained an overall H-NOX-like fold and is therefore commonly termed the α_1 H-NOX domain. During signaling, the binding of NO to heme in the β_1 subunit leads to the formation of a pentacoordinated Fe−NO complex with proximal histidine bond breakage.[13−15] The structural change due to this event is transferred to the cyclase domain, which in turn enhances cGMP production. How this structural change is translated to increased catalytic activity is poorly understood. Moreover, elusive structural details for sGC have

Received: November 8, 2013
Revised: December 12, 2013
Published: December 16, 2013

hampered the understanding of allosteric regulation in the protein. Structures of individual sGC domains such as the β_1 coiled-coil homodimer,[16] the α_1 PAS domain,[17] and the α_1/β_1 heterodimeric cyclase domain[18] have recently been determined. Insight into the H-NOX and PAS domains comes from the structures of prokaryotic homologous proteins,[10,19−21] yet an understanding of how these domains are arranged in the functional NO sensor remains unknown.

Small molecule stimulators of sGC have been discovered, opening new doors for drug discovery in the treatment of cardiovascular diseases.[22] The first of these is compound YC-1, a benzylindazole derivative that inhibits platelet activation through stimulating sGC.[23] YC-1 stimulates sGC 2−4-fold in the absence of NO but acts synergistically with CO or NO to achieve several hundred-fold activation.[24,25] Binding of YC-1 can also overcome the inhibitory phosphorylation of sGC.[26] Compound BAY 63-2521 (riociguat), a YC-1 derivative, has just completed phase III clinical trials[27−30] and has been approved by the Food and Drug Administration for treatment of pulmonary hypertension (as Adempas). These compounds stimulate sGC activity in an NO-independent and heme-dependent manner, but how they bind to sGC and how they stimulate catalytic activity are unknown. Studies aimed at determining the binding site for YC-1 family compounds have suggested the pseudosymmetric site in the cyclase domain,[31,32] the α_1 H-NOX domain,[33,34] and the β_1 H-NOX domain.[35−38] A second class of compounds that function through replacing the sGC heme, which can be lost upon oxidation, have also been developed.[22] Prominent among these are compounds BAY 58-2667 (cinaciguat)[39] and HMR1766 (ataciguat).[40]

We developed sGC from the tobacco hornworm/hawkmoth (*Manduca sexta*) for biophysical and biochemical characterization and to help with uncovering the mechanism underlying YC-1 stimulation.[33,41−43] *M. sexta* sGC (*Ms* sGC) is highly homologous to its mammalian counterparts and responds well to YC-1 family compounds. Expression of N-terminal heterodimeric constructs lacking the α_1/β_1 cyclase domains (*Ms* sGC-NT constructs) leads to proteins that preserve YC-1 binding. Binding of YC-1 to *Ms* sGC leads to enhanced CO and NO binding[33] and to the trapping of CO in the heme pocket after laser photolysis, leading to rebinding with heme before escape from the protein (geminate recombination).[41] *Ms* sGC-NT is an elongated molecule with a central parallel coiled-coil domain, based on chemical cross-linking, mass spectrometry, and small-angle X-ray scattering (SAXS) studies.[43] In this model, the coiled-coil domain acts as an organizing center for the PAS, H-NOX, and, presumably, cyclase domains. Here, we demonstrate that the α subunit serves to keep the β subunit heme domain in a conformation with reduced affinity for CO and that YC-1 binds directly to the β subunit, inducing a high-affinity heme domain conformation.

EXPERIMENTAL PROCEDURES

Materials. All chemicals were obtained from Sigma-Aldrich, restriction enzymes from Fermentas, and purification columns from GE Healthcare unless otherwise indicated. Pfizer compound 25 targeted to sGC (PF-25) was kindly provided by L. Roberts of Pfizer Inc.[44] DEA/NO was kindly provided by K. Miranda (The University of Arizona).

sGC Protein Expression Vectors. Construct *Ms* sGC CT1 (α_1 residues 272−699 and β_1 residues 199−600) was obtained by polymerase chain reaction (PCR) amplification from a full-length *Ms* sGC pETDuet1 construct.[33] Forward primer 5′-ggatccgaccaaagtgacagattt-3′ and reverse primer 5′-gcggccgcctaagttggttcttct-3′ were used for the α_1 subunit, and the PCR product was cloned into the pETDuet1 vector using the BamHI and NotI restriction sites. Similarly, the *Ms* sGC CT1 β_1 fragment was obtained by PCR amplification from the *Ms* sGC full-length pETDuet1 construct using primers 5′-catatgacgttgtctcttgaacca-3′ and 5′-gatatcttaatggatcttcctggt-3′, and the PCR product was cloned into the same pETDuet1 vector using the NdeI and EcoRV restriction sites. The final construct had a His_6 purification tag fused to the N-terminus of the α_1 subunit. Stop codons were inserted at α_1 Asn 451 and β_1 Thr 381 using the QuikChange lightning site-directed mutagenesis kit (Stratagene, La Jolla, CA), leading to constructs containing just the PAS and coiled-coil domains (α_1 residues 272−450 and β_1 residues 199−380).

Possible boundaries for stable PAS domain expression were surveyed using the *Ms* sGC α_1 PAS-CC-cyclase (residues 272−699) and β_1 PAS-CC-cyclase (residues 199−600) cloned into a single plasmid (pETDuet-1, Novagen) or cloned individually into the pETDuet-1 (α_1) or pET28a+ (β_1) plasmid. Domain boundaries were examined through introduction of stop codons, using the QuikChange mutagenesis kit. The *Ms* sGC β_1 PAS construct (residues 199−319) in pET28a+ was obtained by inserting a stop codon at position 320. The *Ms* sGC α_1 PAS domain, spanning residues 279−425, was cloned into the pETHSUL vector, kindly provided by the Loll laboratory.[45] A ligation-independent cloning (LIC) approach was undertaken as described previously,[45] using forward primer 5′-agattggtggcatcggcgtggctagcttctgc-3′ and reverse primer 5′-gaggagagtttagacttaaccatcctgagccctagcc-3′ (LIC overhang residues are underlined). The vector was made ready for ligation using the direct digestion method with BseRI (New England Biolabs). A stop codon was introduced at position 405 to yield wild-type construct *Ms* sGC-P25α, spanning residues 279−404. A triple cysteine-to-alanine mutant (C285A/C352A/C374A, *Ms* sGC-P35α) was produced to assist in crystallization.[17] All mutations were introduced using the QuikChange lightning site-directed mutagenesis kit. Vector pSUPER, containing a dual-tagged catalytic domain of SUMO hydrolase (dtUD1) fused to the N-terminus of SUMO, was also kindly provided by the Loll laboratory.[45] *Ms* sGC β_1(1−380), containing the H-NOX and PAS domains and most of the CC domain, was amplified by PCR and subcloned into the pGEM-T vector. The fragment was then cut with the restriction enzymes NcoI and NotI and inserted into the pET28c vector, yielding a C-terminal His_6 tag.

A single-step insertion methodology[46] was used for insertion of the BirA recognition sequence (Avi-tag, GLNDIFEAQKIEWHE) at the C-terminus of the *Ms* sGC-NT21 β_1 subunit (residue 380, ref 43) and *Ms* sGC β_1(1−380) using forward primers 5′-ggaattggaaaaacagaagggtggcggtctgaacgacatcttcgaggctcaaaaaatagagtggcacgagtaggacaggcttctttactcagtg-3′ and 5′-ggaattggaaaaacagaagggtggcggtctgaacgacatcttcgaggctcaaaaaatagagtggcacgaggcggccgcactcgagcaccaccac-3′ and common reverse primer 5′-cttctgtttttccaattccagctctcggaatgtttgttgaag-3′. The Avi tags with two N-terminal glycine linker residues are underlined. Similarly, a C-terminal Avi tag was added to α_1 PAS domain construct *Ms* sGC-P25α using forward primer 5′-gactcttcatatccgatataggtggcggtctgaacgacatcttcgaggctcaaaaaatagagtggcacgagtgacttcatgatgcgacgagag-3′ and reverse primer 5′-tatatcggatatgaagagtccccttccagtcagaccttcgag-3′. *Escherichia coli* biotin protein ligase BirA in vector pGEX-4T-1, with an N-terminal GST tag linked to a thrombin cleavage site and a C-terminal His_6 tag,

was kindly provided by M. Kuhns (The University of Arizona). The thrombin cleavage site was changed to a TEV cleavage site using forward primer 5′-ccatcctccaaaatcgggcgaaaacttgtatttccaggatccaaggataacaccg-3′ and reverse primer 5′-cggtgttatccttggatccctggaaatacaagttttcgcccgattttggaggatgg-3′ (TEV cleavage site underlined). Additionally, a stop codon was inserted in front of the His_6 tag.

Expression and Purification of *Ms* sGC PAS Domains. *Ms* sGC α_1 PAS with an N-terminal His-tagged SUMO fusion was expressed in *E. coli* strain BL21(DE3) pLysS. Cells were grown at 37 °C to an OD_{600} of 0.6 before being induced with 0.5 mM isopropyl 1-thio-β-D-thiogalactopyranoside (IPTG) and then grown at 20 °C; cells were harvested after 16 h. Purification steps were performed at 4 °C. Cell pellets were resuspended in lysis buffer [50 mM sodium phosphate (pH 7.4), 300 mM NaCl, 20 mM imidazole, 0.1 mg/mL DNase I, 2 mM $MgCl_2$, 1 mM phenylmethanesulfonyl fluoride (PMSF), 1 mM benzamidine, and 1 μg/mL aprotinin, leupeptin, and pepstatin], disrupted using a French press cell (1000 psi), clarified by ultracentrifugation (45Ti rotor, 40000 rpm for 30 min), supplemented with 10% glycerol (w/v) and 5 mM β-mercaptoethanol, and loaded onto a 5 mL Ni-NTA column previously equilibrated with binding buffer [50 mM sodium phosphate (pH 7.4), 300 mM NaCl, 20 mM imidazole, and 5 mM β-mercaptoethanol]. The column was washed with binding buffer until the baseline was reached, and bound protein was eluted using an imidazole gradient ranging from 20 to 300 mM over 100 mL (20 bed volumes) by mixing binding buffer and elution buffer (binding buffer supplemented with 500 mM imidazole). Cleavage of the N-terminal His-tagged SUMO domain was achieved by adding 1 mg of purified SUMO hydrolase (dtUD1) to the pooled PAS-containing fractions followed by overnight dialysis at 4 °C against two changes of dialysis buffer [50 mM sodium phosphate (pH 7.4), 300 mM NaCl, 5% glycerol (w/v), and 10 mM β-mercaptoethanol]. The dialyzed product was again loaded onto the Ni-NTA column to remove the His-tagged SUMO and SUMO hydrolase proteins, followed by concentration to ∼3 mL and further purification over an S-200 size exclusion column previously equilibrated with equilibration buffer [50 mM Tris-HCl (pH 7.4), 200 mM NaCl, 5% glycerol (w/v), and 5 mM dithiothreitol]. The final material was concentrated to 10−15 mg/mL using a Vivaspin concentrator (Sartorius Stedim Biotech) and stored at −80 °C. A final yield of 2−3 mg of highly pure protein was obtained per liter of cell culture.

Ms sGC β_1 PAS was expressed in *E. coli* strain Rosetta pLysS. Cells were grown at 37 °C to an OD_{600} of 1.0 and induced with 0.2 mM IPTG, after which they were grown while being slowly shaken (90 rpm) at 18 °C for 18 h before being harvested. The cell lysate was obtained as described for the α_1 PAS domain, and the protein was purified using Ni-NTA followed by S-200 size exclusion chromatography. A yield of 30−40 mg was obtained per liter of cell culture.

SUMO hydrolase (dtUD1) was expressed in strain BL21-(DE3) pLysS. Cells were grown at 37 °C until the OD_{600} reached 0.6, induced with 0.5 mM IPTG, and grown at 30 °C for 6 h before being harvested. Purification was performed using Ni-NTA column chromatography as described previously.[45]

BirA was expressed in strain BL21(DE3) pLysS. Cells were grown at 37 °C to an OD_{600} of 1.0, and expression was induced with 0.5 mM IPTG, followed by growth at 16 °C for 20 h before being harvested. Cells were lysed by sonication at 4 °C in lysis buffer and clarified by ultracentrifugation, and the supernatant was loaded onto a GSTrap FF column previously equilibrated with 50 mM sodium phosphate buffer (pH 7.4) containing 300 mM NaCl. Bound GST-tagged BirA was eluted with the buffer described above supplemented with 20 mM glutathione. Fractions were incubated for 24 h with 5 μM His_6-tagged TEV protease, and the mixture was loaded onto a GSTrap FF column in tandem with a Ni-NTA column. The flow through was collected and the protein concentrated and stored at −80 °C.

TEV protease with N-terminal polyhistidine, C-terminal polyarginine, and mutation S219V was prepared from a previously described pRK793 vector.[47] TEV protease was expressed in *E. coli* strain BL21(DE3) pLysS. Cells were grown to an OD_{600} of 0.6 at 37 °C, induced with 1 mM IPTG, and grown at 30 °C for 6 h before being harvested. Cell pellets were resuspended in binding buffer [50 mM sodium phosphate (pH 7.4), 300 mM NaCl, and 20 mM imidazole], disrupted using a French press cell (1000 psi), and clarified by ultracentrifugation (45Ti rotor, 40000 rpm for 30 min). The supernatant was supplemented with 10% glycerol (w/v) and 5 mM β-mercaptoethanol before being loaded onto a 5 mL Ni-NTA column previously equilibrated with binding buffer [50 mM sodium phosphate (pH 7.4), 300 mM NaCl, 20 mM imidazole, and 5 mM β-mercaptoethanol]. The column was washed with binding buffer until the baseline was reached, and bound protein was eluted using an imidazole gradient ranging from 20 to 300 mM over 100 mL (20 bed volumes) by mixing binding buffer and elution buffer (binding buffer supplemented with 500 mM imidazole). Fractions containing TEV protease were pooled, buffer exchanged with final storage buffer [50 mM sodium phosphate (pH 7.4), 300 mM NaCl, 25% glycerol, 1 mM EDTA, and 1 mM DTT], concentrated to a final concentration of ∼4 mg/mL, and frozen at −80 °C.

Expression and Purification of Heme-Containing *Manduca* and Bovine sGC Proteins. *Ms* sGC-NT13, *Ms* sGC-NT19, and *Ms* sGC-NT21 were expressed in *E. coli* and purified using Ni-NTA, StrepTactin (*Ms* sGC-NT19), and size exclusion chromatography, as previously described.[33,43] *Ms* sGC β_1(1−380) was expressed in *E. coli* strain Rosetta pLysS. Cells were grown at 37 °C to an OD_{600} of 1.0 and cooled on ice before being induced. The culture was induced with 0.5 mM IPTG, supplemented with 25 μM δ-aminolevulinic acid, and grown at 30 °C for 6 h before being harvested. Cell pellets were resuspended in lysis buffer B [50 mM Tris-HCl (pH 8.5), 10 mM NaCl, 0.1 mg/mL DNase I, 2 mM $MgCl_2$, 1 mM PMSF, 1 mM benzamidine, 1 μg/mL aprotinin, 1 μg/mL leupeptin, 1 μg/mL pepstatin, and 1 mM dithionite], disrupted with a French pressure cell, and clarified by ultracentrifugation. The supernatant was supplemented with 10% (w/v) glycerol, 5 mM β-mercaptoethanol, and an ∼100-fold excess of dithionite (∼1 mM, assuming 2 mg of protein/L of cell culture). The sample was loaded onto a DEAE anion exchange column or Q-FF Sepharose column previously equilibrated with buffer A [20 mM Tris-HCl (pH 8.5), 1 mM EDTA, and 5 mM β-mercaptoethanol], the column washed with buffer A, and protein eluted with a 0 to 300 mM NaCl elution gradient (200 mL) using buffer A (0 mM NaCl) and buffer B (buffer A with 500 mM NaCl). Colored fractions were pooled and loaded onto the Ni-NTA column and eluted with 30 mM EDTA in a single-step elution. Fractions were supplemented with fresh dithionite and tris(2-carboxyethyl)phosphine (TCEP), concentrated, and further purified by being run through a size

exclusion S200 column previously equilibrated with gel filtration buffer [50 mM potassium phosphate buffer (pH 7.4), 100 mM KCl, 2 mM EDTA, 5% glycerol, and 1 mM TCEP], where it ran as a monomer. The purified protein was supplemented with dithionite, concentrated to 5−10 mg/mL, and stored at −80 °C.

For the bovine sGC β_1 H-NOX and β_1 H-NOX-PAS, we used a systematic site-directed mutagenesis approach to determine the appropriate C-terminal ends for optimal expression and solubility of the proteins (J. Hines, L. Rassouli-Taylor, J. Burstyn, and E. Garcin, Raman studies of bovine soluble guanylate cyclase, manuscript in preparation). We used the untagged β_1(1−385) (residues 1−385) construct cloned into the pET30b plasmid (kind gift of J. Burstyn) and introduced stop codons at various positions using the QuikChange mutagenesis kit. *Bt* sGC β_1 H-NOX (residues 1−197) and sGC β_1 H-NOX-PAS (residues 1−359) in pET30b were obtained by inserting a stop codon at positions 198 and 360, respectively. These constructs displayed the highest levels of expression and solubility in *E. coli* cells. Purification of both constructs was performed as follows. Each construct was expressed in *E. coli* strain BL21(DE3) pRIPL. Cells were grown at 37 °C to an OD_{600} of 1.0 and cooled on ice before being induced. The culture was induced with 0.4 mM IPTG, supplemented with 450 μM δ-aminolevulinic acid and ferric citrate, and grown at 20 °C for 24 h before being harvested. Cell pellets were resuspended in lysis buffer [20 mM Tris-HCl (pH 7.5), 50 mM NaCl, DTT, 0.5 mg/mL lysozyme, 300 units of benzonase (SIGMA), and one tablet of EDTA-free protease inhibitor cocktail tablet/50 mL (Roche)], disrupted by sonication, and clarified by ultracentrifugation. We used 10 mM DTT to keep the β_1 H-NOX protein reduced and 1 mM DTT for the β_1 H-NOX-PAS construct. The clarified lysate was loaded onto a Q-FF Sepharose column previously equilibrated with buffer A [20 mM Tris-HCl (pH 7.5), 50 mM NaCl, and DTT], and the protein was eluted with a 0.05 to 1 M NaCl elution gradient (buffer B being buffer A with 1 M NaCl). Colored fractions were pooled, dialyzed into buffer A, and loaded onto an S75 size exclusion column equilibrated in buffer A. Colored fractions were pooled and loaded onto a second QFF column pre-equilibrated in buffer C [20 mM Tris-HCl (pH 8.5), 50 mM NaCl, and TCEP]. The protein was eluted with a 0.05 to 1 M NaCl gradient (buffer D being buffer C with 1 M NaCl). The colored fractions were pooled and dialyzed into buffer C (10 and 1 mM TCEP for β_1 H-NOX and β_1 H-NOX-PAS, respectively). The purified protein was concentrated to ∼10 mg/mL and stored at −80 °C.

Determination of Dissociation Constants for CO. CO dissociation constants were measured by titrating CO from a saturated solution into sGC protein and monitoring the appearance of the CO-bound Soret absorption band, as described previously.[33,43] The *Ms* sGC β_1(1−380) and *Bt* sGC β_1(1−197) samples were prepared in Ar-purged buffer supplemented with excess dithionite. CO binding experiments were performed in a 10 cm path length cuvette for *Ms* sGC-β_1(1−380) and *Ms* sGC-NT21 using a Cary 50 spectrophotometer (Varian) with a modified sample holder. Binding data in the presence and absence of 50 μM YC-1 were plotted using a single-site saturation ligand binding model in SigmaPlot (SPSS, Inc., Chicago, IL).

To extract linked equilibrium binding behavior, CO binding assays were performed for *Ms* sGC-NT21 (10 cm cuvette) and *Ms* sGC-NT13 (1 cm cuvette) at various YC-1 concentrations. The stimulation of CO binding in the presence of YC-1 was described with a cooperative two-site model with four states: free protein, protein bound to CO only, protein bound to YC-1 only, and protein bound to both CO and YC-1. Independent binding of CO and independent binding of YC-1 are described with association constants K_a^{CO} and $K_a^{YC\text{-}1}$, respectively, with an assumed cooperativity constant K_{int} representing coupling between the two binding processes. This model is described with a binding polynomial of the form

$$Z = 1 + K_a^{CO}[CO] + K_a^{YC\text{-}1}[YC\text{-}1] + (K_a^{CO}[CO])(K_a^{YC\text{-}1}[YC\text{-}1])K_{int} \quad (1)$$

in which each term represents the statistical weight for one of the four states. The fraction of CO sites occupied is given by the ratio of the weights for states with CO bound to all four states:

$$\theta = [K_a^{CO}[CO] + (K_a^{CO}[CO])(K_a^{YC\text{-}1}[YC\text{-}1])K_{int}]/Z \quad (2)$$

Estimates for the model parameters K_a^{CO}, $K_a^{YC\text{-}1}$, and K_{int} were obtained from a global fit of θ to the normalized absorbance changes at wavelengths of 423 and 433 nm, using MATLAB (The MathWorks, Inc., Natick, MA). The product $K_a^{YC\text{-}1}K_{int}$ indicates the association constant for binding of YC-1 to the CO-bound complex, so its inverse represents the dissociation constant $K_d^{YC\text{-}1'}$. Similarly, $K_d^{CO'}$ may be estimated from the inverse of the product $K_a^{CO}K_{int}$.

To directly measure the binding of YC-1 family compounds to *Ms* sGC-NT-CO, an ∼2 nm shift in the Soret band maxima was monitored as a function of compound concentration. The compound was titrated into a 1 or 10 cm cuvette containing a CO-saturated protein solution. The K_d for ligand binding in the presence of CO was calculated by plotting the Soret shift difference with respect to the increasing concentrations of the ligand and fitting to a single-site saturation ligand binding model in SigmaPlot.

Fluorescence Anisotropy. Fluorescence anisotropy was measured using a JASCO J-815 CD fluorescence spectrometer equipped with an anisotropy attachment (JASCO). Average anisotropy was measured at 20 °C for 60 s using an excitation wavelength of 325 nm. Anisotropy was calculated using total fluorescence above 380 nm, which was measured 90° incident to the excitation beam. Initial anisotropy was measured for a 2 μM YC-1 solution in 10 mM Tris-HCl (pH 7.5) by titrating *Ms* sGC α_1 P25α or β_1 PAS or lysozyme, and the sample was mixed thoroughly for 30 s before anisotropy measurements were taken. Data were fit using a one-site total binding model implemented in GraphPad (GraphPad Software, Inc.).

Surface Plasmon Resonance Binding Experiments. *In vitro* biotinylation of Avi-tagged *Ms* sGC-NT21, *Ms* sGC α_1 PAS, and *Ms* sGC β_1(1−380) was performed using *E. coli* BirA biotin ligase. A reaction mixture containing 30−40 μM Avi-tagged protein, 1−2 μM purified BirA, 0.5 mM biotin, 10 mM magnesium acetate, and 10 mM ATP was incubated at 4 °C for 6 h and loaded onto a Ni-NTA column (*Ms* sGC-NT21) or Superdex-75 analytical gel filtration column [*Ms* sGC α_1 PAS and *Ms* sGC β_1(1−380)] to remove excess reaction components. Biotinylation was confirmed by a monoclonal anti-biotin antibody (Sigma-Aldrich) Western blot. All SPR studies were performed on a Biacore T100 instrument at 20 °C. Both reference and sample CM5 sensor chip surfaces (GE Healthcare) were prepared by an amine coupling methodology

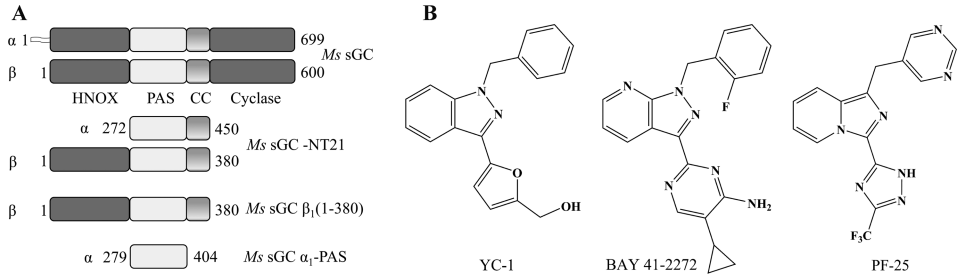

Figure 1. sGC constructs and ligand structures. (A) Schematic representation of the heterodimeric *Ms* sGC domains, expression constructs, and their boundaries. Constructs used in this study but not shown in the diagram are *Ms* sGC-NT13 (α_1 residues 49−450 and β_1 residues 1−380), *Bt* sGC β_1(1−197), and *Bt* sGC β_1(1−359). (B) Structures of YC-1, BAY 41-2272, and PF-25.

following the procedures in the Biacore T100 instrument manual. The chip surfaces were first activated by using a mixture of *N*-hydroxysuccinimide (NHS) and 1-ethyl-3-[3-(dimethylamino)propyl]carbodiimide (EDC). NeutrAvidin (Pierce), 100 μg/mL in 10 mM NaOAc (pH 4.5), was then immobilized to 10000 response units by passing it over the activated surfaces. Running buffer consisted of 10 mM HEPES (pH 7.4), 150 mM NaCl, 1 mM EDTA, and 0.05% Tween 20. Any remaining active esters were blocked with ethanolamine, and the immobilized NeutrAvidin chip surface was washed three times with a 30 s pulse of 10 mM HCl. Biotinylated *Ms* sGC proteins were captured onto the NeutrAvidin-coated chip surfaces by injecting 25 μM protein at a flow rate of 10 μL/min until ∼10000 response units had been achieved. Running buffer consisted of 50 mM potassium phosphate buffer (pH 7.4), 100 mM KCl, 2 mM EDTA, and 1 mM TCEP. The surfaces were washed with running buffer for 2 h at a flow rate of 100 μL/min until a stable response was obtained, indicating no further dissociation of the biotinylated proteins. Each chip has four flow cells allowing simultaneous measurements on one reference and three active surfaces. The Biacore T100 MIX function was used to mix DEA/NO or NaOH alone (0.5 mM DEA/NO stock in 10 mM NaOH and 1% DMSO, contained in an Ar-purged sealed Biacore vial) with varied concentrations of PF-25 in 50 mM potassium phosphate buffer (pH 7.4), 100 mM KCl, 2 mM EDTA, and 1 mM TCEP containing 1% DMSO to achieve a final DEA/NO concentration of 25 μM. Various concentrations of PF-25 containing DEA/NO or NaOH were injected over the surface at a rate of 25 μL/min with 115 s association and 240 s dissociation times. Running buffer consisted of 50 mM potassium phosphate buffer (pH 7.4), 100 mM KCl, 2 mM EDTA, 1 mM TCEP, and 1% DMSO. Solvent correction curves were used to compensate for any mismatch between the sample buffer and the running buffer. Data were analyzed with Biacore T100 evaluation software to obtain the offset corrected response [*R*, measured in response units (RU)] and the expected maximal response (R_{max}) based on the response from the immobilized protein (R_{immob}) and the relative molecular weights of ligand and analyte:

$$R_{max} = (\text{MW PF-25/MW protein})\, R_{immob}(\text{stoichiometric ratio}) \quad (3)$$

For measurements in cases in which binding was very weak (−NO), the dissociation constant was obtained from a single-site saturation ligand binding model with R_{max} constrained, while for tighter binding (+NO), R_{max} was allowed to be fit. Fitting was conducted with SigmaPlot:

$$R = (R_{max}[\text{PF-25}])/(K_d + [\text{PF-25}]) + \text{offset} \quad (4)$$

RESULTS

The sGC α Chain Inhibits CO Capture by Heme in the β Chain. To begin to understand how the affinity of NO and CO for sGC heme is modulated, we examined binding of CO to a variety of sGC proteins lacking specific domains but retaining heme. Measurements were taken in the presence or absence of YC-1 or related compounds. We focused on CO binding because its affinity for ferrous heme was lower than that of NO, allowing for the measurement of equilibrium dissociation constants, and because of its clear response to YC-1 binding. Measurements were taken with *Ms* sGC-NT constructs (Figure 1), taking advantage of their high stability and high yields from bacterial expression.[33,41−43] *Ms* sGC-NT constructs are heterodimeric proteins lacking the C-terminal cyclase domains while retaining YC-1 binding. We previously demonstrated that YC-1 binding leads to tighter CO and NO binding and to a geminate recombination phase upon CO photolysis.[33,41] Here, we extend these studies to include proteins completely lacking the α_1 chain and, where needed, using a cuvette with a path length of 10 cm, allowing for more precise measurement of the tighter binding constants that occur in the presence of YC-1 (Figure 2 and Table 1).

The *Ms* sGC coiled-coil domain likely ends at α_1 Pro 460 and β_1 Pro 390.[16,42,43] We trimmed the C-terminal end of *Ms* sGC-NT2 by 21 residues to remove a portion of the linker between the coiled-coil and cyclase domains, as well as a small portion of the coiled-coil domain, yielding *Ms* sGC-NT13 and *Ms* sGC-NT19, which are identical except for addition of a *Strep* purification tag to *Ms* sGC-NT19. Both proteins display a small increase in CO binding affinity in the absence of YC-1, but no significant change in CO affinity in the presence of YC-1 (Table 1). Values for K_d^{CO} obtained with these proteins varied from 50−90 μM in the absence of YC-1 to 0.8−2.8 μM in the presence of YC-1 (termed $K_d^{CO\prime}$). Removal of the α_1 H-NOX domain (*Ms* sGC-NT21) led to considerable tightening of CO binding [K_d^{CO} = 2.2 μM, and $K_d^{CO\prime}$ = 0.2 μM (Table 1)]. These measurements were taken in a 10 cm cuvette, allowing protein concentrations as low as 50 nM to be used and minimizing the depletion of free CO through heme binding. Thus, *Ms* sGC-NT21 binds CO 20−40-fold tighter than *Ms* sGC proteins containing the α_1 H-NOX domain and still responds to YC-1, displaying a 10-fold increase in CO binding affinity when YC-1 is present. These data are consistent with previous studies indicating YC-1 family compounds stimulate NO-dependent catalysis in sGC proteins lacking the first 259 residues of α_1.[48−50]

dx.doi.org/10.1021/bi4015133 | *Biochemistry* 2014, 53, 101−114

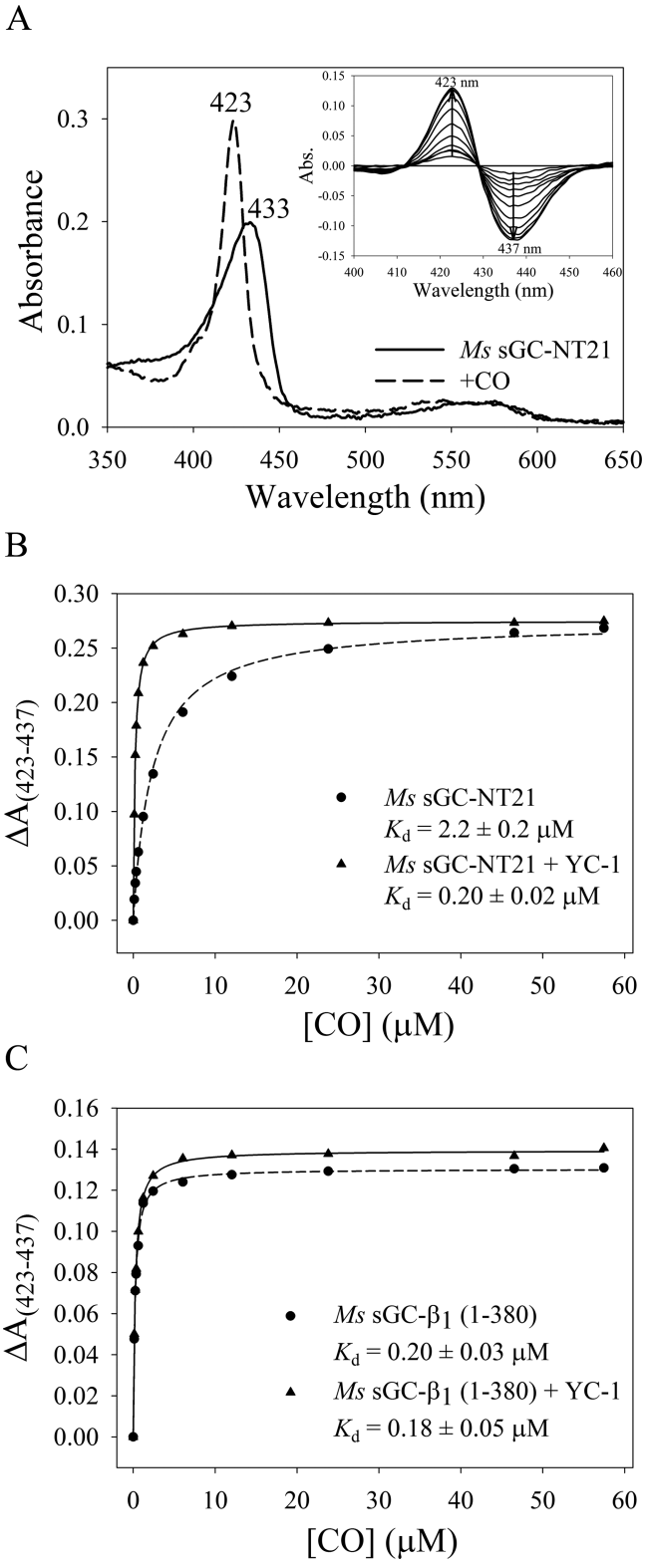

Figure 2. CO saturation binding analysis. (A) Absorption spectra of purified *Ms* sGC-NT21 before and after CO saturation. The A_{433}/A_{280} ratio for the unliganded protein is ~1.8, consistent with high purity and full heme incorporation. The inset shows difference spectra for *Ms* sGC-NT21 upon CO titration. (B) CO saturation binding curve for *Ms* sGC-NT21 with or without YC-1, which displays a 10-fold tightening of the CO dissociation constant upon YC-1 binding. (C) CO saturation binding curve for *Ms* sGC-β_1(1−380) with or without YC-1, which displays little change in CO binding affinity upon YC-1 binding. Titrations were performed in a 10 cm cuvette at room temperature with 0.1 μM protein in buffer containing 50 mM potassium phosphate (pH 7.4), 100 mM KCl, 5% glycerol, and 50 μM YC-1. The data were corrected for dilution upon addition of CO-saturated buffer and were fit to a single-site saturation model to obtain the CO dissociation constants.

To further narrow the YC-1 binding location, we examined an *Ms* sGC protein lacking the entire α_1 chain. This protein binds CO with high affinity (~0.2 μM) in the presence or absence of YC-1 (Figure 2 and Table 1). Thus, YC-1 appears to have no effect on CO binding affinity in the absence of the α chain, and importantly, CO binding is as tight in the absence of the α chain as it is in the presence of YC-1 for any of the heterodimeric *Ms* sGC proteins, displaying a K_d^{CO} value of ~200 nM. We conclude that both the α_1 PAS and H-NOX domains lower the CO affinity for the sGC heme. Binding of YC-1 appears to relieve this restraint.

We examined the bovine β_1 subunit to extend our results to a mammalian sGC. The bovine protein displays the same overall domain structure as *Ms* sGC and has an overall level of sequence identity of 60% with the β_1 subunit and 39% with the α_1 subunit. We produced two *Bt* sGC forms, one containing just the H-NOX domain and one containing the H-NOX and PAS domain. As with *Ms* sGC β_1, neither *Bt* sGC β_1 construct displayed YC-1 sensitivity (Table 1). Binding of CO to the bovine protein was less tight, however, and differed between the H-NOX domain- and H-NOX-PAS domain-containing proteins, with the shorter construct having the greatest affinity (~1 μM) and the longer construct binding with ~10-fold less affinity. Homodimer formation in *Bt* sGC β_1(1−359) may contribute to the lower CO affinity [*Ms* sGC β_1(1−380) behaves as a monomer].

Binding Affinity of YC-1 for *Ms* sGC. The data in Table 1 indicate the YC-1 binding site is within the *Ms* sGC-NT21 construct and, furthermore, that YC-1 enhancement of CO binding requires an intact α_1 PAS domain. Measurement of the binding affinity of YC-1 for sGC, which is needed to clarify where on the protein binding takes place, is frustrated by the poor solubility of YC-1 in aqueous solutions and by the tendency for YC-1 to bind nonspecifically to proteins. We therefore employed a multidimensional binding assay to extract the YC-1 dissociation constant through analysis of the linked equilibria between CO binding and YC-1 binding (Figure 3 and Table 2). For a system displaying linked equilibria, binding of either ligand, in this case CO or YC-1, will affect the binding of the other. We therefore measured CO binding affinity as a function of YC-1 concentration for *Ms* sGC-NT21 (10 cm cuvette) and *Ms* sGC-NT13 (1 cm cuvette). Linked equilibrium analyses yielded $K_d^{YC\text{-}1}$ values of 9.3 and 21 μM, respectively, for the two proteins in the absence of NO and CO (Table 2). Cooperativity factors of 14 and 19 (Table 3), reflecting the influence of one ligand on binding of the other, were also derived from these data, from which the dissociation constant for the binding of YC-1 to the CO-saturated protein ($K_d^{YC\text{-}1\prime}$) can be derived. These values were 0.7 and 1.1 μM for *Ms* sGC-NT21 and *Ms* sGC-NT13, respectively (Table 2).

We also directly measured binding of YC-1 to CO-saturated heterodimeric *Ms* sGC proteins by monitoring the ~2 nm blue shift in the Soret absorption band that occurs upon YC-1 binding.[41,51] Monitoring of this shift while titrating in YC-1 allowed the estimation of compound affinity (Figure 4, Table

Table 1. CO Dissociation Constants for sGC Proteins[a]

protein	α_1 residues	β_1 residues	K_d^{CO} (μM)	$K_d^{CO\prime}$ (μM) (ligand)	ref
Bt sGC (full length)	1–691	1–619	127	~26 (YC-1)	51
			97		76
Hs sGC (full length)	1–690	1–619	260		77
Ms sGC-NT2	49–471	1–401	77 ± 7	1.7 ± 0.1 (YC-1)	33
			90 ± 9	1.0 ± 0.1 (YC-1)	43
Ms sGC-NT13	49–450	1–380	53 ± 4	2.8 ± 0.4 (YC-1)	this work
				2.9 ± 0.2 (PF-25)	this work
				0.25 ± 0.02[b] (BAY)	this work
Ms sGC-NT19	49–450	1–380	50 ± 3	0.8 ± 0.1 (YC-1)	43
Ms sGC-NT21	272–450	1–380	2.2 ± 0.2[b]	0.20 ± 0.02[b] (YC-1)	this work
				0.24 ± 0.01[b] (PF-25)	this work
				0.07 ± 0.01[b] (BAY)	this work
Ms sGC β_1(1–380)	absent	1–380	0.20 ± 0.03[b]	0.18 ± 0.05[b] (YC-1)	this work
Bt sGC β_1(1–197)	absent	1–197	1.6 ± 0.2[c]	1.2 ± 0.2[c] (YC-1)	this work
Bt sGC β_1(1–359)	absent	1–359	15 ± 4	10 ± 3 (YC-1)	this work

[a]Titration binding data were measured using gastight syringes and 1 or 10 cm cuvettes fitted with rubber septa. The protein concentration was 1 μM unless otherwise indicated. Where included for measuring $K_d^{CO\prime}$, the YC-1 and PF-25 concentrations were 50 μM and the BAY 41-2272 concentration was 2.5 μM (*Ms* sGC-NT21) or 10 μM (*Ms* sGC-NT13). Values are means and the standard deviation of at least three independent measurements. [b]Measured in a 10 cm cuvette, using 0.1 μM protein. [c]Measured in a 1 cm cuvette, using 0.5 μM protein.

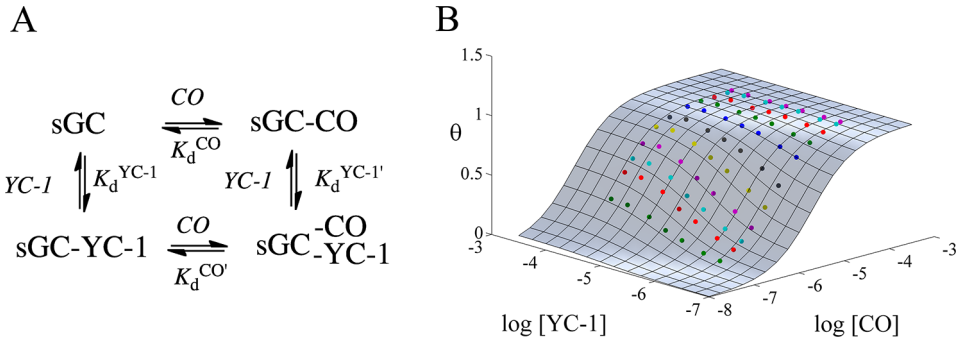

Figure 3. Ligand binding and linked equilibria in sGC. (A) Linked equilibrium diagram showing four different states for binding of CO and YC-1 to sGC. (B) Global fitting of the fraction of CO sites occupied (θ) to the normalized $\Delta A_{(423-437)}$ for *Ms* sGC-NT21 (10 cm cuvette) using MATLAB. The surface represents the extent of CO binding as a function of CO and YC-1 concentration. Colored points indicate the measured $\Delta A_{(423-437)}$. Titrations were performed in a 10 cm cuvette at room temperature with 0.1 μM protein in buffer containing 50 mM potassium phosphate (pH 7.4), 100 mM KCl, 5% glycerol, and YC-1 concentrations ranging from 0 to 50 μM.

Table 2. YC-1, PF-25, and BAY 41-2272 Dissociation Constants for sGC Proteins (micromolar)

	without NO or CO			with CO			with NO
protein	K_d^{YC-1}	K_d^{PF-25}	K_d^{BAY}	$K_d^{YC-1\prime}$	$K_d^{PF-25\prime}$	$K_d^{BAY\prime}$	$K_d^{PF-25\prime}$
Ms sGC-NT13	21 ± 5[a]	155 ± 11[a]	17 ± 3[b]	1.1 ± 0.3[a]	3.0 ± 0.3[a]	0.08 ± 0.01[e]	
				0.8 ± 0.1[d]	2.8 ± 0.2[d]		
Ms sGC-NT21	9.3 ± 0.8[a]	73 ± 21[a]	2.0 ± 0.5[a]	0.67 ± 0.06[a]	3.8 ± 1.4[a]	0.03 ± 0.01[a]	11 ± 2[c]
		153 ± 5[c]		0.6 ± 0.1[e]	0.9 ± 0.3[d]	0.09 ± 0.02[e]	
Ms sGC β_1(1–380)		92 ± 5[c]					7 ± 1[c]
Ms sGC α_1 PAS		NB[c]					NB[c]
Bt sGC (full length)	52[f]			~8[h]			
	~20[g]						

[a]From global fitting of multidimensional titration data (see the text). For *Ms* sGC-NT13, titration occurred in a 1 cm cuvette with 1 μM protein. For *Ms* sGC-NT21, titration occurred in a 10 cm cuvette with 0.1 μM protein. Values are means and the standard deviation of three independent measurements. Values for $K_d^{YC-1\prime}$ were obtained using the cooperativity factors listed in Table 3. [b]Estimated assuming linked equilibria: $(K_d^{CO}/K_d^{CO\prime})K_d^{BAY\prime}$. [c]From SPR (see the text). Values in the absence of NO were fit with a calculated R_{max}, and those in the presence of NO were fit with a floating R_{max}. Errors are from the fitting. NB means no binding. [d]From fitting of the Soret shift (1 cm cuvette). Values are means and the standard deviation of three to five independent measurements. For YC-1, 1 μM protein was used. For PF-25, both 1 and 0.5 μM protein was used. [e]From fitting of the Soret shift (1 and 10 cm cuvettes). Values are means and the standard deviation of 3–10 independent measurements. For YC-1 (10 measurements), measurements with protein concentrations of 0.1 μM (10 cm cuvette) and 0.5 and 1.0 μM (1 cm cuvette) were included. For BAY 41-2272 (three measurements), protein concentrations of 0.05 and 0.1 μM were included (10 cm cuvette). [f]From ref 32, measured in the presence of Mn^{2+}. [g]From ref 24, with an EC_{50} value for stimulating bovine sGC in the absence of NO or CO. [h]From ref 51, measured in the presence of GTP.

Table 3. Cooperativity Factors for sGC Proteins

	K_{int} (CO)[a]			$K_d^{CO}/K_d^{CO'}$			$K_d^{PF\text{-}25}/K_d^{PF\text{-}25'}$ (NO)
protein	YC-1	PF-25	BAY	YC-1	PF-25	BAY	PF-25
Ms sGC-NT13	19 ± 2	53 ± 3	NM[b]	19 ± 3	18 ± 2	212 ± 23	
Ms sGC-NT21	13.8 ± 0.3	19 ± 4	58 ± 7	11 ± 1	9 ± 1	31 ± 5	14 ± 3
Ms sGC β_1(1−380)							13 ± 2

[a]From global fitting. [b]Could not be readily measured by global fitting because of the large cooperativity factor, requiring that both 1 and 10 cm cuvettes be used.

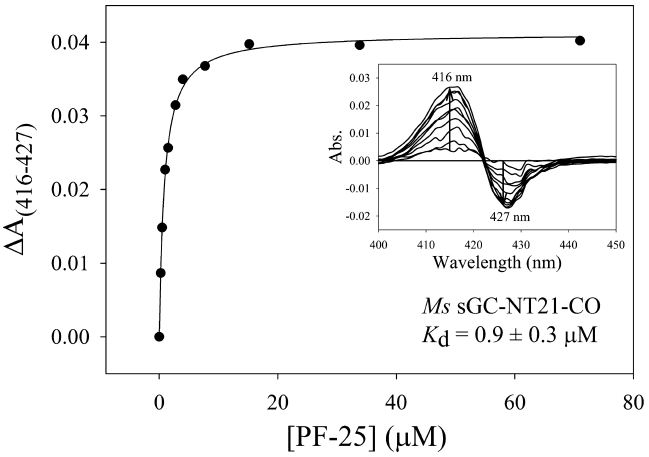

Figure 4. Binding of YC-1 to *Ms* sGC-NT-CO. Representative curve for binding of PF-25 to *Ms* sGC-NT21-CO. *Ms* sGC-NT-CO complexes were prepared in either 1 cm (1 μM protein, shown) or 10 cm (0.1 μM protein, BAY 41-2272) septum-capped cuvettes containing CO-saturated buffer [50 mM potassium phosphate (pH 7.4), 100 mM KCl, and 5% glycerol]. YC-1 family compounds (1 or 15 mM in ethanol) were titrated into the cuvettes, and the shift in the Soret band was monitored [$\Delta A_{(416-427)}$]. The data were fit to a single-site saturation model to obtain the dissociation constants for binding of the compound to the *Ms* sGC-NT-CO complex. The inset shows difference spectra upon compound titration. Ethanol or DMSO alone or other unrelated ring-containing compounds do not generate a shift in the Soret band (data not shown).

2). We examined binding of YC-1 to *Ms* sGC-NT21-CO and *Ms* sGC-NT13-CO in 10 and 1 cm cuvettes, respectively, which yielded values nearly identical to those obtained from the linked equilibrium analysis (Table 2). Likewise, estimating cooperativity factors by linked equilibrium analysis or by the ratio of K_d^{CO} to $K_d^{CO'}$ yielded similar values (Table 3), indicating good internal consistency between the two approaches. A shift in Soret band maxima was not observed for *Ms* sGC β_1(1−380).

Relative YC-1, BAY 41-2272, and PF-25 Binding Affinities. We examined binding by compounds BAY 41-2272, which is active at concentrations lower than those of YC-1,[22] and Pfizer compound 25 (PF-25), a recently described compound with greater aqueous solubility.[44] PF-25 behaves like other YC-1 family compounds, stimulating human sGC in the presence of NO (EC_{20} = 80 nM) and relaxing preconstricted aortic rings (IC_{50} = 60 nM). Both compounds are derived from YC-1 (Figure 1), differing mainly through substitution of the YC-1 furan ring. Affinity measurements were taken using linked equilibria and/or the Soret band shift. Interestingly, differences were observed among the compounds for binding to both the unliganded and CO-liganded proteins, and for their associated cooperativity factors. As with CO, YC-1 family compounds also bind tighter to *Ms* sGC-NT21 than to *Ms* sGC-NT13, indicating that the α_1 H-NOX domain not only interferes with CO binding but also interferes with YC-1 family compound binding (Table 2). The effect of H-NOX removal on stimulator binding is greater for BAY 41-2272 (~9-fold) than for YC-1 or PF-25 (~2-fold).

Binding of stimulator compounds to the CO complexes is much tighter than binding to the unliganded proteins. The greatest enhancement is seen for BAY 41-2272, which binds to the CO complex with a K_d of 30−90 nM, whereas YC-1 binds with a K_d of ~1 μM and PF-25 with a K_d of ~3 μM (Table 2). PF-25 binds particularly poorly to the unliganded proteins (70−150 μM).

Measuring PF-25 Binding Using Surface Plasmon Resonance. We hypothesized that YC-1 family compounds bind to the α_1 PAS domain because (i) PAS domains commonly bind small molecules in their capacity as signaling proteins,[11] (ii) the α_1 PAS domain is required for observing a YC-1-dependent enhancement in CO affinity (Table 1), and (iii) addition of YC-1 did not lead to a shift in the Soret absorption band for any of the proteins lacking the α chain. To directly address whether YC-1 binds to the α_1 PAS domain, we used surface plasmon resonance (SPR), allowing for binding measurements that were not dependent on heme spectra. To accomplish this, we specifically biotinylated *Ms* sGC NT21, α_1 PAS, and β_1(1−380) at their C-termini, using biotin ligase (BirA) and sGC proteins modified to contain the BirA recognition sequence.[52] The biotinylated proteins were captured in the SPR instrument on a NeutrAvidin-coated sensor chip, and analyte binding was examined. Unfortunately, neither YC-1 nor BAY 41-2272 was suitable for SPR binding measurements because of their poor solubility in aqueous buffer. Introducing these compounds required a percentage of DMSO greater than the percentage that was well tolerated by the protein over the course of the measurements, which take hours to complete. We therefore turned to PF-25, a compound better suited to SPR measurements because of its greater aqueous solubility.

Binding of PF-25 to *Ms* sGC NT21 was clearly observed in the SPR instrument (Figure 5). Binding was rapid, as expected from our CO titration experiments, making k_{on} measurements unreliable. Release was also rapid and difficult to quantify. Ligand affinity was therefore estimated through saturation binding, leading to a $K_d^{PF\text{-}25}$ of 153 μM, a value similar to that observed through analysis by linked equilibria. Unexpectedly, binding to *Ms* sGC β_1(1−380) was also observed ($K_d^{PF\text{-}25}$ = 92 μM). In contrast, binding to *Ms* sGC α_1 PAS was not observed. Thus, these data indicated PF-25 binds to the β_1 chain between residues 1 and 380.

Measuring binding of PF-25 to the CO-saturated protein was not possible because the SPR instrument has an in-line degasser to prevent bubble formation. We therefore examined binding after addition of NO to the heme-containing constructs, which could be saturated with small amounts of NO released *in situ*. Unlike with CO, only nanomolar concentrations of NO were

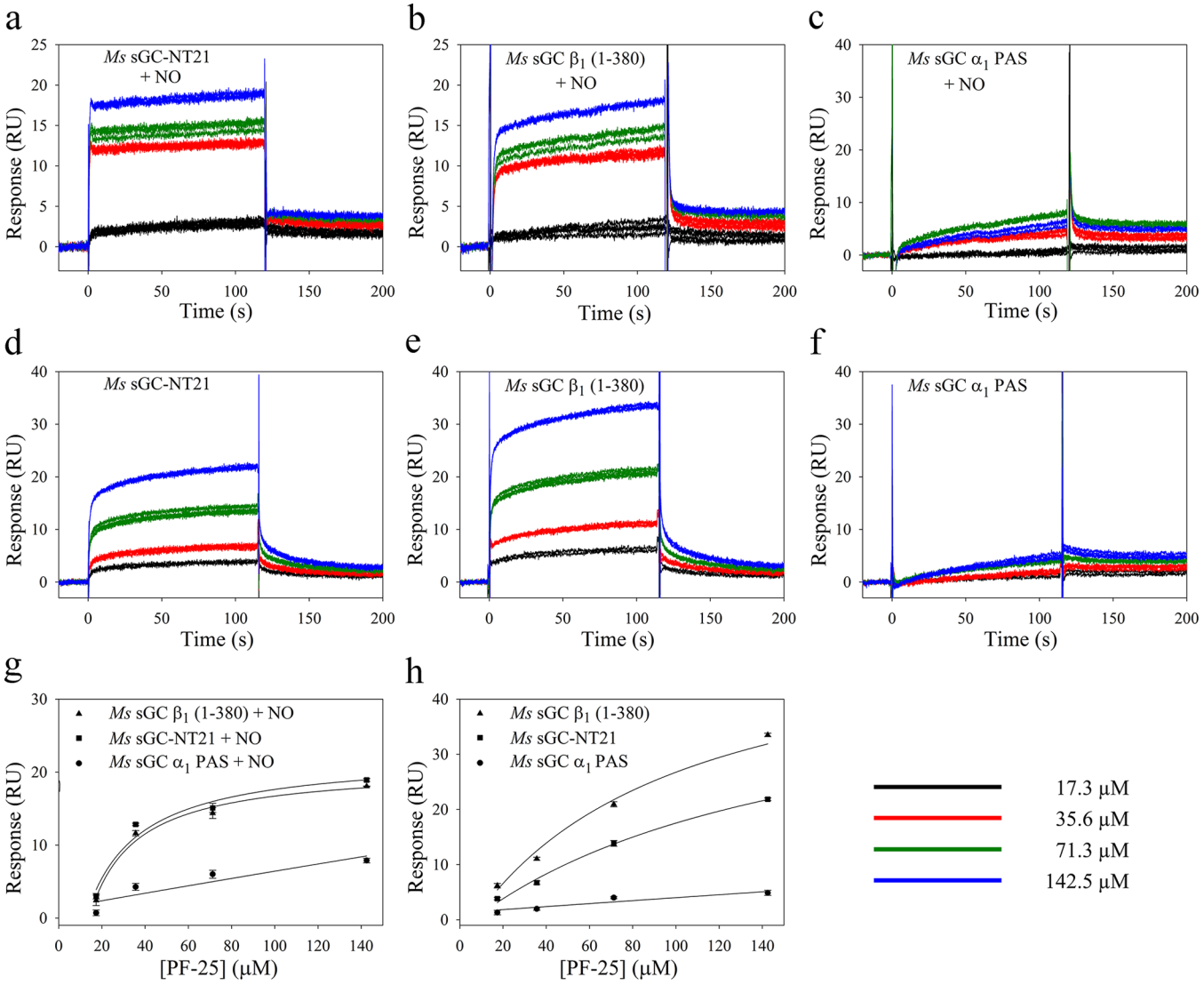

Figure 5. Binding of PF-25 to *Ms* sGC constructs examined by surface plasmon resonance. Biotinylated *Ms* sGC-NT21, *Ms* sGC α_1 PAS, and *Ms* sGC β_1(1−380) were captured on an SPR chip containing immobilized NeutrAvidin. Solutions of PF-25 with or without DEA/NO were injected into the chip, and the response change was recorded. The injected samples contained 50 mM potassium phosphate buffer (pH 7.4), 100 mM KCl, 2 mM EDTA, 1 mM TCEP, 1% DMSO, PF-25 (0−142.5 μM), and, where included, 25 μM DEA/NO. Shown are representative sensorgrams for PF-25 binding in the presence (a−c) and absence (d−f) of DEA/NO. Three trials are shown for each PF-25 concentration. Binding data were analyzed with the Biacore T-100 evaluation software. Values for K_d were obtained using a single-site saturation model (SigmaPlot) by plotting the response (RU) with respect to PF-25 concentration using a floating R_{max} (g) or a calculated R_{max} (h).

required for these measurements because of the high affinity of NO for sGC heme (picomolar to nanomolar) and the small amount of protein captured on the chip surface (picomoles). Binding of NO to heme enhanced binding of PF-25 to *Ms* sGC NT21 as expected ($K_d^{PF\text{-}25\prime}$ = 11 μM) but, in contrast to CO, also enhanced binding of PF-25 to *Ms* sGC β_1(1−380) (Figure 5 and Table 2), yielding a $K_d^{PF\text{-}25\prime}$ of 7 μM. Surprisingly, PF-25 also bound slightly weaker to *Ms* sGC-NT21-NO than to *Ms* sGC-NT21-CO. The reason for these differences in binding is not yet clear but is presumably due to differences in the conformations of the NO and CO complexes.

Binding of YC-1 to *Ms* sGC PAS Domains Is Not Observed by Fluorescence Anisotropy. We examined binding of YC-1 to PAS domains in solution using fluorescence anisotropy. Various proteins were titrated into a YC-1-containing solution, and changes in YC-1-dependent fluorescence anisotropy were monitored. Weak binding (>100 μM) was indicated for *Ms* sGC α_1 PAS, but not for lysozyme. However, the data were extremely noisy, nonsaturable, and slow to equilibrate, suggesting the observed interaction was nonspecific. Likewise, a weak signal was also seen for the β_1 PAS domain, although it was less substantial, and also likely to be due to nonspecificity. Binding to heme-containing *Ms* sGC proteins could not be measured because of signal quenching by the heme. Although inconclusive, these data indicate the individual sGC PAS domains do not contain the YC-1 binding site, consistent with our SPR data.

DISCUSSION

YC-1 family compounds show great promise for the treatment of cardiovascular disease through their stimulation of sGC, yet their mechanism of action remains unknown. Likewise, the mechanism by which binding of NO to sGC heme stimulates cyclase activity is unclear. Here, we show that (i) the α_1 PAS

dx.doi.org/10.1021/bi4015133 | *Biochemistry* 2014, 53, 101−114

domain inhibits binding of CO, and presumably NO, to the β_1 heme domain, (ii) binding of YC-1 overcomes this inhibition, (iii) binding of YC-1 and CO or NO to heterodimeric sGC displays linked equilibria, with binding of one enhancing binding of the other, (iv) monomeric β_1 sGC displays high CO affinity and loss of CO−YC-1 linked equilibria, and (v) YC-1 binds to the β_1 chain, most likely in the heme domain. A model emerges from our study in which the α_1 H-NOX and PAS domains act to inhibit the β_1 H-NOX domain, which, in turn, acts to inhibit the cyclase domain. Activation of cyclase can occur through the relieving of either inhibitory contact; maximal activity occurs when both inhibitory contacts are removed. In what follows, we expand upon these findings.

YC-1 Binding to or near the sGC Heme Domain. Discovery of the YC-1 binding site has been challenging because of the difficulty in working with sGC protein. Suggestions in the literature for where YC-1 binds invoke nearly all sGC domains, including the α_1 H-NOX domain,[33,34,53] the catalytic domain,[31,32,54] and the heme domain.[35−38,55,56] Here, using SPR, we demonstrate that binding is to the N-terminal portion of the β_1 chain. Because binding to the β_1 PAS domain could not be detected by fluorescence anisotropy measurements, binding is most likely to the heme-containing β_1 H-NOX domain. Additionally, a recent report notes that a human sGC construct lacking both H-NOX domains is not stimulated by BAY 41-2272, while full-length sGC is.[57]

Binding of YC-1 leads to an ∼2 nm shift in the Soret absorption band for the CO complex,[38,41,55] which we used to determine the YC-1 dissociation constants to be 0.8 and 0.6 μM for *Ms* sGC-NT13-CO and *Ms* sGC NT21-CO, respectively (Figure 4 and Table 2). Others have used this shift in absorbance,[38,55] or a shift in the Raman heme spectrum upon addition of YC-1 or BAY 41-2272,[35−37,56,58] to argue that YC-1 family compounds bind to the heme domain. However, the high concentrations of YC-1 used in those studies (generally 200 μM) raise the concern that the spectral changes may have arisen from nonspecific binding. Here, we demonstrate that only nanomolar quantities of YC-1 are required for inducing the shift in the *Ms* sGC-NT-CO Soret absorption band, consistent with a specific binding event.

YC-1 readily enhances CO binding in *Ms* sGC-NT proteins (Table 1 and ref 33), which lack the cyclase domain, but does not stimulate the isolated cyclase domains.[59] YC-1 also readily enhances binding of CO to *Ms* sGC-NT21 (Table 1 and ref 43), which does not contain the α_1 H-NOX domain, ruling out the possibility of the α_1 H-NOX domain containing the binding site. A similar conclusion was reached for truncated versions of mammalian sGC proteins.[48−50] These data, taken together with our SPR and spectral data, provide a compelling argument for heme domain binding of YC-1 family compounds.

Results using the bovine protein are qualitatively the same as those for the *Manduca* protein but differ in the dissociation constants for CO binding. *Bt* sGC β_1(1−197) binds CO ∼8-fold less tightly than *Ms* sGC β_1(1−380) (Table 1), while binding by *Bt* sGC β_1(1−359) is weaker yet, ∼9-fold weaker than binding by *Bt* sGC β_1(1−197). Neither bovine protein displays a significant response to YC-1. The difference in CO affinity between *Bt* sGC β_1(1−197) and *Bt* sGC β_1(1−359) may result from stabilization of the lower-affinity form of the H-NOX domain upon homodimer formation in the larger protein or from interactions between the H-NOX and PAS domains.

YC-1 Binding Relieves Inhibition of the β_1 Heme Domain by the α_1 H-NOX and PAS Domains. Perhaps our most unexpected finding is that the affinity of CO for heme in the β_1 H-NOX domain is as high in the absence of other domains as it is in the presence of YC-1 (Table 1). We showed previously that YC-1 binding leads to tighter CO binding in *Ms* sGC-NT constructs[33] and that binding leads to the development of a geminate recombination phase upon CO photolysis.[41] Negrerie and co-workers recently showed that the isolated human H-NOX domain [β_1(1−190)] also displays a geminate rebinding phase whereas the full-length protein does not.[60] This tighter binding and trapped CO correlate with increased cyclase activity for full-length sGC proteins.[25,61] We now show that both the α_1 PAS and α_1 H-NOX domains impair CO binding (Table 1). Removal of the α_1 H-NOX domain enhances CO binding by 24-fold, and complete removal of the α_1 chain enhances CO binding by 265-fold (Table 1). Binding of CO to *Ms* sGC β_1(1−380) in the absence of YC-1 is as tight (K_d^{CO} = 0.20 μM) as binding to any of the *Ms* sGC-NT proteins in the presence of YC-1. Cooperativity in binding of CO to any of the constructs missing the α_1 chain is now largely absent (K_{int} ∼ 1), and YC-1 binding does not appreciably enhance CO binding (Table 1). In addition to tightly binding CO, *Ms* sGC β_1(1−380) presumably also binds tightly to YC-1 and BAY 41-2272.

The situation with NO binding is similar to that for CO but apparently differs with respect to cooperativity. Unlike CO binding, NO binding leads to proximal histidine cleavage and a five-coordinate Fe−NO complex. NO release is multiphasic. We previously showed that binding of YC-1 to *Ms* sGC-NT-NO eliminated the faster of two NO release rates, yielding a protein with higher NO affinity, much like what occurs with CO.[33] However, unlike with CO, the data in Table 2 indicate that binding of NO enhances binding of PF-25 to *Ms* sGC β_1(1−380) by ∼10-fold, indicating that cooperativity occurs for NO with this protein but not for CO. The reason for this difference is unclear but may have to do with the difference in heme domain conformation for the five-coordinate and six-coordinate *Ms* sGC proteins.

We recently determined the crystal structure of *Ms* sGC α_1 PAS[17] and a molecular model for domain packing based on homology modeling, chemical cross-linking, and SAXS analysis.[43] These data indicate a direct contact between one face of helix Fα in *Ms* sGC α_1 PAS, involving residues Glu 340 and Lys 343, and the subdomain containing proximal His 105 that is proposed to be involved in signal transduction[62−64] (Figure 6). This contact in the intact protein may serve to stabilize the H-NOX domain in a low-affinity conformation. A pocket in this subdomain identified in our homology model may be the YC-1 binding site and provide a means for counteracting the effects of α_1 PAS inhibition. Our cross-linking data also indicate direct contact between the α_1 and β_1 H-NOX domains (Figure 6). This contact is farther from the heme and may serve to enhance the α_1 PAS−β_1 H-NOX interaction.

Binding Affinity of YC-1 Family Compounds. Just as YC-1 binding enhances binding of CO to heterodimeric sGC, CO binding enhances YC-1 binding, highlighting both the allosteric nature of sGC and the linked equilibria between CO and YC-1 binding events. Binding to *Ms* sGC-NT13 in the absence of CO (Figure 3 and Table 2) varies from ∼20 μM for YC-1 and BAY 41-2272 to 155 μM for PF-25. Binding to *Ms* sGC-NT21 is slightly tighter than to *Ms* sGC-NT13, particularly for BAY 41-2272, indicating that the α_1 H-NOX

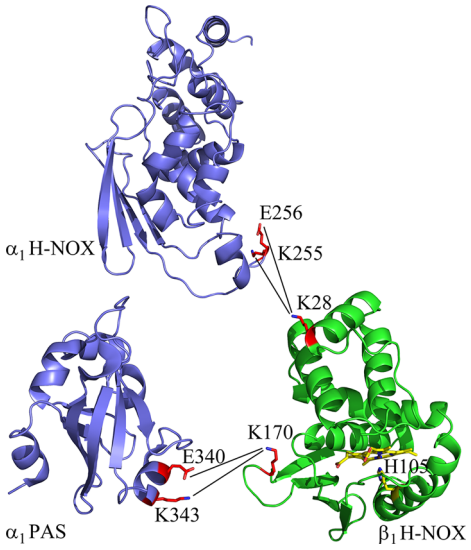

Figure 6. Contact residues of α_1 H-NOX, α_1 PAS, and β_1 H-NOX domains. Shown is the crystal structure for the α_1 PAS domain (Protein Data Bank entry 4GJ4[17]) and homology models for the α_1 and β_1 H-NOX domains. Cross-links between the two domains identified by mass spectrometry are shown,[43] as are the heme and proximal histidine in the β_1 H-NOX domain. This figure was prepared using PyMOL (W. L. DeLano, http://www.pymol.org).

domain inhibits not only CO binding but also binding by stimulator compounds.

Binding of YC-1 family compounds to *Ms* sGC-NT-CO complexes is 10−200-fold tighter than that to *Ms* sGC-NT (Figure 4 and Tables 2 and 3). BAY 41-2272 binds particularly tightly to the CO complexes, displaying dissociation constants of 30−90 nM. Thus, the enhanced stimulation of sGC by BAY 41-2272 as compared to that with other YC-1 family compounds appears to be due to especially tight binding to the active conformation.

Binding of PF-25 to the *Ms* sGC-NT21-NO complex, examined using SPR, was ∼2-fold weaker than binding to the *Ms* sGC β_1(1−380)-NO complex, consistent with the unliganded and CO-bound binding studies (Table 2), and consistent with a model in which the α_1 PAS domain inhibits binding of CO, NO, or YC-1 family compounds. Interestingly, binding of PF-25 to the *Ms* sGC-NT21-NO complex is 3−12-fold weaker than binding to the *Ms* sGC-NT21-CO complex.

The YC-1 dissociation constants we measure for the unliganded and truncated *Ms* sGC proteins are similar to those reported for binding and stimulating the full-length protein. Binding to full-length bovine lung sGC was monitored using equilibrium dialysis, yielding a K_d of 52 μM when measured in the presence of Mn^{2+},[32] and by the effective concentration needed to achieve 50% maximal stimulation of unliganded bovine sGC, yielding an EC_{50} of ∼20 μM.[24] These values compare favorably with those of a stimulator binding to *Ms* sGC-NT13 ($K_d^{YC\text{-}1}$ = 21 μM). Additionally, similar concentrations are needed for BAY 41-2272 to bind *Ms* sGC-NT21-CO ($K_d^{BAY'}$ = 0.09 μM) and for BAY 41-2272 to stimulate sGC in preconstricted aortic rings (EC_{50} = 0.3 μM[34]). This agreement between binding affinity for *Ms* sGC-NT and the concentration needed to stimulate activity in the full-length protein provides confidence that our measurements reflect the functionally important binding events.

A Model for sGC Regulation. The model that emerges from our data is one in which the low-energy state for the heme pocket differs between the isolated β_1 H-NOX domain and heterodimeric sGC (Figure 7). In the isolated domain, the

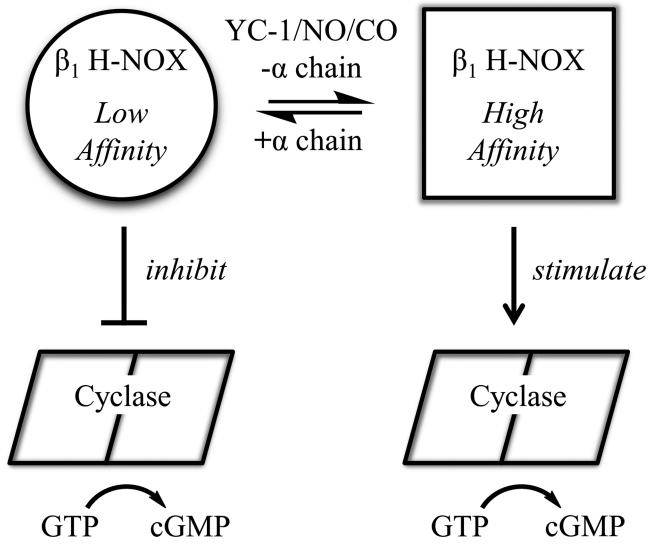

Figure 7. Model for sGC regulation. Shown is a proposed model for allosteric regulation in sGC in which the β_1 H-NOX is in equilibrium between high- and low-affinity conformations. YC-1, NO, CO, and the absence of α_1 chain H-NOX and PAS domains all shift the equilibria toward high affinity, while the α_1 chain H-NOX and PAS domains shift the equilibria toward low affinity. The low-affinity conformer is inhibitory toward the cyclase domains, while the high-affinity conformer is noninhibitory or possibly stimulatory.

heme pocket traps CO and NO, leading to high affinity for these ligands. In heterodimeric sGC, the heme pocket changes conformation such that NO and CO can more readily escape and binding affinity is reduced. Binding of YC-1 family compounds to heterodimeric sGC alters or severs the connection between the heme domain and α_1 subunit, returning the heme domain to its high-affinity conformation. A prediction of this model is that CO or NO binding will induce the high-affinity heme domain conformation, leading to tighter binding by YC-1 family compounds. Linked equilibria were in fact observed: YC-1 family compounds bind 10−200-fold more tightly in the presence of CO or NO than in their absence (Table 2).

A second prediction of this model is that the low-affinity H-NOX conformation inhibits cyclase activity, while the high-affinity conformation relieves this inhibition or is stimulatory. In this way, binding of either YC-1 or CO/NO leads to cyclase activation, and binding of both yields full sGC activation. Support for this model comes from studies of sGC mutant β_1H105C, in which the heme proximal histidine is mutated to cysteine, leading to heme-free sGC and a presumably high-affinity conformation for the H-NOX domain. This protein displays high basal catalytic activity and can still be stimulated by YC-1.[65,66] Additional support for the model comes from studies of the rat cyclase domain alone and after addition of the H-NOX domain in trans, which leads to inhibition of cyclase activity[67] and protection of cyclase from hydrogen−deuterium exchange.[64] Although inhibition was insensitive to NO, these data support a model in which the H-NOX domain directly binds to and inhibits the cyclase domain.[67] The possibility that

the high-affinity heme domain conformation may in fact stimulate cyclase activity rather than simply remove an inhibitory contact is suggested by experiments with sGC lacking both H-NOX domains, which displays only basal catalytic activity.[57] Interestingly, this protein is also insensitive to BAY 41−2272.

A third prediction of this model is that linked equilibria should exist between nucleotide binding to the cyclase domain and ligand binding to the heme domain. The fact that such a link exists has been previously described.[68−70] In the presence of nucleotide, NO release is slowed,[69] full stimulation by NO enhanced,[68] and desensitization delayed.[70]

How the β_1 H-NOX domain switches from low to high CO and NO affinity is unknown. One recently proposed possibility is that the proximal heme pocket is strained in the low-affinity form, leading to heme distortion and inherently poor CO and NO binding affinity. Upon bond breakage, CO and NO escape rather than re-bind to heme.[38,60,71,72] In the high-affinity state, proximal strain is relieved by movement of the proximal histidine and heme iron into the plane of the porphyrin ring, yielding greater CO or NO affinity and a higher capture rate.[72] This model is reminiscent of the "relaxed" and "tense" states described for hemoglobin.

A second possibility is for the heme domain to adopt "open" and "closed" conformations, in which the closed conformation hinders the escape of CO or NO and favors capture by heme. This is the strategy employed by *Rhodnius prolixus* nitrophorin 4, an NO transport protein. In nitrophorin 4, two loops collapse into the heme pocket at low pH, generating a closed conformation, an increased level of geminate recombination, and a higher affinity for NO.[73−75] Distinguishing between these models awaits determination of high-resolution structures.

AUTHOR INFORMATION

Corresponding Author

*Department of Chemistry and Biochemistry, The University of Arizona, 1041 E. Lowell St., Tucson, AZ 85721. E-mail: montfort@email.arizona.edu. Telephone: (520) 621-1884. Fax: (520) 626-9204.

Funding

This work was supported in part by grants from the National Institutes of Health (HL062969 to W.R.M. and U54 CA143924 to W.R.M. and M.J.G.) and the American Heart Association (11PRE7610113 to R.P. and 10SDG2600345 to E.D.G.).

Notes

The authors declare no competing financial interest.

ACKNOWLEDGMENTS

We thank Alex Hailey and Scott Ogley for help with evaluating expression of PAS domains containing differing C-termini. We are grateful to Jacquie Brailey for help with protein expression and to Dr. Patrick Loll for providing us with his SUMO fusion ligation-independent cloning vector. We thank Dr. Lee Roberts for Pfizer compound PF-25 and Dr. Katrina Miranda for DEA/NO. SPR data were acquired by the Arizona Proteomics Consortium supported by National Institute of Environmental Health Sciences Grant ES06694 to the Southwest Environmental Health Sciences Center, National Cancer Institute Grant CA023074 to the Arizona Cancer Center, and the BIO5 Institute of The University of Arizona. The Biacore T100 biosensor was provided though generous support of the Prescott Friends of the Sarver Heart Center with leadership gifts from Jim and Linda Lee, Ron and Laura James, and Swayze and Kathy McCraine.

ABBREVIATIONS

sGC, soluble guanylyl cyclase; *Ms* sGC, *M. sexta* sGC; *Bt* sGC, *Bos taurus* (bovine) sGC; DEA/NO, 2-(*N*,*N*-diethylamino)-diazenolate 2-oxide; CC, coiled coil; PAS, Per-ARNT-Sim; H-NOX, heme-nitric oxide/oxygen binding; SPR, surface plasmon resonance; SAXS, small-angle X-ray scattering.

REFERENCES

(1) Ignarro, L. J., Ed. (2010) *Nitric Oxide Biology and Pathobiology*, 2nd ed., Academic Press, San Diego.

(2) Bian, K., Doursout, M. F., and Murad, F. (2008) Vascular system: Role of nitric oxide in cardiovascular diseases. *J. Clin. Hypertens. (Hoboken, NJ, U.S.) 10*, 304−310.

(3) Coggins, M. P., and Bloch, K. D. (2007) Nitric oxide in the pulmonary vasculature. *Arterioscler., Thromb., Vasc. Biol. 27*, 1877−1885.

(4) Li, H., and Poulos, T. L. (2005) Structure-function studies on nitric oxide synthases. *J. Inorg. Biochem. 99*, 293−305.

(5) Stuehr, D. J., Tejero, J., and Haque, M. M. (2009) Structural and mechanistic aspects of flavoproteins: Electron transfer through the nitric oxide synthase flavoprotein domain. *FEBS J. 276*, 3959−3974.

(6) Brunton, T. L. (1867) Use of Nitrite of Amyl in Angina Pectoris. *Lancet 90*, 97−98.

(7) Murrell, W. (1879) Nitro-glycerine as a remedy for angina pectoris. *Lancet 113*, 113−115.

(8) Derbyshire, E. R., and Marletta, M. A. (2012) Structure and regulation of soluble guanylate cyclase. *Annu. Rev. Biochem. 81*, 533−559.

(9) Cary, S. P., Winger, J. A., Derbyshire, E. R., and Marletta, M. A. (2006) Nitric oxide signaling: No longer simply on or off. *Trends Biochem. Sci. 31*, 231−239.

(10) Nioche, P., Berka, V., Vipond, J., Minton, N., Tsai, A. L., and Raman, C. S. (2004) Femtomolar sensitivity of a NO sensor from *Clostridium botulinum*. *Science 306*, 1550−1553.

(11) Moglich, A., Ayers, R. A., and Moffat, K. (2009) Structure and signaling mechanism of Per-ARNT-Sim domains. *Structure 17*, 1282−1294.

(12) Liu, Y., Ruoho, A. E., Rao, V. D., and Hurley, J. H. (1997) Catalytic mechanism of the adenylyl and guanylyl cyclases: Modeling and mutational analysis. *Proc. Natl. Acad. Sci. U.S.A. 94*, 13414−13419.

(13) Dierks, E. A., Hu, S., Vogel, K. M., Yu, A. E., Spiro, T. G., and Burstyn, J. N. (1997) Demonstration of the role of scission of the proximal histidine-iron bond in the activation of soluble guanylyl cyclase though metalloporphyrin substitution studies. *J. Am. Chem. Soc. 119*, 7316−7323.

(14) Stone, J. R., and Marletta, M. A. (1996) Spectral and kinetic studies on the activation of soluble guanylate cyclase by nitric oxide. *Biochemistry 35*, 1093−1099.

(15) Wedel, B., Humbert, P., Harteneck, C., Foerster, J., Malkewitz, J., Böhme, E., Schultz, G., and Koesling, D. (1994) Mutation of His-105 in the β1 subunit yields a nitric oxide-insensitive form of soluble guanylate cyclase. *Proc. Natl. Acad. Sci. U.S.A. 91*, 2592−2596.

(16) Ma, X., Beuve, A., and van den Akker, F. (2010) Crystal structure of the signaling helix coiled-coil domain of the β1 subunit of the soluble guanylyl cyclase. *BMC Struct. Biol. 10*, 2.

(17) Purohit, R., Weichsel, A., and Montfort, W. R. (2013) Crystal structure of the α subunit PAS domain from soluble guanylyl cyclase. *Protein Sci. 22*, 1439−1444.

(18) Allerston, C. K., von Delft, F., and Gileadi, O. (2013) Crystal structures of the catalytic domain of human soluble guanylate cyclase. *PLoS One 8*, e57644.

(19) Pellicena, P., Karow, D. S., Boon, E. M., Marletta, M. A., and Kuriyan, J. (2004) Crystal structure of an oxygen-binding heme domain related to soluble guanylate cyclases. *Proc. Natl. Acad. Sci. U.S.A. 101*, 12854−12859.

(20) Ma, X., Sayed, N., Baskaran, P., Beuve, A., and van den Akker, F. (2008) PAS-mediated Dimerization of Soluble Guanylyl Cyclase Revealed by Signal Transduction Histidine Kinase Domain Crystal Structure. *J. Biol. Chem. 283*, 1167−1178.
(21) Ma, X., Sayed, N., Beuve, A., and van den Akker, F. (2007) NO and CO differentially activate soluble guanylyl cyclase via a heme pivot-bend mechanism. *EMBO J. 26*, 578−588.
(22) Evgenov, O. V., Pacher, P., Schmidt, P. M., Hasko, G., Schmidt, H. H., and Stasch, J. P. (2006) NO-independent stimulators and activators of soluble guanylate cyclase: Discovery and therapeutic potential. *Nat. Rev. Drug Discovery 5*, 755−768.
(23) Ko, F. N., Wu, C. C., Kuo, S. C., Lee, F. Y., and Teng, C. M. (1994) YC-1, a novel activator of platelet guanylate cyclase. *Blood 84*, 4226−4233.
(24) Friebe, A., Schultz, G., and Koesling, D. (1996) Sensitizing soluble guanylyl cyclase to become a highly CO-sensitive enzyme. *EMBO J. 15*, 6863−6868.
(25) Stone, J. R., and Marletta, M. A. (1998) Synergistic activation of soluble guanylate cyclase by YC-1 and carbon monoxide: Implications for the role of cleavage of the iron-histidine bond during activation by nitric oxide. *Chem. Biol. 5*, 255−261.
(26) Ramanathan, S., Mazzalupo, S., Boitano, S., and Montfort, W. R. (2011) Thrombospondin-1 and angiotensin II inhibit soluble guanylyl cyclase through an increase in intracellular calcium concentration. *Biochemistry 50*, 7787−7799.
(27) Belik, J. (2009) Riociguat, an oral soluble guanylate cyclase stimulator for the treatment of pulmonary hypertension. *Curr. Opin. Invest. Drugs 10*, 971−979.
(28) Mittendorf, J., Weigand, S., Alonso-Alija, C., Bischoff, E., Feurer, A., Gerisch, M., Kern, A., Knorr, A., Lang, D., Muenter, K., Radtke, M., Schirok, H., Schlemmer, K. H., Stahl, E., Straub, A., Wunder, F., and Stasch, J. P. (2009) Discovery of riociguat (BAY 63-2521): A potent, oral stimulator of soluble guanylate cyclase for the treatment of pulmonary hypertension. *ChemMedChem 4*, 853−865.
(29) Ghofrani, H. A., Galie, N., Grimminger, F., Grunig, E., Humbert, M., Jing, Z. C., Keogh, A. M., Langleben, D., Kilama, M. O., Fritsch, A., Neuser, D., and Rubin, L. J. (2013) Riociguat for the treatment of pulmonary arterial hypertension. *N. Engl. J. Med. 369*, 330−340.
(30) Ghofrani, H. A., D'Armini, A. M., Grimminger, F., Hoeper, M. M., Jansa, P., Kim, N. H., Mayer, E., Simonneau, G., Wilkins, M. R., Fritsch, A., Neuser, D., Weimann, G., and Wang, C. (2013) Riociguat for the treatment of chronic thromboembolic pulmonary hypertension. *N. Engl. J. Med. 369*, 319−329.
(31) Lamothe, M., Chang, F. J., Balashova, N., Shirokov, R., and Beuve, A. (2004) Functional characterization of nitric oxide and YC-1 activation of soluble guanylyl cyclase: Structural implication for the YC-1 binding site? *Biochemistry 43*, 3039−3048.
(32) Yazawa, S., Tsuchiya, H., Hori, H., and Makino, R. (2006) Functional characterization of two nucleotide-binding sites in soluble guanylate cyclase. *J. Biol. Chem. 281*, 21763−21770.
(33) Hu, X., Murata, L. B., Weichsel, A., Brailey, J. L., Roberts, S. A., Nighorn, A., and Montfort, W. R. (2008) Allostery in recombinant soluble guanylyl cyclase from *Manduca sexta*. *J. Biol. Chem. 283*, 20968−20977.
(34) Stasch, J.-P., Becker, E. M., Alonso-Alija, C., Apeler, H., Gerzer, R., Minuth, T., Perzborn, E., Pleiss, U., Schröder, H., Schroeder, W., Stahl, E., Steinke, W., Straub, A., and Schramm, M. (2001) NO-independent regulatory site on soluble guanylate cyclase. *Nature 410*, 212−215.
(35) Ibrahim, M., Derbyshire, E. R., Marletta, M. A., and Spiro, T. G. (2010) Probing soluble guanylate cyclase activation by CO and YC-1 using resonance Raman spectroscopy. *Biochemistry 49*, 3815−3823.
(36) Ibrahim, M., Derbyshire, E. R., Soldatova, A. V., Marletta, M. A., and Spiro, T. G. (2010) Soluble guanylate cyclase is activated differently by excess NO and by YC-1: Resonance Raman spectroscopic evidence. *Biochemistry 49*, 4864−4871.
(37) Martin, E., Czarnecki, K., Jayaraman, V., Murad, F., and Kincaid, J. (2005) Resonance Raman and infrared spectroscopic studies of high-output forms of human soluble guanylyl cyclase. *J. Am. Chem. Soc. 127*, 4625−4631.
(38) Yoo, B. K., Lamarre, I., Rappaport, F., Nioche, P., Raman, C. S., Martin, J. L., and Negrerie, M. (2012) Picosecond to second dynamics reveals a structural transition in *Clostridium botulinum* NO-sensor triggered by the activator BAY-41-2272. *ACS Chem. Biol. 7*, 2046−2054.
(39) Schmidt, P. M., Schramm, M., Schroder, H., Wunder, F., and Stasch, J. P. (2004) Identification of residues crucially involved in the binding of the heme moiety of soluble guanylate cyclase. *J. Biol. Chem. 279*, 3025−3032.
(40) Schindler, U., Strobel, H., Schonafinger, K., Linz, W., Lohn, M., Martorana, P. A., Rutten, H., Schindler, P. W., Busch, A. E., Sohn, M., Topfer, A., Pistorius, A., Jannek, C., and Mulsch, A. (2006) Biochemistry and pharmacology of novel anthranilic acid derivatives activating heme-oxidized soluble guanylyl cyclase. *Mol. Pharmacol. 69*, 1260−1268.
(41) Hu, X., Feng, C., Hazzard, J. T., Tollin, G., and Montfort, W. R. (2008) Binding of YC-1 or BAY 41-2272 to Soluble Guanylyl Cyclase Induces a Geminate Phase in CO Photolysis. *J. Am. Chem. Soc. 130*, 15748−15749.
(42) Fritz, B. G., Hu, X., Brailey, J. L., Berry, R. E., Walker, F. A., and Montfort, W. R. (2011) Oxidation and loss of heme in soluble guanylyl cyclase from *Manduca sexta*. *Biochemistry 50*, 5813−5815.
(43) Fritz, B. G., Roberts, S. A., Ahmed, A., Breci, L., Li, W., Weichsel, A., Brailey, J. L., Wysocki, V. H., Tama, F., and Montfort, W. R. (2013) Molecular Model of a Soluble Guanylyl Cyclase Fragment Determined by Small-Angle X-ray Scattering and Chemical Cross-Linking. *Biochemistry 52*, 1568−1582.
(44) Roberts, L. R., Bradley, P. A., Bunnage, M. E., England, K. S., Fairman, D., Fobian, Y. M., Fox, D. N., Gymer, G. E., Heasley, S. E., Molette, J., Smith, G. L., Schmidt, M. A., Tones, M. A., and Dack, K. N. (2011) Acidic triazoles as soluble guanylate cyclase stimulators. *Bioorg. Med. Chem. Lett. 21*, 6515−6518.
(45) Weeks, S. D., Drinker, M., and Loll, P. J. (2007) Ligation independent cloning vectors for expression of SUMO fusions. *Protein Expression Purif. 53*, 40−50.
(46) Liu, H., and Naismith, J. H. (2008) An efficient one-step site-directed deletion, insertion, single and multiple-site plasmid mutagenesis protocol. *BMC Biotechnol. 8*, 91.
(47) Kapust, R. B., Tozser, J., Fox, J. D., Anderson, D. E., Cherry, S., Copeland, T. D., and Waugh, D. S. (2001) Tobacco etch virus protease: Mechanism of autolysis and rational design of stable mutants with wild-type catalytic proficiency. *Protein Eng. 14*, 993−1000.
(48) Koglin, M., and Behrends, S. (2003) A functional domain of the α1 subunit of soluble guanylyl cyclase is necessary for activation of the enzyme by nitric oxide and YC-1 but is not involved in heme binding. *J. Biol. Chem. 278*, 12590−12597.
(49) Kraehling, J. R., Busker, M., Haase, T., Haase, N., Koglin, M., Linnenbaum, M., and Behrends, S. (2011) The amino-terminus of nitric oxide sensitive guanylyl cyclase α_1 does not affect dimerization but influences subcellular localization. *PLoS One 6*, e25772.
(50) Sharina, I. G., Jelen, F., Bogatenkova, E. P., Thomas, A., Martin, E., and Murad, F. (2008) α1 soluble guanylyl cyclase (sGC) splice forms as potential regulators of human sGC activity. *J. Biol. Chem. 283*, 15104−15113.
(51) Kharitonov, V. G., Sharma, V. S., Magde, D., and Koesling, D. (1999) Kinetics and equilibria of soluble guanylate cyclase ligation by CO: Effect of YC-1. *Biochemistry 38*, 10699−10706.
(52) Chen, I., Howarth, M., Lin, W., and Ting, A. Y. (2005) Site-specific labeling of cell surface proteins with biophysical probes using biotin ligase. *Nat. Methods 2*, 99−104.
(53) Pal, B., and Kitagawa, T. (2010) Binding of YC-1/BAY 41-2272 to soluble guanylate cyclase: A new perspective to the mechanism of activation. *Biochem. Biophys. Res. Commun. 397*, 375−379.
(54) Makino, R., Yazawa, S., Hori, H., and Shiro, Y. (2012) Interactions of soluble guanylate cyclase with a P-site inhibitor: Effects of gaseous heme ligands, azide, and allosteric activators on the binding of 2′-deoxy-3′-GMP. *Biochemistry 51*, 9277−9289.

(55) Sharma, V. S., and Magde, D. (1999) Activation of soluble guanylate cyclase by carbon monoxide and nitric oxide: A mechanistic model. *Methods 19*, 494−505.
(56) Li, Z., Pal, B., Takenaka, S., Tsuyama, S., and Kitagawa, T. (2005) Resonance Raman evidence for the presence of two heme pocket conformations with varied activities in CO-bound bovine soluble guanylate cyclase and their conversion. *Biochemistry 44*, 939−946.
(57) Sharina, I., Sobolevsky, M., Doursout, M. F., Gryko, D., and Martin, E. (2012) Cobinamides are novel coactivators of nitric oxide receptor that target soluble guanylyl cyclase catalytic domain. *J. Pharmacol. Exp. Ther. 340*, 723−732.
(58) Denninger, J. W., Schelvis, J. P. M., Brandish, P. E., Zhao, Y., Babcock, G. T., and Marletta, M. A. (2000) Interaction of soluble guanylate cyclase with YC-1: Kinetic and resonance Raman studies. *Biochemistry 39*, 4191−4198.
(59) Derbyshire, E. R., Fernhoff, N. B., Deng, S., and Marletta, M. A. (2009) Nucleotide regulation of soluble guanylate cyclase substrate specificity. *Biochemistry 48*, 7519−7524.
(60) Yoo, B. K., Lamarre, I., Martin, J. L., and Negrerie, M. (2012) Quaternary structure controls ligand dynamics in soluble guanylate cyclase. *J. Biol. Chem. 287*, 6851−6859.
(61) Friebe, A., and Koesling, D. (1998) Mechanism of YC-1-induced activation of soluble guanylate cyclase. *Mol. Pharmacol. 53*, 123−127.
(62) Baskaran, P., Heckler, E. J., van den Akker, F., and Beuve, A. (2011) Identification of residues in the heme domain of soluble guanylyl cyclase that are important for basal and stimulated catalytic activity. *PLoS One 6*, e26976.
(63) Baskaran, P., Heckler, E. J., van den Akker, F., and Beuve, A. (2011) Aspartate 102 in the heme domain of soluble guanylyl cyclase has a key role in NO activation. *Biochemistry 50*, 4291−4297.
(64) Underbakke, E. S., Iavarone, A. T., and Marletta, M. A. (2013) Higher-order interactions bridge the nitric oxide receptor and catalytic domains of soluble guanylate cyclase. *Proc. Natl. Acad. Sci. U.S.A. 110*, 6777−6782.
(65) Martin, E., Lee, Y. C., and Murad, F. (2001) YC-1 activation of human soluble guanylyl cyclase has both heme-dependent and heme-independent components. *Proc. Natl. Acad. Sci. U.S.A. 98*, 12938−12942.
(66) Martin, E., Sharina, I., Kots, A., and Murad, F. (2003) A constitutively activated mutant of human soluble guanylyl cyclase (sGC): Implication for the mechanism of sGC activation. *Proc. Natl. Acad. Sci. U.S.A. 100*, 9208−9213.
(67) Winger, J. A., and Marletta, M. A. (2005) Expression and characterization of the catalytic domains of soluble guanylate cyclase: Interaction with the heme domain. *Biochemistry 44*, 4083−4090.
(68) Russwurm, M., and Koesling, D. (2004) NO activation of guanylyl cyclase. *EMBO J. 23*, 4443−4450.
(69) Cary, S. P., Winger, J. A., and Marletta, M. A. (2005) Tonic and acute nitric oxide signaling through soluble guanylate cyclase is mediated by nonheme nitric oxide, ATP, and GTP. *Proc. Natl. Acad. Sci. U.S.A. 102*, 13064−13069.
(70) Tsai, A. L., Berka, V., Sharina, I., and Martin, E. (2011) Dynamic ligand exchange in soluble guanylyl cyclase (sGC): Implications for sGC regulation and desensitization. *J. Biol. Chem. 286*, 43182−43192.
(71) Tsai, A. L., Martin, E., Berka, V., and Olson, J. S. (2012) How do heme-protein sensors exclude oxygen? Lessons learned from cytochrome c′, *Nostoc puntiforme* heme nitric oxide/oxygen-binding domain, and soluble guanylyl cyclase. *Antioxid. Redox Signaling 17*, 1246−1263.
(72) Tsai, A. L., Berka, V., Martin, E., and Olson, J. S. (2012) A "sliding scale rule" for selectivity among NO, CO, and O_2 by heme protein sensors. *Biochemistry 51*, 172−186.
(73) Weichsel, A., Andersen, J. F., Roberts, S. A., and Montfort, W. R. (2000) Reversible nitric oxide binding to nitrophorin 4 from *Rhodnius prolixus* involves complete distal pocket burial. *Nat. Struct. Biol. 7*, 551−554.
(74) Kondrashov, D. A., and Montfort, W. R. (2007) Nonequilibrium dynamics simulations of nitric oxide release: Comparative study of nitrophorin and myoglobin. *J. Phys. Chem. B 111*, 9244−9252.
(75) Benabbas, A., Ye, X., Kubo, M., Zhang, Z., Maes, E. M., Montfort, W. R., and Champion, P. M. (2010) Ultrafast dynamics of diatomic ligand binding to nitrophorin 4. *J. Am. Chem. Soc. 132*, 2811−2820.
(76) Stone, J. R., and Marletta, M. A. (1995) The ferrous heme of soluble guanylate cyclase: Formation of hexacoordinate complexes with carbon monoxide and nitrosomethane. *Biochemistry 34*, 16397−16403.
(77) Martin, E., Berka, V., Bogatenkova, E., Murad, F., and Tsai, A. L. (2006) Ligand selectivity of soluble guanylyl cyclase: Effect of the hydrogen-bonding tyrosine in the distal heme pocket on binding of oxygen, nitric oxide, and carbon monoxide. *J. Biol. Chem. 281*, 27836−27845.

APPENDIX C

IDENTIFICATION OF AN ALLOSTERIC BINDING POCKET IN SOLUBLE GUANYLATE CYCLASE

Contributions. Identification of an Allosteric Pocket in Soluble Guanylate Cyclase. Expression and purification of all proteins were solely my work. All mutant constructs were prepared by me except for those in human sGC. Dr. Andrzej Weichsel and Ms. Jessica Wales performed the cGMP measurements. I made all kinetic measurements and analyses. I performed all CO binding measurements and YC-1 family compounds binding measurements. I prepared the manuscript. Dr. William R. Montfort provided overall guidance for the project and edited the manuscript.

Identification of an Allosteric Pocket in Soluble Guanylyl Cyclase from *Manduca sexta*

Rahul Purohit, Jessica Wales, Andrzej Weichsel and William R. Montfort[1]

From the [†]Department of Chemistry and Biochemistry, University of Arizona, Tucson, AZ 85721

[1]Corresponding author: William R. Montfort, Department of Chemistry and Biochemistry, The University of Arizona, 1041 E. Lowell St., Tucson, AZ 85721; Tel: (520) 621-1884; Fax: (520) 626-9204; E-mail: montfort@email.arizona.edu.

Running Title: Allosteric pocket in sGC

Funding Sources: This work was supported in part by grants from the National Institutes of Health (HL062969 to WRM and U54 CA143924 to WRM), and the American Heart Association (11PRE7610113 to RP and 14GRNT2008006 to WRM).

ABBREVIATIONS

sGC, soluble guanylyl cyclase; *Ms* sGC, *Manduca sexta* sGC; DEA/NO, 2-(N,N-Diethylamino)-diazenolate-2-oxide; CC, coiled coil; PAS domain, Per-ARNT-Sim domain; H-NOX domain, heme-nitric oxide / oxygen binding domain.

ABSTRACT:

Soluble guanylate cyclase (sGC) is the primary nitric oxide receptor protein and plays an important role in regulating cardiovascular physiology. NO binding to sGC heme leads to proximal histidine bond breakage and increased catalytic conversion of GTP to cGMP. The mechanism of this signal propagation upon NO binding is not clearly understood. YC-1 family compounds activate sGC in synergy with NO and CO, but ambiguity about the mode of action of these compounds and the binding site still remains. Here, we investigate a newly identified pocket in sGC and its importance in allosteric regulation and signal transduction. Using a truncated form of *Manduca sexta* sGC (*Ms* sGC-NT), we examined the effect of mutations on the cavity. Mutations L98F/A154F, designed to decrease the internal cavity volume, lead to a protein with low affinity for CO (K_d >200 μM). Unlike with wild type sGC, binding of YC-1 did not enhance the CO binding. Introducing these mutations into full-length human sGC also leads to a protein that responds weakly to NO and YC-1 stimulation and exhibits a higher K_m for GTP. Mutations to an alternative possible YC-1 binding pocket have only a small effect on CO binding, whereas mutation D45A in the loop connecting αB and αC leads to heme-free sGC. Additionally, we demonstrate that the coiled-coil domain plays an important role in regulating the rate of histidine release and propose a model in which signal propagation proceeds through the coiled-coil.

INTRODUCTION:

Once regarded as toxic pollutant gas, nitric oxide (NO) is now highly studied for its potent role in maintaining numerous physiological processes, most importantly vascular tone (*1*). NO is produced by nitric oxide synthase (NOS) upon oxidation of L-arginine to L-citrulline (*2, 3*). NO rapidly diffuses within the same cell or passes through cell membrane into nearby cells, where it acts as a biological messenger through binding to its primary receptor protein, soluble guanylate cyclase (sGC). sGC is a multi-domain, heterodimeric ferrous heme containing enzyme that converts GTP to cGMP. NO binding to sGC leads to an ~200 fold enhancement of catalytic activity resulting in a cGMP-dependent signaling cascade (*4*). Impaired NO-sGC-cGMP signaling has been implicated in multiple cardiovascular diseases including pulmonary hypertension, diminished antiplatelet activity and formation of plaques that can lead to heart attack and stroke (*5, 6*). More recently, genome wide association studies indicate mutations in the sGC α-subunit lead to loss of function and increased risk of myocardial infarction and moyamoya disease (*7, 8*). This makes sGC an interesting target for drug discovery for treatment of cardiovascular diseases.

sGC is a heterodimeric protein composed of homologous α and β subunits, which are evolutionarily linked through a gene duplication event (*9, 10*). Several isoforms of each subunit have been isolated but the most common isoforms are the α_1 and β_1 subunits (*11, 12*). Both α and β subunits of sGC consist of four recognizable domains, an N-terminal Heme-Nitric Oxide Oxygen (H-NOX) domain (*13*) (only the β subunit contains

heme), a Per-ARNT-Sim (PAS) domain (*14*), a coiled-coil domain required for dimerization (*15*), and a C-terminal catalytic cyclase domain (*16*).

While a structure of full length sGC has yet to be determined, individual domains have been more amenable to crystallization, and structures of the α_1 PAS domain (*17*), β_1 coiled-coil homodimer (*18*), and the α_1/β_1 heterodimeric cyclase domain (*19, 20*) have recently been determined. Structures of prokaryotic *Ns* H-NOX and *Tt* H-NOX proteins provide insight into the sGC β_1 H-NOX domain (*21-23*). Recent small-angle X-ray scattering (SAXS) studies on a *Manduca sexta* N-terminal fragment (*24*) and single particle electron microscopy (EM) on full length *Rattus norvegicus* sGC provide a molecular architecture for sGC (*25*). Structural changes in the N-terminal fragment upon NO binding appear small as suggested by both the SAXS and EM studies (*24*).

The precise details of how the signal from NO binding propagates from the regulatory domain to the effector domain are not clearly understood. NO binding to the heme leads to breakage of the iron-histidine bond, conformational changes in the protein, and activation of cyclase activity (*4, 26, 27*). Chemical cross-linking and mass spectrometry analyses of *Manduca sexta* sGC (*Ms* sGC) N-terminal constructs revealed key interdomain contacts between the β_1 H-NOX domain with the α_1 chain, the latter of which was shown to keep the β_1 H-NOX domain in an inhibited conformation (*24, 28*). Studies from the Marletta lab indicated inhibition of the cyclase domain occurs through direct contact with the β_1 H-NOX domain and suggest relief of inhibition upon NO binding (*29, 30*). In contrast, a recent study shows that the cyclase domain exhibits low

activity even in the absence of the β_1 H-NOX domain (*20*). Other studies suggest signal transduction might propagate through the PAS and coiled-coil domains (*31, 32*). In the absence of a full-length structure, key details about how the domains are arranged as well as the molecular details of signal transduction upon NO binding are unknown.

sGC can be stimulated by heme dependent/NO independent compounds that act synergistcally with CO and NO (*33*). The first such compound described in this family was YC-1, which was discovered to be an antiplatelet compound targeted to sGC (*34-36*). A series of modifications to the core benzylindazole scaffold in YC-1 led to the development of the drug Riociguat (BAY 63-2521), which is the only approved drug targeted to sGC and currently in use for the treatment of pulmonary arterial hypertension (*37*). Another class of compounds activates sGC independently of heme or NO by replacing heme in the apo protein, which can occur through oxidation and loss of heme. BAY 58-2667 (Cinaciguat) is the most promising of these compounds. A crystal structure of Cinaciguat bound to a prokaryotic H-NOX protein confirmed that the compound can mimic heme and fill the empty heme pocket (*38*).

Unlike with the heme mimetic activators, mechanism of binding and the binding location of YC-1 family compounds remain unclear. We previously showed that sGC exhibits a linked equilibrium between binding of CO or NO and YC-1 family compounds; binding of one leads to enhanced binding of the other *(28)*. The possibility of YC-1 binding to the α_1 H-NOX domain (*39-41*) or to the pseudosymmetric site in the

cyclase domain (*42-44*) has been suggested, but appears unlikely based on more recent data, which indicate the β_1 H-NOX domain as the likely binding site (*28, 45-49*).

We previously reported recombinant expression of several heterodimeric N-terminal constructs of sGC from *Manduca sexta (*hawkmoth), which is highly homologous to the mammalian sGC and functions similarly (*24, 39, 50, 51*). Here, we report identification of a new pocket in the previously developed homology model of the *Ms* sGC β_1 H-NOX domain (*24*), which lies near the proximal region of the heme. We altered this pocket and an alternative possible binding site through site-directed mutagenesis to uncover their roles in YC-1 binding and signal transduction. We also evaluated the effect of coiled coil domain truncation or elongation on proximal histidine release rates since the domain has also been implicated in signal transduction.

MATERIAL AND METHODS:

Materials. All chemicals were obtained from Sigma-Aldrich and chromatography columns from GE Healthcare unless otherwise indicated. 2-(*N*,*N*-Diethylamino)diazenolate-2-oxide (DEA/NO) was kindly provided by Dr. Katrina Miranda (University of Arizona). HEK293T cells were obtained from ATCC. EZview red ANTI-FLAG M2 affinity gel beads were purchased from Sigma. QuikChange Lightning Mutagenesis kits were obtained from Aligent Technologies. TurboFect was purchased from Fermentas. Protease inhibitor cocktail was obtained from Sigma. cGMP was measured using a commercially available homogeneous time-resolved fluorescence (HTRF) immunoassay (Cisbio).

Expression and Purification of *Ms* sGC Constructs. All mutations were introduced using the QuikChange lightning site-directed mutagenesis kit. *Ms* sGC-NT13, *Ms* sGC-NT19 and *Ms* sGC-NT21 wild type (WT) proteins were expressed in *E. coli* and purified using Ni-NTA, StrepTactin (*Ms* sGC-NT19) and size exclusion chromatography, as previously described (*24, 39*). *Ms* sGC-NT25 and Ms sGC-NT32 were purified similarly to *Ms* sGC-NT19. All mutant constructs were partially purified using Ni-NTA affinity column chromatography.

Determination of Dissociation Constants for CO. CO dissociation constants were measured by titrating CO from a saturated solution into sGC protein and monitoring

the appearance of the CO-bound Soret absorption band, as described previously (*24*, *39*). The *Ms* sGC β_1(1-380) double mutant samples were prepared in Ar-purged buffer supplemented with ~100fold excess sodium dithionite. CO binding experiments were performed in a 1 cm pathlength cuvette using a Cary 50 spectrophotometer (Varian). Binding data in the presence and absence of 50 μM YC-1 were plotted using a single site saturation ligand binding model in SigmaPlot (SPSS, Inc., Chicago, IL). Binding constants for YC-1 family compounds to *Ms* sGC-NT-CO complexes were determined using a Soret shift analysis as previously described (*28*). For this, YC-1 was titrated into a 1 cm cuvette containing a CO saturated protein solution and K_d for compound binding was determined by plotting the Soret shift difference with respect to the increasing concentrations of the ligand, and fitting to a single-site saturation ligand binding model in SigmaPlot.

Kinetics of Histidine Release Rate upon NO Binding. The rate of His105 release from heme iron upon NO binding in the β_1 H-NOX domain was measured at 10 ^oC by mixing 1 μM protein and 10 μM NO in an RSM-1000 stopped-flow spectrophotometer (OLIS, Inc.) as previously described (*24, 39*). Desired protein samples were prepared in argon-purged buffer and transferred to the stopped-flow device in a gastight syringe. NO solutions were also prepared in argon-purged buffer in a gastight syringe from a stock DEA/NO solution and then connected to the stopped flow device. DEA/NO decomposition was allowed to proceed for 20 min at room temperature before

the sample was transferred to the instrument, where the solution was allowed to equilibrate to the desired temperature for 5 min. Absorbance changes (A_{420}) were fit to single- or double-exponential equations using SigmaPlot; values reported are the average and standard deviation of five to ten consecutive measurements.

Expression of Human Soluble Guanylate Cyclase. Human sGC-α_1 (ATTCC clone MC-33150) was previously cloned into pCMV-3Tag-9 (Clonetech) between the *BamHI* and *HindIII* sites, which added a C-terminal myc-tag (WM397). Human sGC-β_1 was previously cloned into pCMV-3Tag-3A (Clonetech) between the *SacI* and *XhoI* sites, which added a C-terminal FLAG-tag (WM434) (*52*). The sGC β_1 L98F/A154F double mutant, referred to as sGC_LA, was generated by introducing L98F and A154F mutations into sGC-β1 (WM434) using the QuikChange Lightning Mutagenesis kit. Mutations were confirmed by DNA sequencing.

HEK293T cells were cultured in Dublecco's Modified Eagle's Medium (DMEM) supplemented with 10% fetal bovina serum (FBS), 1% Pencillin/Streptomycin, and 2 mM L-glutamine. All experiments were performed prior to reaching passage 20. HEK293T cells were grown in 10 cm dishes to 70-80% confluence, and were transfected with a mixture of 10 µg WM397, 10 µg WM434 and 25 µL transfection reagent TurboFect. Transfected cells were incubated at 37 °C, 5% CO_2 and harvested 13 hr post transfection.

Transfected cells were washed twice with 10 mL tris-buffered saline (TBS) (50 mM Tris HCl, pH 7.4, 150 mM NaCl), and suspended in 2 mL lysis buffer (50 mM Tris

HCl, pH 7.4, 100 mM NaCl, 1 mM EDTA, 1 mM TCEP, 1 mM PMSF, 10 µg/mL leupeptin, and a 1:100 diluted protease inhibitor cocktail). Cells were lysed by homogenization, and cell debris was removed by centrifugation at 13,500 x g for 10 min at 4 °C. FLAG-tagged sGC was immunoprecipitated by adding 15 µL EZview red ANTI-FLAG M2 affinity gel beads to the cell lysate from $2x10^6$ cells. The mixture was incubated for 2 hr at 4 °C while nutating. The beads were washed 3 times with 500 µL TBS by centrifugation at 8,500 x g for 30 s at 4 °C, and divided into 90 µL aliquots per condition.

cGMP Activity Assays. Reaction buffer (50 mM HEPES, pH 7.4, 8 mM $MgCl_2$, 1 mM GTP) was freshly prepared as a 10x stock solution, and 10 µL was added to each condition. A final concentration of 50 µM DEA/NO or a vehicle control was added to the indicated conditions, and the samples were incubated at 37 °C for the specified times (5, 10, 20 or 30 min). The reaction was terminated by the addition of 50 µL conjugate lysis buffer (50 mM phosphate buffer, pH 7.0, 1M KF, 1.25% Triton X-100), along with flash freezing in liquid nitrogen. cGMP concentrations were determined with the use of the Cisbio HTRF immunoassay kit.

To determine K_m for GTP, reaction buffer was freshly prepared as a 10x stock solution, with the final concentration of GTP ranging between 10 µM – 1 mM. Immunoprecipitated wild type or mutant sGC protein was obtained from ~100 µg total cell lysate for each condition. Due to the tight binding of the FLAG epitope to the

EZview beads, sGC proteins could not be eluted without significant loss of activity. Activity was therefore measured directly on the bead, and final enzyme concentrations were unknown. Relative enzyme concentration was determined and normalized using western blots. 10 µL of reaction buffer was added to the indicated conditions, along with 50 µM of DEA/NO or vehicle control. Samples were incubated at 37 °C for 15 min, and the reaction was terminated by adding 50 µL conjugate lysis buffer and flash freezing in liquid nitrogen. cGMP concentrations were determined using the HTRF immunoassay kit.

RESULTS:

Identification of a Pocket in the β_1 H-NOX Domain. Despite much work, the binding location of YC-1 family compounds in sGC remains unclear. Recent studies by our group and others have hinted towards the role of the β_1 H-NOX domain in binding of these small molecules (*28, 49*). To test if the β_1 H-NOX domain might contain such a binding pocket, we examined a previously developed homology model of the *Ms* sGC β_1 H-NOX domain and identified a pocket in the proximal region of the heme domain, using the CASTp server (*53*). The pocket lies in a similar region to where a small internal cavity was previously identified in the H-NOX protein from *Nostoc* specie (*Ns* H-NOX) (*21*). Compared to the *Ns* H-NOX cavity, the pocket in the *Ms* sGC H-NOX model is bigger and extends from heme to the solvent accessible pocket mouth. Total volume of the pocket calculated by CASTp is 496 $Å^3$ and contains two openings to solvent. Residues lining this pocket come from helices αF (Phe97, Leu98) and αG (Val150, Ala154, Thr160), and from beta strands β1 (Phe120), β2 (Leu131) and β4 (Ile180) (Figure 1). Importantly, all residues lining this pocket are highly conserved among sGC proteins from insect to mammals (Figure 1). CASTp also identified a tunnel network in the *Ms* sGC β_1 H-NOX domain that has previously been implicated in the regulation of gaseous ligand flux in *Ns* H-NOX (*54*). We examined both the newly identified pocket (labeled as Site 1) and the tunnel 2 region (labeled as Site 2, Figure 2) for their roles in binding YC-1 family compounds and in signal transduction using site-directed mutagenesis approach.

A

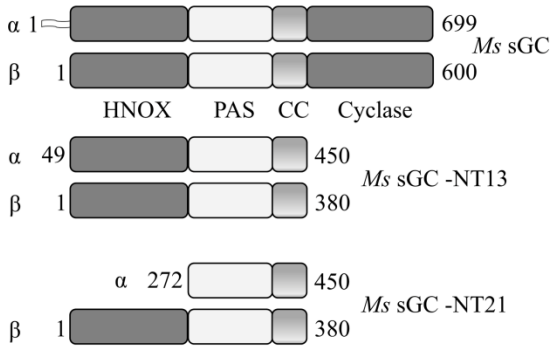

B

```
Bovine sGC β1        MYGFVNHALELLVIRNYGPEVWEDIKKEAQLDEEGQFLVRIIYDDSKTYDLVAAASKVLN  60
Human sGC β1         MYGFVNHALELLVIRNYGPEVWEDIKKEAQLDEEGQFLVRIIYDDSKTYDLVAAASKVLN  60
Rat sGC β1           MYGFVNHALELLVIRNYGPEVWEDIKKEAQLDEEGQFLVRIIYDDSKTYDLVAAASKVLN  60
Manduca sGC β1       MYGFVNYALELLVMKTFDEETWETIKKKADVAMEGSFLVRQIYEDEITYNLITAAVEVLQ  60
                     ******:******:::.:  *.** ***:*::  **.**** **:*. **:*::** :**:

Bovine sGC β1        LNAGEILQMFGKMFFVFCQESGYDTILRVLGSNVREFLQNLDALHDHLATIYPGMRAPSF  120
Human sGC β1         LNAGEILQMFGKMFFVFCQESGYDTILRVLGSNVREFLQNLDALHDHLATIYPGMRAPSF  120
Rat sGC β1           LNAGEILQMFGKMFFVFCQESGYDTILRVLGSNVREFLQNLDALHDHLATIYPGMRAPSF  120
Manduca sGC β1       IPADAILELFGKTFFEFCQDSGYDKILQVLGATPRDFLQNLDGLHDHLGTLYPGMRSPSF  120
                     : *  **::*** ** ***:****.**:***:. *:******.*****.*:*****:***

Bovine sGC β1        RCTDADKGKGLILHYYSEREGLQDIVIGIIKTVAQQIHGTEIDMKVIQQRNEECDHTQFLI 181
Human sGC β1         RCTDAEKGKGLILHYYSEREGLQDIVIGIIKTVAQQIHGTEIDMKVIQQRNEECDHTQFLI 181
Rat sGC β1           RCTDAEKGKGLILHYYSEREGLQDIVIGIIKTVAQQIHGTEIDMKVIQQRSEECDHTQFLI 181
Manduca sGC β1       RCTERPEDGALVLHYYSDRPGLEHIVIGIVKTVASKLHNTEVKVEILK-TKEECDHVQFLI 180
                     ***:  :  .*:*****:* **:.*****:****.::* **:.:::::  .*****.****
```

Figure 1. sGC constructs and β_1 H-NOX domain alignment. (A) Schematic representation of *Ms* sGC domains, expression constructs and their boundaries. Constructs used in the present study but not shown in the diagram are *Ms* sGC-NT23 (α_1 49−459, β_1 1−389) and *Ms* sGC-NT23 (α_1 272−459, β_1 1−389). (B) Sequence alignment of the β_1 H-NOX domain from bovine, human, rat and *Manduca*. Alignment was generated using Clustal Omega (*55*) showing absolutely conserved residues marked with an asterisk. Residues mutated in the present study are highlighted as green for invariant residues and yellow for similar residues.

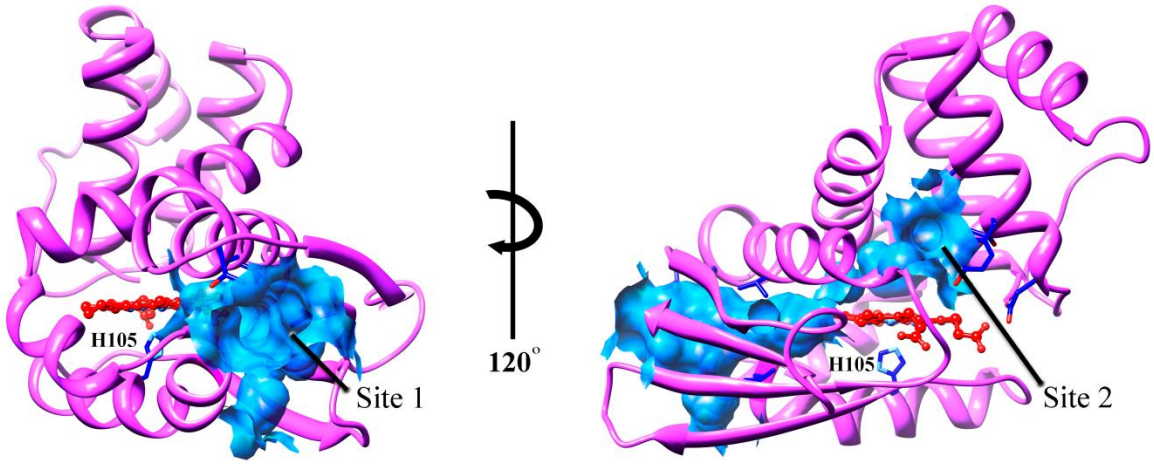

Figure 2. Possible ligand binding pockets in the *Ms* sGC β_1 H-NOX domain. The identified pocket labeled Site 1 is shown in blue (left) with targeted residues lining the pocket (Leu 98, Val 150, Ala 154, Thr 160 and Ile 180) shown in blue. An alternative possible binding site (*56*) (residues Asp 45, Thr 48 and Tyr 49) is shown on the right (Site 2). This pocket is near tunnel 2 previously identified in *Ns* H-NOX (*54*).

Mutations at Site 1 in *Ms* sGC-NT Proteins Affect CO Binding. Since the pocket volume at Site 1 is similar to the volume of YC-1 family compounds (~258 $Å^3$ for YC-1), we hypothesized that this is the binding site for these compounds. To test this possibility, we mutated the individual residues lining the pocket (Leu 98, Ala 154, Val 150, Thr 160, Ile 180) to either phenylalanine or tryptophan in order to fill the pocket and potentially interfere with binding. We probed the effect of the mutations on CO binding affinity for ferrous sGC heme, in the presence and absence of YC-1, since CO binding is weaker than NO binding and changes in affinity more easily estimated. All single mutations at Site 1 were initially made in the heterodimeric *Ms* sGC-NT13 construct (Figure 1), which retains the YC-1 binding site and the YC-1 enhancement of CO binding (*39*, *51*).

We mutated residues lining the inside of the Site 1 pocket or located at the pocket mouth. All of the *Ms* sGC-NT13 mutant proteins retained heme and displayed Soret absorption spectra similar to the WT *Ms* sGC-NT constructs (434 nm), indicating no change in the heme pocket (Figure 3A). Two mutations were made at the entry to Site 1, T160W, located at the loop connecting helix αG to β sheet strand β3, and I180W, located at the end of β sheet strand β4. Both mutated proteins responded to YC-1 binding similarly to the wild type protein (Table 1). In contrast, mutations within the Site 1 pocket had substantial effects on the CO binding affinity in the presence and absence of YC-1. Mutation L98F, located on helix αF, led to ~3 fold weaker CO affinity (K_d^{CO} = 165 μM) and ~7 fold weaker CO affinity in presence of YC-1 ($K_d^{CO'}$ = 20 μM, Table 1).

Three mutations on helices αG were also introduced: V150W, A154F and A154W. Mutation V150W had no effect of CO binding affinity in the absence of YC-1, but had ~5-fold weaker CO affinity in presence of YC-1. Mutations A154F and A154W mutations lowered CO affinity ~1.5-fold and ~2-fold in the absence of YC-1, and ~5-fold and ~9-fold in the presence of YC-1, respectively. Overall, YC-1 enhanced CO binding only 3-5 fold for these mutants compared to the 19-fold enhancement seen with the WT *Ms* sGC-NT13 (*28*). These results indicated the pocket might be important for regulating gaseous ligand binding, YC-1 binding and/or allosteric response. Previous mutations close to the heme pocket on helix αF (D102A) and on β sheet strand β1 (F120A) led to heme loss in rat sGC, indicating the importance of these residues in heme stability (*57*).

We then examined whether the effects of mutation to Leu 98, Val 150 and Ala 154 were additive, creating the L98F/A154F (LA) and L98F/V150F (LV) double mutants. Mutant *Ms* sGC-NT13_LV behaved similarly to mutant *Ms* sGC-NT13_L98F, with further diminished YC-1 enhancement of CO binding. *Ms* sGC-NT13_LA mutant displayed very weak CO binding affinity and a dissociation constant of more than 200 μM, which could not be measured reliably due to the relatively low solubility of CO (~1mM at saturation). Moreover, YC-1 enhancement of CO binding in the *Ms* sGC-NT13_LA mutant was largely absent, with $K_d^{CO'}$ = ~150 μM, a value ~53-fold weaker CO binding in the presence of YC-1 compared to WT *Ms* sGC-NT13 (Figure 3). *Ms* sGC-NT13_LA is thus stabilized in a low affinity heme conformation, and YC-1 is unable to induce tighter CO binding. Additionally, an ~2 nm blue shift in the Soret band upon

binding YC-1 to wild type *Ms* sGC-NT13 is absent in *Ms* sGC-NT13_LA suggesting YC-1 binding was severely compromised.

To further test whether *Ms* sGC-NT13_LA had completely lost YC-1 binding or was overly stabilized in the low affinity conformation, we introduced the L98F/A154F mutation into construct *Ms* sGC-NT21. The resulting construct, *Ms* sGC-NT21_LA, is identical to *Ms* sGC-NT13_LA except that it lacks the α chain H-NOX domain (Figure 1). A similar CO binding profile was observed for the *Ms* sGC-NT21_LA mutant; however, the effect of the mutations was now much more pronounced. CO binding to the *Ms* sGC-NT21_LA mutant was ~85 fold and ~450 fold weaker in the absence and presence of YC-1, respectively, compared to WT *Ms* sGC-NT21. CO binding in the mutant protein was also largely unresponsive towards YC-1, which only enhanced CO binding 2-fold. Nonetheless, YC-1 addition led to an ~2 nm blue shift in the Soret absorption band for the CO complex, indicating YC-1 binding was still present. Titration of YC-1 into the CO saturated *Ms* sGC-NT21_LA mutant yielded K_d = 4.5 μM for the YC-1 binding, a value ~7 fold weaker than that for the WT *Ms* sGC-NT21 protein. These results indicated YC-1 is still able to bind but is unable to potentiate the CO binding in the double mutant *Ms* sGC-NT proteins.

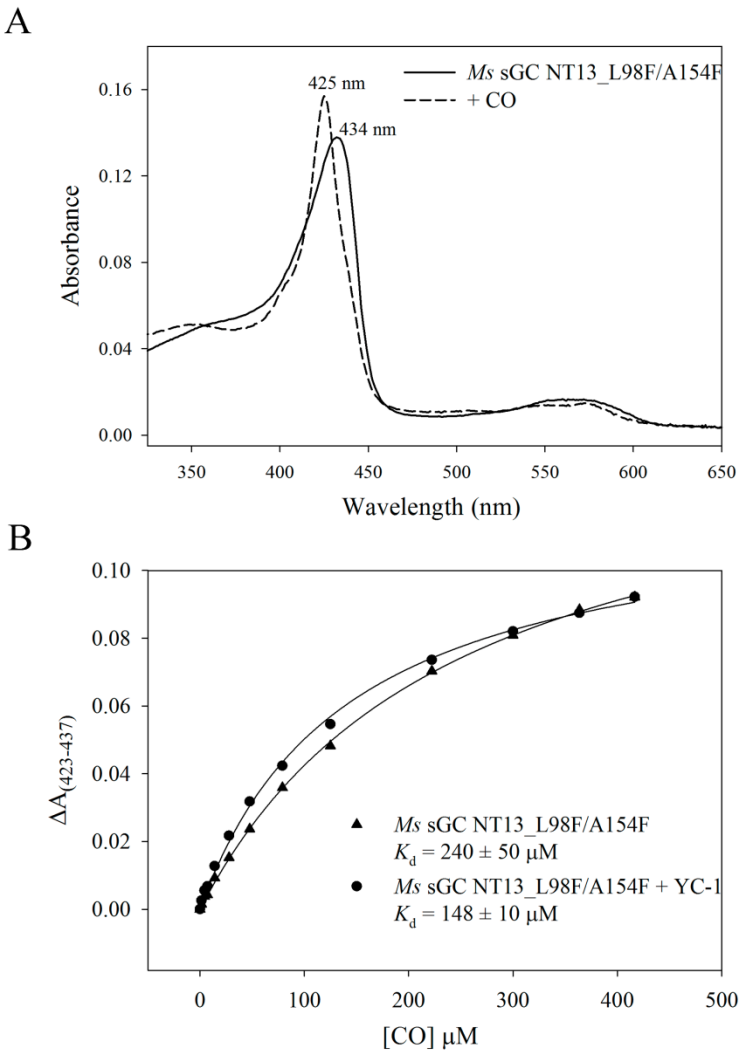

Figure 3. CO saturation binding analysis for L98F/A154F mutant. (A) Absorption spectra of the *Ms* sGC-NT13_LA double mutant before and after CO saturation. (B) CO saturation binding curve for *Ms* sGC-NT13_LA mutant ± YC-1, displaying weak CO binding and little tightening of CO binding upon addition of YC-1. Titrations were performed in a 1 cm cuvette at room temperature with 1 µM protein in buffer containing 50 mM potassium phosphate, pH 7.4, 100 mM KCl, 5% glycerol, and ± 50 µM YC-1. The data were corrected for dilution upon addition of CO-saturated buffer and were fitted to a single-site saturation model to obtain the CO dissociation constants. K_d values shown are the average and standard deviation of three independent measurements.

Mutations to the Alternative YC-1 Binding Site. An alternative binding site for YC-1 family compounds has previously been proposed, based on results from a study using molecular dynamics (*56*). The identified binding site cluster lies close to the predicted tunnel 2 in the *Ns* H-NOX crystal structure (*54*). We also tested the role of this predicted region in YC-1 binding through mutagenesis (illustrated in Figure 2). Both residues at the tunnel mouth, Thr 48 and Tyr 49, are highly conserved in sGC across species (Figure 1). We mutated both Site 2 residues to larger amino acids to see if YC-1 binding could be blocked. Mutation of Tyr 49 to Ala, Phe or Trp in *Ms* sGC-NT13 had no effect on CO binding in the absence or presence of YC-1. Mutation of Thr 48 to Trp led to ~1.8-fold weaker CO affinity; YC-1 binding was slightly less effective, yielding a 9-fold enhancement of CO binding as compared to the ~19-fold enhancement seen with wild type *Ms* sGC-NT13.

The loop connecting helices αB and αC in the β_1 H-NOX domain has also been predicted to be crucially important in sGC activation (*58*), particularly residue Asp 45 (*23*). cGMP activity studies on D45A mutant resulted in NO insensitive enzyme (*29*, *59*). Mutation of Asp 45 to Ala in *Ms* sGC-NT13 led to a protein with almost no heme loading, displaying only a small broad peak around 400 nm, indicating presence of only a small amount of oxidized heme. Addition of sodium dithionite shifted the Soret to ~427 nm (as opposed to 433 nm in the wild type protein) and the protein could now bind CO, yielding a Soret maxima of ~424 nm.

TABLE 1. CO and YC-1 Dissociation Constants for sGC Proteins

Protein[a]	Mutation	K_d^{CO} (μM)[b]	$K_d^{CO'}$(+YC1, μM)	$K_d^{YC1'}$(+CO, μM)[e]
Ms sGC-NT13	WT	53 ± 4[c]	2.8 ± 0.4[c]	0.8 ± 0.1
Ms sGC-NT13	L98F	165 ± 6	20 ± 2	1.7
Ms sGC-NT13	V150F	42	2.5	1.3
Ms sGC-NT13	V150W	55 ± 2	15 ± 4	
Ms sGC-NT13	A154F	81 ± 3	15 ± 3	3.1
Ms sGC-NT13	A154W	108 ± 10	26 ± 1	
Ms sGC-NT13	L98F/V150F	135 ± 2	35 ± 10	
Ms sGC-NT13	L98F/A154F	240 ± 50	148 ± 10	No Shift in Soret
Ms sGC-NT13	T160W	38	1.5	
Ms sGC-NT13	I180W	28	2.4	
Ms sGC-NT21	WT	2.2 ± 0.2[c,d]	0.2 ± 0.0[c,d]	0.6 ± 0.1
Ms sGC-NT13	Y49A	46	2.4	
Ms sGC-NT21	Y49F	48	2.3	
Ms sGC-NT21	Y49W	65	2	
Ms sGC-NT21	T48W	95	11	
Ms sGC-NT21Avi	L98F/A154F	192	90	4.5
Ms sGC β_1(1-380)	WT	0.20 ± 0.03[c,d]	0.18 ± 0.05[c,d]	
Ms sGC β_1(1-380)	A154F	0.29[c]	0.18[c]	
Ms sGC β_1(1-380)	L98F/A154F	17	10	
Ms sGC β_1(1-205)	L98F/A154F	22	22 (BAY)[c]	

[a]NT13: α_1(49-450), β_1(1-380); NT21: α_1(272-450), β_1(1-380); NT21Avi, same as NT21 but with an Avitag at the C-terminus of the β_1-subunit. [b]CO affinity was measured through titration and fitting to a single-site saturation ligand binding model. The protein concentration was 1 μM and YC-1 concentration, when present, was 50 μM. [c]From Purohit *et. al.* (*28*). [d]Measured in a 10 cm cuvette, using 0.1 μM protein. [e]From fitting of the shift in Soret band maxima. Values shown without errors are currently being replicated and errors will be incorporated in the final manuscript.

Double Mutant sGC Shows Diminished cGMP Activity. To examine the effect of the L98F/A154F mutations on the activity of full length human sGC, we measured basal and NO stimulated catalytic activity in transiently transfected HEK-293T cells. The sGC_LA mutant exhibited poor stimulation in the presence of NO and displayed impaired overall activity as compared with the wild-type protein (Figure 5). We further characterized the sGC_LA double mutant by measuring the kinetic parameters and determined the effect of the mutations on K_m and V_{max}. Immunoprecipitated wild type sGC showed a decrease in K_m and an increase in V_{max} values upon NO stimulation, consistent with previously reported values (*52, 60, 61*). Preliminary K_m and V_{max} values obtained for basal wild type sGC activity were 350 µM and 0.4 pmol cGMP min^{-1}, and for NO stimulated wild type sGC were 50 µM and 3.8 pmol cGMP min^{-1}. The sGC LA mutant protein displayed high value for K_m (K_m = 363 µM) in the presence of NO. V_{max} value was 0.3 pmol cGMP min^{-1} in the presence of NO, suggesting the mutant sGC is not stimulated by NO (Figure 4). These studies are preliminary and are being completed by Jessica Wales. Further activity assays will be performed in the presence of YC-1 compounds and these data will be included as figure 4 and table 3 for publication.

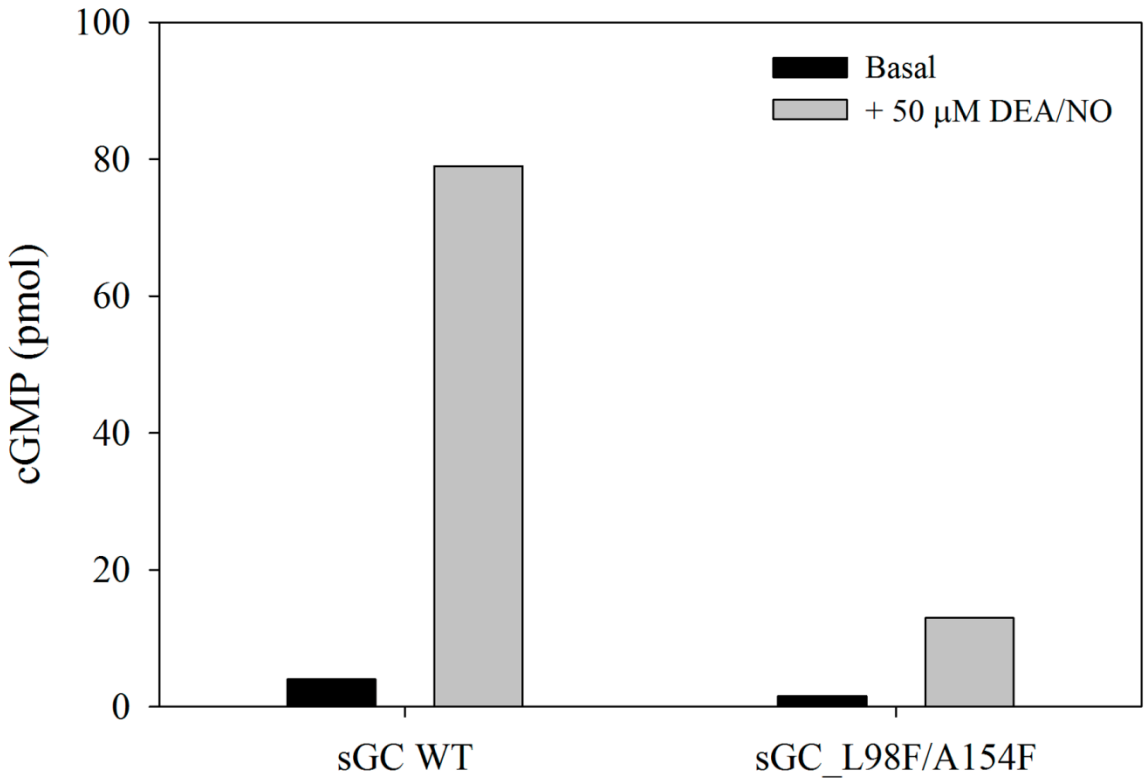

Figure 4. Preliminary cyclase activity of full-length wild-type human sGC and LA mutant. The production of cGMP from GTP by immunoprecipitated sGC from HEK-293 cells was measured using an HTRF immunoassay. 50 μM DEA/NO or a vehicle control were added to the samples just prior to measurement; samples were incubated at 37 °C for 20 min.

Double Mutant Exhibits Slow Histidine Release Rate Upon NO Binding. NO binding to sGC proceeds through a transient 6-coordinate intermediate followed by release of the proximal histidine to yield a 5-coordinated nitrosyl complex and, presumably, fully activated protein. We examined His 105 release in the mutant proteins to access whether release rates were affected. As with wild type, mixing of NO and *Ms* sGC-NT13_LA and *Ms* sGC-NT21_LA in a stopped flow spectrophotometer led to rapid formation of the 6-coordinated intermediate, occurring within the mixing dead time of the instrument. We measured the rate of histidine release in both *Ms* sGC-NT13_LA and *Ms* sGC-NT21_LA double mutant constructs at 10 °C, as previously described (*24, 39*). We were able to observe the six coordinate intermediate and measured histidine release rates of 2.7 s^{-1} and 3.5 s^{-1} for *Ms* sGC-NT13_LA and *Ms* sGC-NT21_LA double mutants (Figure 5, Table 2). The observed rates for the double mutants are very slow compared to the wild type constructs, for which histidine release rates were very fast and not measurable (Table 2) (*24*).

Coiled-Coil Regulates the Histidine Release Rate in the N-terminal sGC Constructs. The release of the proximal histidine has been attributed to the activation of the cyclase domain but the mechanistic details of the signal transduction to the cyclase domain are still not clear (*4, 26*). To understand the role of the coiled-coil in signal transduction, we examined the histidine release rates of various *Ms* sGC NT constructs with varied coiled-coil length. Homology modeling predicted the *Ms* sGC coiled-coil to end at α_1 Pro 460 and β_1 Pro 390, followed by a turn and a small additional helix on each

chain, ending at α_1 471 and β_1 401 (*18, 24*). We previously reported that the histidine release rate in construct *Ms* sGC NT2 (α_1 49-471 and β_1 1-401) is similar to full length sGC (*24*, *39*) and that shortening of the coiled-coil domain by 21 residues leads to dramatically faster proximal histidine release (*24*). We further extended these studies by measuring the rate in constructs *Ms* sGC-NT23 (α_1 272-459 and β_1 1-489) and *Ms* sGC-NT25 (α_1 49-459 and β_1 1-389), which are similar to *Ms* sGC NT21 and *Ms* sGC NT13, respectively, except the coiled-coil terminus on both subunits has been extended by another 9 residues. The six-coordinate transient intermediate was observed with rate 32.7 s^{-1} and 65 s^{-1} for *Ms* sGC-NT25 and *Ms* sGC-NT23, respectively (Table 2). These results indicate a potential role for the coiled-coil in signal transduction from the β_1 H-NOX domain to the cyclase domain upon NO binding.

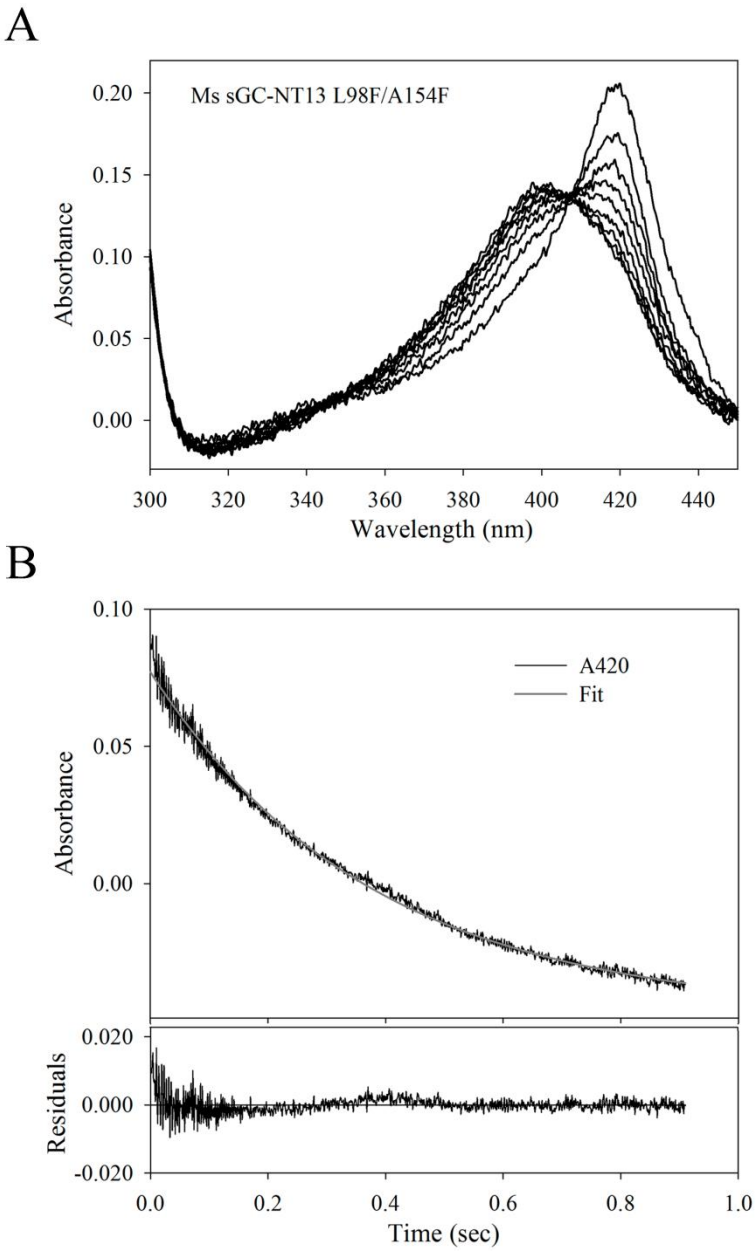

FIGURE 5. Kinetics for proximal histidine release examined by stopped-flow spectroscopy. *A*, transient spectra after NO mixing with mutant *Ms* sGC-NT13 L98F/A154F mutant. *B*, typical fitting of the change in absorbance (420 nm) *versus* time (0–900 ms) using a single exponential decay model. Residuals of the fit are also shown.

Table 2. Histidine Release Rates for Six-Coordinate Nitrosyl Complex[a]

Ms sGC protein	*Domain Boundaries*	$k_{6\text{-}5}$ (s^{-1})	*Ref*
Ms sGC-NT1	α_1 1−471, β_1 1−401	12.8 ± 0.4	(*39*)
	α_1 1−471, β_1 1−401	11.1 ± 0.5	(*24*)
Ms sGC-NT2	α_1 49−471, β_1 1−401	14.5 ± 0.6	(*24*)
Ms sGC-NT13	α_1 49-450, β_1 1-380	>100[b]	(*24*)
Ms sGC-NT19	α_1 49-450, β_1 1-380-Strep	>100[b]	(*24*)
Ms sGC-NT21	α 272-450, β 1-380	>100[b]	(*24*)
Ms sGC-NT13_LA	α_1 49-450, β_1 1-380	2.7 ± 0.5	*This work*
Ms sGC-NT21Avi_LA	α 272-450, β 1-380	3.5 ± 0.2	*This work*
Ms sGC-NT21Avi	α 272-450, β 1-380	>100[b]	*This work*
Ms sGC-NT25	α_1 49-459, β_1 1-389	32.7 ± 2	*This work*
Ms sGC-NT23	α_1 272-459, β_1 1-389	~62*	*This work*

[a]Rate constants for proximal histidine release from the transient six-coordinate nitrosyl complex to the more stable five-coordinate nitrosyl complex. Measured at 10 °C in a stopped-flow spectrophotometer. [b]Unobserved. *Measurement will be repeated for standard deviation before manuscript submission.

DISCUSSION:

Despite much study, how NO binding to the β_1 H-NOX sensory domain, or binding of YC-1 family stimulatory compounds, leads to enhanced catalysis by the C-terminal cyclase domain remains unclear. Here, we investigated a newly-identified predicted pocket for its possible role in YC-1 binding and allosteric signal transduction. We show that introduction of mutations designed to fill this cavity leads to a protein with hampered CO binding, loss of YC-1 stimulation and reduced NO stimulated catalytic activity. We also examined the role of the coiled coil in signal transduction and show that a modest change in length leads to dramatic change in the rate for proximal histidine release upon NO binding to heme. In what follows, we discuss the implications for signal transduction and propose a new model for signaling through the central coiled-coil.

Mutations in the Proximal Pocket Affect CO Binding Affinity to the Ferrous Heme. Baskaran *et. al*. previously predicted the presence of a cavity in the rat sGC β_1 H-NOX homology model near the heme proximal pocket (*57*). In our *Ms* sGC β_1 H-NOX homology model, this internal cavity (Site 1) appears to be bigger and has a solvent accessible opening. Since the predicted model ends at the C-terminal end of the domain, and right at the end of this cavity, the opening is poorly described and may be modified or closed off by the linker residues to the PAS domain. Mutation of individual residues to fill the pocket leads to significantly reduced CO binding affinity and NO-stimulated catalysis, suggesting that the predicted pocket is involved in signal transduction from H-

NOX domain to cyclase domain. Moreover, YC-1 enhancement of CO binding is no longer present in the mutant protein, indicating disruption of the linked equilibria in the system. Linked-equilibria would also predict weaker binding for YC-1 to the mutant proteins. The binding affinity of YC-1 in the mutant *Ms* sGC-NT-CO proteins, as estimated from the Soret shift, is indeed several fold weaker compared to the wild type proteins. Overall, the residues predicted to fill the pocket lead to loss of ligand binding, reduced catalysis and disrupted linked equilibria.

Aspartate 102 has been implicated to have an important role in NO activation of sGC and mutations D102N and D102E in the rat sGC β_1 H-NOX lead to poor YC-1 stimulation (*57*). Although Asp 102 is not part of the pocket in *Ms* sGC, it might be important in maintaining pocket dynamics through interaction with Phe 120, which forms a part of the pocket wall. Mutations D102A and F120A on the αF helix and the β1 strand lead to sGC without heme, possibly because Asp 102 lies in close proximity to the heme moiety and mediates key interactions possibly required for the heme stability (*57*). All of the Site 1 pocket mutants in *Ms* sGC N-terminal proteins retain heme and show spectral characteristics similar to those of the wild type NT proteins.

How Site 1 Mutations Lead to Low CO/NO Affinity? One possibility is that the pocket mutations lead to an altered porphyrin conformation that restricts the in-plane heme movement and stabilizes the heme in a low affinity state that cannot be activated by YC-1. That such a non-activatable state exists has been predicted before using Raman

resonance studies on an I149Y mutant sGC (*45*). A second possibility is that mutations lead to conformational change in the distal heme pocket causing steric hindrance to ligand binding. Similar steric hindrance to NO binding has been observed with studies on I145Y mutat sGC (*62*).

Additionally, both *Ms* sGC-NT13_LA and *Ms* sGC-NT21_LA double mutants display markedly slow histidine release rates upon NO binding compared to their wild type counterparts, for which release rates were too fast to measure with the stopped-flow instrument (*24*). It is likely that the L98F/A154F mutations introduce additional constraints in the proximal region thereby hindering in-plane movement of the heme, leading to weaker CO binding and slower histidine release rates (*63*). A sliding scale rule (*64*) has been proposed by Tsai *et. al.*, which suggests proximal strain and/or distal sterics play an important role in restricting ligand binding to NO sensors. Overall, these results suggest the importance of this pocket in tuning the strain enough to prevent O_2 binding and rapid signal transduction upon NO binding.

Exploring the Alternate Pocket. Mutational studies indicate residues in the loop connecting helices αB-αC, helix αF and beta sheet strand β1 are crucially required for sGC activation (*58*). Mutations D44A and R40A lead to heme loss indicating the residues in the loop are also important for heme stability (*58, 59*). Asp 45 has been suggested to be critical for sGC activation and mutating it to Alanine leads to an NO and BAY 41-2272 unresponsive enzyme, but one that could be stimulated in the presence of

both NO and BAY 41-2272, though it is unclear if heme was present in these studies (*59*). Here, we show that mutation D45A in *Ms* sGC-NT13 leads to the protein with minimal heme loading and rapid heme oxidation. Addition of dithionite leads to a shift in the Soret absorption peak that can now bind CO. This correlates with the observation that no stimulation occurred with separate addition of NO and BAY 41-2272. That a dose dependent activation was observed in the presence of the both ligands could possibly be due to either the presence of small fraction of heme containing sGC or stabilization of the mutant by the cyclase domains. Additionally, mutating Thr 48 to Trp leads to weaker CO binding in the presence and absence of YC-1, which is in contrast to *Ns* H-NOX where the T48W mutation led to tightening of CO binding by ~2.5 fold. Mutations of Tyr 49 at the Site 2 pocket mouth had no effect on CO binding affinity in the presence or absence of YC-1 and all three mutants (Y49A, Y49W and Y49F) behaved similar to the wild type protein.

YC-1 Binding Site. An *In silico* study predicted the binding site for YC-1 family compounds in the β_1 H-NOX domain (*56*). Interestingly the predicted binding site is close to where Winter *et. al.* predicted tunnel 2 for diatomic ligand escape in *Ns* H-NOX (*54*). Although our mutations near Site 2 have no pronounced effect on YC-1 binding, it does not rule out the possibility of Site 2 as potential binding site; additional mutations will be required to resolve this issue. Previously, Raman resonance studies have predicted heme planarization upon YC-1 binding possibly due to weakened H-bonding between the

YXSXR motif and propionate side chains (*45*). The possibility of YC-1 binding to predicted Site 2 needs to be further evaluated, where YC-1 binding at Site 2 could potentially lead to structural changes in the β_1 H-NOX domain leading to perturbation of heme stabilizing interactions between propionate residues and the YXSXR residues. Our binding studies on the Site 1 mutants show loss of YC-1 stimulation of CO binding and weaker YC-1 binding. Although the data suggests Site 1 as the probable YC-1 binding site, since we observe the Soret shift upon YC-1 binding to the *Ms* sGC-NT21_LA mutant CO complex, the possibility of this pocket as the binding site for the YC-1 family compounds remains inconclusive.

Role of the Site 1 Pocket in Allostery. cGMP activity measurements in mutant L98F/A154F for full-length sGC reveal diminished activity in the presence of NO and YC-1, which is consistent with the observed weaker CO binding and slower histidine release rates. Similar activity profiles were observed with β I145Y (*62*) and β I149Y (*45*) mutants, possibly due to direct steric interference with NO binding to the heme, and structural changes in the heme pocket, respectively. The L98F/A154F double mutant protein also exhibits a high K_m for GTP binding, suggesting mutations in the pocket leads to an altered cyclase domain conformation, which now binds poorly to GTP and displays low cGMP activity. One plausible explanation is the mutant protein not only restricts the heme to a low affinity conformation but also restricts the cyclase to the low activity conformation. This suggests the pocket confers the flexibility to the proximal heme

subdomain to undergo conformational changes upon NO binding that are required for signal transduction. Since the mutant proteins display full heme loading, exhibit Soret characteristics similar to wild type heme, and forms a penta-coordinated nitrosyl complex upon NO binding, it is more likely that the signal transduction event post NO binding and His 105 bond cleavage is disrupted. It further suggests His 105 bond breakage is not the only step required for signal transduction but that signaling through the PAS and the coiled-coil domains is also required and disrupted by mutation. Recent hydrogen/deuterium exchange mass spectrometry (HDX-MS) studies also suggest NO induced conformational changes propagate through the PAS and coiled-coil domains (*32*).

Signal Transduction Through the Coiled-Coil. The role of the coiled-coil domain in signal transduction is not yet clear, and ambiguity about its role still remains. Although the crystal structure of the rat sGC β_1 coiled-coil domain reveals an anti-parallel arrangement, modeling by Ma *et. al. (18)* as well as our chemical cross-linking studies (*24*) and recent electron microscopy model (*25*) all indicate a parallel arrangement for the coiled-coil helices. We previously reported a drastic increase in the histidine release rate and rapid formation of penta-coordinated NO bound species when the coiled coil is truncated by ~21 residues (*24*).

These data supported a model in which the signal transduction propagates through the coiled-coil, leading to sGC activation. Here, we report that upon extending the coiled

coil by 9 residues to the predicted end of the coiled-coil (α_1 459 and β_1 389) in both *Ms* sGC-NT19 and *Ms* sGC-NT25, the histidine release rate becomes slower, suggesting the C-terminus of the coiled coil domain plays a crucial role in regulating the rate of histidine release. Since our modeling studies put the C-terminus of the coiled-coil away from the β_1 H-NOX domain, and the link between coiled-coil and the N-terminal signaling complex appears quite flexible by EM (*25*), it is tempting to speculate that signal transduction is not through direct contact between H-NOX and cyclase domains, but rather through passage of the coiled-coil. Recently, FRET studies in sGC also implicate the shorter helix after the proline induced turn at the C-terminus of the coiled-coil domain to be in close contact with the cyclase domain suggesting it might be involved in the signal transduction upon NO binding (*31*). Moreover, the HDX-MS studies also show large changes in exchange rates in both the α_1 and β_1 coiled-coil domains upon NO binding, suggesting the coiled-coil domain is involved in signal propagation (*32*).

Our studies favor a model in which a low activity conformation is coupled to a low affinity heme domain (Figure 6). Binding of NO or YC-1 to the N-terminal portion of the protein leads to realignment of the coiled-coil, which in turn aligns the active site residues in a high activity conformation. Support for this comes from the cGMP activity studies on the isolated cyclase domains, which display only basal level activity and require alignment of the key residues for activation. This suggests inhibition through contact with the β_1 H-NOX domain is not the only mechanism and other domains are required for activation (*20*). One possibility is that activity in sGC could be modulated by

a mechanism in which coiled-coil rotation upon NO binding could provide a torque required for aligning the residues in the cyclase domain for activation. That such a mechanism exists is shown in the recently reported crystal structure of the dihydroxyacetone kinase transcription regulator (DhaR) (*65*), where coiled-coil rotation transmits the signal of complex formation to the DNA-binding domain. Additionally, the crystal structure of a light activated histidine kinase (*66*) provides detailed insight into the role of a coiled-coil realignment to activate the kinase domain at one end of the coiled-coil after light is absorbed at the other end.

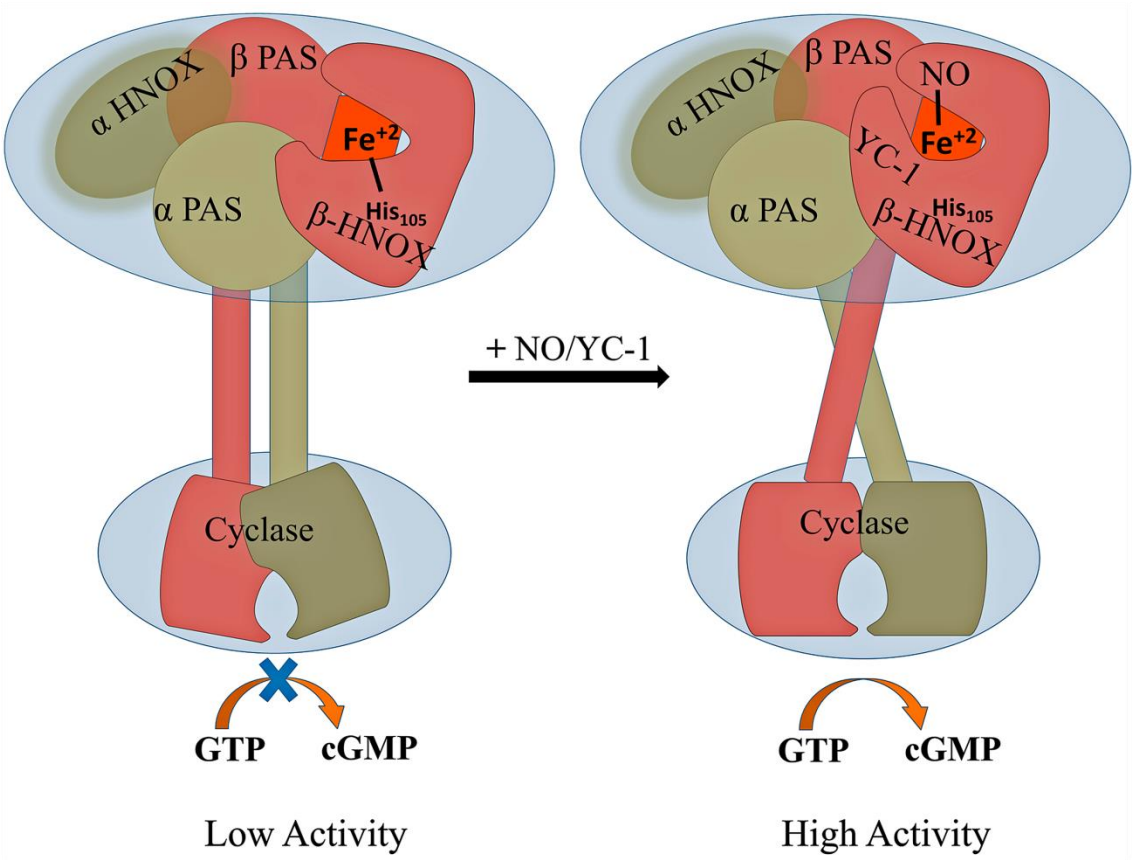

Figure 6. Model for sGC activation and regulation. Shown is a proposed model for allosteric regulation in sGC in which the β_1 H-NOX is kept in a low activity conformation through interactions with PAS domain and has high proximal strain. The coiled-coil in turn restricts the cyclase domain to a basal activity conformation. Binding of NO or YC-1 leads to a closed heme pocket which, through the coiled-coil conformational change, aligns the cyclase domain in a high activity conformation.

References:

1. Ignarro, L. J., (Ed.) (2010) *Nitric Oxide Biology and Pathobiology*, Second ed., Academic Press, San Diego.

2. Li, H., and Poulos, T. L. (2005) Structure-function studies on nitric oxide synthases, *J. Inorg. Biochem. 99*, 293-305.

3. Stuehr, D. J., Tejero, J., and Haque, M. M. (2009) Structural and mechanistic aspects of flavoproteins: electron transfer through the nitric oxide synthase flavoprotein domain, *FEBS J. 276*, 3959-3974.

4. Stone, J. R., and Marletta, M. A. (1996) Spectral and kinetic studies on the activation of soluble guanylate cyclase by nitric oxide, *Biochemistry 35*, 1093-1099.

5. Bian, K., Doursout, M. F., and Murad, F. (2008) Vascular system: role of nitric oxide in cardiovascular diseases, *J. Clin. Hypertens. (Greenwich) 10*, 304-310.

6. Coggins, M. P., and Bloch, K. D. (2007) Nitric oxide in the pulmonary vasculature, *Arterioscler. Thromb. Vasc. Biol. 27*, 1877-1885.

7. Erdmann, J., Stark, K., Esslinger, U. B., Rumpf, P. M., Koesling, D., de Wit, C., Kaiser, F. J., Braunholz, D., Medack, A., Fischer, M., Zimmermann, M. E., Tennstedt, S., Graf, E., Eck, S., Aherrahrou, Z., Nahrstaedt, J., Willenborg, C., Bruse, P., Braenne, I., Nothen, M. M., Hofmann, P., Braund, P. S., Mergia, E., Reinhard, W., Burgdorf, C., Schreiber, S., Balmforth, A. J., Hall, A. S., Bertram, L., Steinhagen-Thiessen, E., Li, S. C., Marz, W., Reilly, M., Kathiresan, S., McPherson, R., Walter, U., Ott, J., Samani, N. J., Strom, T. M., Meitinger, T., Hengstenberg, C., and Schunkert, H. (2013) Dysfunctional nitric oxide signalling increases risk of myocardial infarction, *Nature 504*, 432-436.

8. Herve, D., Philippi, A., Belbouab, R., Zerah, M., Chabrier, S., Collardeau-Frachon, S., Bergametti, F., Essongue, A., Berrou, E., Krivosic, V., Sainte-Rose, C., Houdart, E., Adam, F., Billiemaz, K., Lebret, M., Roman, S., Passemard, S., Boulday, G., Delaforge, A., Guey, S., Dray, X., Chabriat, H., Brouckaert, P., Bryckaert, M., and Tournier-Lasserve, E. (2014) Loss of alpha1beta1 soluble guanylate cyclase, the major nitric oxide receptor, leads to moyamoya and achalasia, *Am J Hum Genet 94*, 385-394.

9. Fitzpatrick, D. A., O'Halloran, D. M., and Burnell, A. M. (2006) Multiple lineage specific expansions within the guanylyl cyclase gene family, *BMC Evol Biol 6*, 26.

10. Schaap, P. (2005) Guanylyl cyclases across the tree of life, *Front. Biosci. 10*, 1485-1498.

11. Braughler, J. M., Mittal, C. K., and Murad, F. (1979) Purification of soluble guanylate cyclase from rat liver, *Proc. Natl. Acad. Sci. USA 76*, 219-222.

12. Budworth, J., Meillerais, S., Charles, I., and Powell, K. (1999) Tissue distribution of the human soluble guanylate cyclases, *Biochem Biophys Res Commun 263*, 696-701.

13. Cary, S. P., Winger, J. A., Derbyshire, E. R., and Marletta, M. A. (2006) Nitric oxide signaling: no longer simply on or off, *Trends Biochem. Sci. 31*, 231-239.

14. Moglich, A., Ayers, R. A., and Moffat, K. (2009) Structure and signaling mechanism of Per-ARNT-Sim domains, *Structure 17*, 1282-1294.

15. Anantharaman, V., Balaji, S., and Aravind, L. (2006) The signaling helix: a common functional theme in diverse signaling proteins, *Biol. Direct 1*, 25.

16. Liu, Y., Ruoho, A. E., Rao, V. D., and Hurley, J. H. (1997) Catalytic mechanism of the adenylyl and guanylyl cyclases: Modeling and mutational analysis, *Proc. Natl. Acad. Sci. USA 94*, 13414-13419.

17. Purohit, R., Weichsel, A., and Montfort, W. R. (2013) Crystal structure of the Alpha subunit PAS domain from soluble guanylyl cyclase, *Protein Sci. 22*, 1439-1444.

18. Ma, X., Beuve, A., and van den Akker, F. (2010) Crystal structure of the signaling helix coiled-coil domain of the beta1 subunit of the soluble guanylyl cyclase, *BMC Struct. Biol. 10*, 2.

19. Allerston, C. K., von Delft, F., and Gileadi, O. (2013) Crystal Structures of the Catalytic Domain of Human Soluble Guanylate Cyclase, *Plos One 8*.

20. Seeger, F., Quintyn, R., Tanimoto, A., Williams, G. J., Tainer, J. A., Wysocki, V. H., and Garcin, E. D. (2014) Interfacial Residues Promote an Optimal Alignment of the Catalytic Center in Human Soluble Guanylate Cyclase: Heterodimerization Is Required but Not Sufficient for Activity, *Biochemistry 53*, 2153-2165.

21. Ma, X., Sayed, N., Beuve, A., and van den Akker, F. (2007) NO and CO differentially activate soluble guanylyl cyclase via a heme pivot-bend mechanism, *EMBO J. 26*, 578-588.

22. Nioche, P., Berka, V., Vipond, J., Minton, N., Tsai, A. L., and Raman, C. S. (2004) Femtomolar sensitivity of a NO sensor from Clostridium botulinum, *Science 306*, 1550-1553.

23. Pellicena, P., Karow, D. S., Boon, E. M., Marletta, M. A., and Kuriyan, J. (2004) Crystal structure of an oxygen-binding heme domain related to soluble guanylate cyclases, *Proc. Natl. Acad. Sci. USA 101*, 12854-12859.

24. Fritz, B. G., Roberts, S. A., Ahmed, A., Breci, L., Li, W., Weichsel, A., Brailey, J. L., Wysocki, V. H., Tama, F., and Montfort, W. R. (2013) Molecular Model of a Soluble Guanylyl Cyclase Fragment Determined by Small-Angle X-ray Scattering and Chemical Cross-Linking, *Biochemistry 52*, 1568-1582.

25. Campbell, M. G., Underbakke, E. S., Potter, C. S., Carragher, B., and Marletta, M. A. (2014) Single-particle EM reveals the higher-order domain architecture of soluble guanylate cyclase, *Proc. Natl. Acad. Sci. USA 111*, 2960-2965.

26. Dierks, E. A., Hu, S., Vogel, K. M., Yu, A. E., Spiro, T. G., and Burstyn, J. N. (1997) Demonstration of the role of scission of the proximal histidine-iron bond in the activation of soluble guanylyl cyclase though metalloporphyrin substitution studies, *J Am Chem Soc 119*, 7316-7323.

27. Wedel, B., Humbert, P., Harteneck, C., Foerster, J., Malkewitz, J., Böhme, E., Schultz, G., and Koesling, D. (1994) Mutation of His-105 in the b1 subunit yields a nitric oxide-insensitive form of soluble guanylate cyclase, *Proc. Natl. Acad. Sci. USA 91*, 2592-2596.

28. Purohit, R., Fritz, B. G., The, J., Issaian, A., Weichsel, A., David, C. L., Campbell, E., Hausrath, A. C., Rassouli-Taylor, L., Garcin, E. D., Gage, M. J., and Montfort, W. R. (2014) YC-1 Binding to the beta Subunit of Soluble Guanylyl Cyclase Overcomes Allosteric Inhibition by the alpha Subunit, *Biochemistry 53*, 101-114.

29. Underbakke, E. S., Iavarone, A. T., and Marletta, M. A. (2013) Higher-order interactions bridge the nitric oxide receptor and catalytic domains of soluble guanylate cyclase, *Proc. Natl. Acad. Sci. USA 110*, 6777-6782.

30. Winger, J. A., and Marletta, M. A. (2005) Expression and characterization of the catalytic domains of soluble guanylate cyclase: interaction with the heme domain, *Biochemistry 44*, 4083-4090.

31. Busker, M., Neidhardt, I., and Behrends, S. (2014) Nitric oxide activation of guanylate cyclase pushes the alpha1 signaling helix and the beta1 heme-binding domain closer to the substrate-binding site, *J. Biol. Chem. 289*, 476-484.

32. Underbakke, E. S., Iavarone, A. T., Chalmers, M. J., Pascal, B. D., Novick, S., Griffin, P. R., and Marletta, M. A. (2014) Nitric Oxide-Induced Conformational Changes in Soluble Guanylate Cyclase, *Structure 22*, 602-611.

33. Evgenov, O. V., Pacher, P., Schmidt, P. M., Hasko, G., Schmidt, H. H., and Stasch, J. P. (2006) NO-independent stimulators and activators of soluble guanylate cyclase: discovery and therapeutic potential, *Nat. Rev. Drug Discov. 5*, 755-768.

34. Friebe, A., and Koesling, D. (1998) Mechanism of YC-1-induced activation of soluble guanylyl cyclase, *Mol Pharmacol 53*, 123-127.

35. Ko, F. N., Wu, C. C., Kuo, S. C., Lee, F. Y., and Teng, C. M. (1994) YC-1, a novel activator of platelet guanylate-cyclase, *Blood 84*, 4226-4233.

36. Wu, C. C., Ko, F. N., Kuo, S. C., Lee, F. Y., and Teng, C. M. (1995) Yc-1 Inhibited Human Platelet-Aggregation through No-Independent Activation of Soluble Guanylate-Cyclase, *Brit. J. Pharmacol. 116*, 1973-1978.

37. Mittendorf, J., Weigand, S., Alonso-Alija, C., Bischoff, E., Feurer, A., Gerisch, M., Kern, A., Knorr, A., Lang, D., Muenter, K., Radtke, M., Schirok, H., Schlemmer, K. H., Stahl, E., Straub, A., Wunder, F., and Stasch, J. P. (2009) Discovery of riociguat (BAY 63-2521): a potent, oral stimulator of soluble

guanylate cyclase for the treatment of pulmonary hypertension, *ChemMedChem 4*, 853-865.

38. Martin, F., Baskaran, P., Ma, X., Dunten, P. W., Schaefer, M., Stasch, J. P., Beuve, A., and van den Akker, F. (2010) Structure of cinaciguat (BAY 58-2667) bound to Nostoc H-NOX domain reveals insights into heme-mimetic activation of the soluble guanylyl cyclase, *J. Biol. Chem. 285*, 22651-22657.

39. Hu, X., Murata, L. B., Weichsel, A., Brailey, J. L., Roberts, S. A., Nighorn, A., and Montfort, W. R. (2008) Allostery in recombinant soluble guanylyl cyclase from Manduca sexta, *J. Biol. Chem. 283*, 20968-20977.

40. Pal, B., and Kitagawa, T. (2010) Binding of YC-1/BAY 41-2272 to soluble guanylate cyclase: A new perspective to the mechanism of activation, *Biochem Biophys Res Commun 397*, 375-379.

41. Stasch, J. P., Becker, E. M., Alonso-Alija, C., Apeler, H., Dembowsky, K., Feurer, A., Gerzer, R., Minuth, T., Perzborn, E., Pleiss, U., Schroder, H., Schroeder, W., Stahl, E., Steinke, W., Straub, A., and Schramm, M. (2001) NO-independent regulatory site on soluble guanylate cyclase, *Nature 410*, 212-215.

42. Lamothe, M., Chang, F. J., Balashova, N., Shirokov, R., and Beuve, A. (2004) Functional characterization of nitric oxide and YC-1 activation of soluble guanylyl cyclase: Structural implication for the YC-1 binding site?, *Biochemistry 43*, 3039-3048.

43. Makino, R., Yazawa, S., Hori, H., and Shiro, Y. (2012) Interactions of soluble guanylate cyclase with a P-site inhibitor: effects of gaseous heme ligands, azide, and allosteric activators on the binding of 2'-deoxy-3'-GMP, *Biochemistry 51*, 9277-9289.

44. Yazawa, S., Tsuchiya, H., Hori, H., and Makino, R. (2006) Functional characterization of two nucleotide-binding sites in soluble guanylate cyclase, *J. Biol. Chem. 281*, 21763-21770.

45. Ibrahim, M., Derbyshire, E. R., Marletta, M. A., and Spiro, T. G. (2010) Probing Soluble Guanylate Cyclase Activation by CO and YC-1 Using Resonance Raman Spectroscopy, *Biochemistry 49*, 3815-3823.

46. Ibrahim, M., Derbyshire, E. R., Soldatova, A. V., Marletta, M. A., and Spiro, T. G. (2010) Soluble Guanylate Cyclase Is Activated Differently by Excess NO and by YC-1: Resonance Raman Spectroscopic Evidence, *Biochemistry 49*, 4864-4871.

47. Li, Z. Q., Pal, B., Takenaka, S., Tsuyama, S., and Kitagawa, T. (2005) Resonance Raman evidence for the presence of two heme pocket conformations with varied activities in CO-bound bovine soluble guanylate cyclase and their conversion, *Biochemistry 44*, 939-946.

48. Martin, E., Czarnecki, K., Jayaraman, V., Murad, F., and Kincaid, J. (2005) Resonance Raman and infrared spectroscopic studies of high-output forms of human soluble guanylyl cyclase, *J Am Chem Soc 127*, 4625-4631.

49. Yoo, B.-K., Lamarre, I., Rappaport, F., Nioche, P., Raman, C. S., Martin, J.-L., and Negrerie, M. (2012) Picosecond to Second Dynamics Reveals a Structural Transition in Clostridium botulinum NO-Sensor Triggered by the Activator BAY-41-2272, *ACS Chem. Biol. 7*, 2046-2054.

50. Fritz, B. G., Hu, X., Brailey, J. L., Berry, R. E., Walker, F. A., and Montfort, W. R. (2011) Oxidation and loss of heme in soluble guanylyl cyclase from Manduca sexta, *Biochemistry 50*, 5813-5815.

51. Hu, X., Feng, C., Hazzard, J. T., Tollin, G., and Montfort, W. R. (2008) Binding of YC-1 or BAY 41-2272 to soluble guanylyl cyclase induces a geminate phase in CO photolysis, *J Am Chem Soc 130*, 15748-15749.

52. Ramanathan, S., Mazzalupo, S., Boitano, S., and Montfort, W. R. (2011) Thrombospondin-1 and angiotensin II inhibit soluble guanylyl cyclase through an increase in intracellular calcium concentration, *Biochemistry 50*, 7787-7799.

53. Dundas, J., Ouyang, Z., Tseng, J., Binkowski, A., Turpaz, Y., and Liang, J. (2006) CASTp: computed atlas of surface topography of proteins with structural and topographical mapping of functionally annotated residues, *Nucleic Acids Research 34*, W116-W118.

54. Winter, M. B., Herzik, M. A., Jr., Kuriyan, J., and Marletta, M. A. (2011) Tunnels modulate ligand flux in a heme nitric oxide/oxygen binding (H-NOX) domain, *Proc. Natl. Acad. Sci. USA 108*, E881-889.

55. Sievers, F., Wilm, A., Dineen, D., Gibson, T. J., Karplus, K., Li, W., Lopez, R., McWilliam, H., Remmert, M., Soeding, J., Thompson, J. D., and Higgins, D. G. (2011) Fast, scalable generation of high-quality protein multiple sequence alignments using Clustal Omega, *Mol. Syst. Biol. 7*.

56. Alisaraie, L., Fu, Y., and Tuszynski, J. A. (2013) Dynamic Change of Heme Environment in Soluble Guanylate Cyclase and Complexation of NO-Independent Drug Agents with H-NOX Domain, *Chem. Biol.Drug Des.81*, 359-381.

57. Baskaran, P., Heckler, E. J., van den Akker, F., and Beuve, A. (2011) Aspartate 102 in the Heme Domain of Soluble Guanylyl Cyclase Has a Key Role in NO Activation, *Biochemistry 50*, 4291-4297.

58. Baskaran, P., Heckler, E. J., van den Akker, F., and Beuve, A. (2011) Identification of Residues in the Heme Domain of Soluble Guanylyl Cyclase that are Important for Basal and Stimulated Catalytic Activity, *Plos One 6*.

59. Rothkegel, C., Schmidt, P. M., Stoll, F., Schroeder, H., Schmidt, H. H. H. W., and Stasch, J.-P. (2006) Identification of residues crucially involved in soluble guanylate cyclase activation, *FEBS Lett. 580*, 4205-4213.

60. Chang, F. J., Lemme, S., Sun, Q., Sunahara, R. K., and Beuve, A. (2005) Nitric oxide-dependent allosteric inhibitory role of a second nucleotide binding site in soluble guanylyl cyclase, *J. Biol. Chem. 280*, 11513-11519.

61. Denninger, J. W., Schelvis, J. P. M., Brandish, P. E., Zhao, Y., Babcock, G. T., and Marletta, M. A. (2000) Interaction of soluble guanylate cyclase with YC-1: Kinetic and resonance Raman studies, *Biochemistry 39*, 4191-4198.

62. Martin, E., Berka, V., Bogatenkova, E., Murad, F., and Tsai, A.-L. (2006) Ligand selectivity of soluble guanylyl cyclase - Effect of the hydrogen-bonding tyrosine in the distal heme pocket on binding of oxygen, nitric oxide, and carbon monoxide, *J. Biol. Chem. 281*, 27836-27845.

63. Tsai, A.-l., Martin, E., Berka, V., and Olson, J. S. (2012) How Do Heme-Protein Sensors Exclude Oxygen? Lessons Learned from Cytochrome c ', Nostoc puntiforme Heme Nitric Oxide/Oxygen-Binding Domain, and Soluble Guanylyl Cyclase, *Antioxid. Redox Signal. 17*, 1246-1263.

64. Tsai, A. L., Berka, V., Martin, E., and Olson, J. S. (2012) A "sliding scale rule" for selectivity among NO, CO, and O(2) by heme protein sensors, *Biochemistry 51*, 172-186.

65. Shi, R., McDonald, L., Cygler, M., and Ekiel, I. (2014) Coiled-Coil Helix Rotation Selects Repressing or Activating State of Transcriptional Regulator DhaR, *Structure 22*, 478-487.

66. Diensthuber, R. P., Bommer, M., Gleichmann, T., and Moeglich, A. (2013) Full-Length Structure of a Sensor Histidine Kinase Pinpoints Coaxial Coiled Coils as Signal Transducers and Modulators, *Structure 21*, 1127-1136.